

INTELLIGENT COMPUTING IN MEDICAL ULTRASONIC SYSTEM

By

NAOMI YAGI

A dissertation submitted in partial fulfillment of the requirements for the degree of

DOCTOR OF ENGINEERING

UNIVERSITY OF HYOGO
JAPAN

MARCH 2014

*To my husband, mother, father, sister, and all members of my family
for helping me build the foundations in my research life and allowing me to give my studies.*

Acknowledgements

First and foremost, I would like to express my sincerest gratitude to my supervisor Professor Yutaka Hata of University of Hyogo, for the continuous support and instilled mental stimulation of my Ph. D study with his motivation and immense knowledge. I also thank to Doctor Syoji Kobashi and Doctor Kei Kuramoto of University of Hyogo for providing lucid and valuable insights throughout my work.

I firmly believe that my research would not be completed without medical support and advice. I would like to appreciate Doctor Osamu Ishikawa, Doctor Yoshitetsu Oshiro, and Doctor Tomomoto Ishikawa of Ishikawa Hospital, and Doctor Nao Shibamura of Kobe Kaisei Hospital. I also owe many thanks to Mister Toshiyuki Sawayama of New Sensor Corporation for providing technical guidance and comment of ultrasonic field. They gave direction when it was most needed. Their advice throughout my process kept me focused on my research topic.

Special thanks are due to Professor Lotfi A. Zadeh of University of California, Doctor Tokuko S. Wiedemann of Fukushima Medical University, Doctor Hiroshi Nakajima of Omron Corporation, and Doctor Kazuhiko Taniguchi of Kinden Corporation. They inspired me to take pride in my research; their enthusiasm for research efforts will have a significant affect on my future projects. Their heartfelt encouragement with consistent quality contributed to my growth as a scientist.

In addition, I am so grateful to Google for granting me Anita Borg scholarship and giving any chances of meeting many active female researchers and students in the field of computer science. They transcend academia and provide a quest for my study. I also sincerely thank all members of Informtaion Systems Laboratory of University of Hyogo for supporting every phase of this work.

Last but not the least, I would like to owe eternal thanks to everyone for supporting me academically and spiritually throughout my research life.

Preface

The medical ultrasonography is a noninvasive and real-time diagnostic technique for the human body structures and tissue in medicine. Furthermore, it is an easy, safe, and repetitive system. The medical ultrasonography is used in the study of many different fields including gastroenterology, cardiology, neonatology, gynecology, and so on. Ultrasonography is an ultrasound-mediated diagnostic imaging technique for visualizing subcutaneous body structures. In real medicine, the medical expert doctors diagnose the tissue using the ultrasonic devices by visual observation. It is so important to automatically and correctly diagnose the tissue for early detection. For example, X-ray computed tomography (CT) and magnetic resonance imaging (MRI) to obtain the detailed image of the brain are widely used. However, they have some serious problems, which they have X-ray exposure in a case of CT and are not real time device. In comparison to them, the ultrasonic diagnosis has some advantages such as low cost and compactness.

Though the frequency up to 50-100 MHz has been experimentally used in a technique known as bio-microscopy in special regions, typical ultrasound diagnostic device operates in the frequency range of 0.4 to 25 MHz. The choice of ultrasonic frequency is a trade-off between spatial resolution of the image and imaging depth. Lower frequencies produce less resolution but image deeper into the body. Higher frequency sound waves have a smaller wavelength and thus are capable of reflecting or scattering from the small structures. On the other hand, higher frequency sound waves have a larger attenuation and thus are more readily absorbed in tissue, limiting the depth of penetration of the sound wave into the body.

This dissertation describes three ultrasonic intelligent computing systems, which are measured ranging from cell level to femur and skull: cell quantity in the bone tissue, surgical replacement of the hip joint for Total Hip Arthroplasty, and human brain diagnosis. These systems are mainly proposed with intelligent computing, which are frequency analysis, and Fuzzy Logic that is pioneered the development by prof. Lotfi A. Zadeh. First, the cell quantity estimation method is introduced. Without destroying cell, it is suggested the ability of intervention in order to produce the desired beneficial effect. Second, the stem determination method is introduced and indicates the indexes in order to judge how degree the stem fits in the clinical treatment for the surgeons. Third, the human brain diagnosis method is introduced. Generally, the general ultrasonic devices are not available for transmitting bone tissue. The ultrasound is rarely used to the bone, because the ultrasound through bone causes large absorption and scattering and the bone tissue has higher attenuation than the other tissue. In order to solve the problems and obtain the clearer ultrasonic images, some data synthesis and analysis are proposed. Moreover, the mobile health care management are suggested with implementation of iPhone/iPad.

It is represented the usability of ultrasound and intelligent computing for secure and accurate medical diagnosis, which are noninvasive, and enable dynamic imaging. It needs the development and technical improvement for new ultrasonic medical diagnosis system. This dissertation presents and discusses the scientific significance and contribution contents as the advanced study.

Contents

ACKNOWLEDGEMENTS	I
PREFACE	II
CONTENTS	III
CHAPTER 1 INTRODUCTION.....	1
CHAPTER 2 CELLULAR QUANTITY MEASUREMENT SYSTEM IN BONE MARROW STROMAL CELLS.....	4
2.1 INTRODUCTION	4
2.2 EXPERIMENTAL ENVIRONMENTS.....	5
<i>2.2.1 Artificial Culture Bone.....</i>	<i>5</i>
<i>2.2.2 Ultrasonic Device.....</i>	<i>6</i>
2.3. EXPERIMENTAL MEASUREMENT	7
<i>2.3.1 Ultrasonic Measurement.....</i>	<i>7</i>
<i>2.3.2 Scanning Electron Microscopy Observation</i>	<i>8</i>
<i>2.3.3 Relationship between Features</i>	<i>8</i>
2.4. CELL QUANTITY ESTIMATION	9
<i>2.4.1 Fuzzy Inference</i>	<i>9</i>
<i>2.4.2 Neural Network.....</i>	<i>11</i>
<i>2.4.3 Multiple Linear Regression Model.....</i>	<i>12</i>
2.5. ESTIMATION RESULTS	14
2.6. DISCUSSION ON FREQUENCY FEATURE	14
2.7. CONCLUSION.....	15
CHAPTER 3 STEM DETERMINATION SYSTEM FOR TOTAL HIP ARTHROPLASTY	17
3.1 INTRODUCTION	17
3.2. TOTAL HIP ARTHROPLASTY.....	18
3.3. PRELIMINARY EXPERIMENT.....	19
3.4. MEASUREMENT SYSTEM.....	20
3.5 ATTENUATION TIME	21
3.6. FUZZY INFERENCE	22
3.7. EXPERIMENTAL RESULTS.....	24
3.8. CONCLUSION.....	25

CHAPTER 4 DIAGNOSIS SYSTEM FOR HUMAN BRAIN IMAGING	26
4.1 TRANS-SKULL ULTRASONIC DOPPLER SYSTEM.....	26
4.1.1 <i>Introduction.....</i>	26
4.1.2 <i>Experimental Devices.....</i>	27
4.1.3 <i>Proposed Method</i>	28
4.1.4 <i>Doppler Effect and COG in Frequency Domain.....</i>	29
4.1.5 <i>Evaluation System</i>	31
4.1.6 <i>Experimental Results.....</i>	33
4.1.7 <i>Conclusion.....</i>	34
4.2 TRANS-SKULL BRAIN IMAGING SYSTEM	34
4.2.1 <i>Introduction.....</i>	34
4.2.2 <i>Experimental Environments</i>	35
4.2.3 <i>Data Synthesis</i>	37
4.2.4 <i>Data Analysis</i>	39
4.2.5 <i>Data Extraction</i>	42
4.2.5.1 <i>Bone Thickness Determination.....</i>	42
4.2.5.2 <i>Sulcus Surface</i>	45
4.2.6 <i>Experimental Results.....</i>	46
4.2.7 <i>Conclusion.....</i>	49
4.3 MOBILE HEALTHCARE MANAGEMENT SYSTEM.....	50
4.3.1 <i>Introduction.....</i>	50
4.3.2 <i>Mobile System Implementation</i>	51
4.3.3 <i>Disscussion.....</i>	53
4.3.4 <i>Conclusion.....</i>	54
CHAPTER 5 CONCLUSION.....	55
BIBLIOGRAPHY	57
AUTHOR’S PAPERS CONCERNING THIS DISSERTATION	62

Chapter 1

Introduction

Ultrasound has been used to image the human body and has become one of the most widely used diagnostic tools in modern medicine. The technology is relatively inexpensive and portable, especially when compared with other modalities, such as magnetic resonance imaging (MRI) and computed tomography (CT), which are time-consuming, and require radioactive tracers. Ultrasound is also used to visualize tissue during routine and emergency prenatal care. As currently applied in the medical field, properly performed ultrasound poses no known risks to the patient. Moreover, it has been shown that it is possible to visualize and measure changes in ultrasound intensities with the use of harmonic gray-scale ultrasound imaging [1], [2].

In regenerative medicine, large bone defects caused by bone tumors and bone fractures are treated by using filling materials because natural healing is untreatable to these bone defects. The human body has an innate response to defend and heal when injured or invaded by various diseases. However, in the case of untreatable injuries and diseases, it is essential to depend on the promising field of regenerative medicine, which is working to restore the structure and function of damaged tissues and organs. Recently, the composites of bone marrow stromal cells (BMSCs)/ β -tricalcium phosphate (β -TCP) have been increasingly used as bone substitutes in bone tissue engineering. In clinical setting, it is important to identify appropriate number of cells in the composites before implanting. Some studies evaluated number of cells by scanning with microscope [3], [4]. However, when evaluating it with these techniques, the composites must be destroyed and are not used for any future study or clinical practice. In order to detect objects and measure distances, X-rays and microwave of high frequency are used, but they destroy some tissue of the products or the cells. Therefore, the novel nondestructive testing method is desired on a field of medical treatment.

In orthopedic surgery, when a damaged joint is replaced with an artificial joint, called prosthesis, a joint replacement surgery, is needed, and the arthritic or dysfunctional joint surface is replaced with an orthopedic prosthesis. For joint replacement surgery, the artificial surfaces of the joint replacement are shaped in such a way as to allow joint movement similar to that of a healthy natural joint. In such a severe case, one may consider a joint replacement as a possible solution. The examinations and tests will be performed to assess the severity of the joint damage. If less invasive alternatives do not alleviate pain and damage, the total joint replacement will be considered. The prosthetic implant used in hip replacement consists of different parts, the acetabular cup, the femoral component and the particular interface. The femoral component is the component that fits in the femur. Bone is removed and the femur is shaped to accept the femoral stem with attached prosthetic femoral head or ball. Options exist for different patients and indications. Correct selection of the prosthesis is important. Regardless of implant design, primary stability of the cement less femoral implants in the femoral canal must be achieved at the time of operation and is really important for osseointegration, long-term fixation and clinical success [5]. The surgeon's experience in choosing the stem to be implanted is fundamental to achieve good fixation. It is difficult to predict the precise size of the implant during the preoperative plan especially when the stem implantation is planned. Moreover, it depends on the surgeon skill, and do not have objective decision measuring. Thus, it is needed to perform more quantitative measurement and more reasonable assessment.

In human brain diagnostic, the imaging of the brain is needed. Stroke remains an important and time-sensitive health concern. CT is the imaging modality most commonly used to assess the

underlying nature of a potential stroke. As a diagnostic tool to aid in decision-making, transcranial ultrasound might constitute a safer, less expensive, more portable alternative to CT for emergency medicine and home health care. In Reference [6], The system acquired fusing 3-D transcranial ultrasound volumes from temporal window. However, it is not portable system and is difficult to transmit ultrasound from the random position. In Reference [7], the transcranial sonography has been proposed using two linear array probes. These array probes consist of 128 elements. However, it is difficult to transmit ultrasound from the random position because the two array probes are set up on both sides of human head. In Reference [8], they employ the spherical array probe that consists of the 448 elements. However, they only described a signal processing. Therefore, a simple and unrestrained system without the large mechanical scanner is strongly needed.

In smart medical system, the more widely used electronic medical record (EHR) operated by the clinicians or the health care providers. It contrasts well with a personal health record (PHR). This is a health record which the patient maintains health data and information for the care [9]. The intention of a PHR is to provide a summary of an individual medical history which is accessible online. The health data on a PHR include patient-reported outcome data from devices collected passively from a smartphone such as wireless electronic weighing scales. The patients may enter PHR directly, either by typing into fields or uploading/transmitting data from a file or another website. In recent years, several formal definitions of the term have been proposed by various organizations [10]. It is desired for physicians and patients to use compact and mobile technology in order to assist with clinical decision-making.

This dissertation proposes three ultrasonic intelligent computing systems by focusing the advantages of ultrasound: Cellular Quantity Measurement System in Bone Marrow Stromal Cells, Stem Determination System for Total Hip Arthroplasty, and Diagnosis System for Human Brain Imaging.

Chapter 2 presents “Cellular Quantity Measurement System in Bone Marrow Stromal Cells”. In order to measure cell quantity, the composite must be crushed and the cell count with an electro microscope. However, the measured composite is not used for a future study and clinic. Therefore, this study proposes the cellular quantity measurement system without destroying some tissue and cells of the products. This system estimates the cell quantity with correlation between cell quantity and two features, which are extracted from the ultrasonic waves: amplitude and frequency. It is attempted to identify cellular quantity with an ultrasonic system and approaches of neural network and fuzzy inference. Amplitude is obtained from the raw ultrasonic wave, and frequency is calculated from frequency spectrum obtained by applying cross-spectrum method. A comparison is done with the multi regression method. Moreover, it is suggested that the superiority of frequency to analyze Bone Marrow Stromal Cells. In order to calculate the frequency value, it is proposed two approaches, which is Fast Fourier Transform and Cross-Spectrum. This study focuses on the attenuation due to viscosity, which is proportional to the squares of the frequency. This chapter has a discussion about the attenuation of frequency. It is employed the ultrasonic waves with the center frequency of 1.0 MHz. The attenuation is proportional to the squares of the frequency. The frequency range of approximate 1.0 MHz value attenuates. This study shows the ability of intervention in order to produce the desired beneficial effect.

Chapter 3 presents “Stem Determination System for Total Hip Arthroplasty”. Total Hip Arthroplasty is surgical replacement of the hip joint with an artificial prosthesis. The selection of the optimum size and type of implant to fit the anatomical characteristics of the individual patient is important in order to avoid postoperative complications such as dislocation or loosening. The surgeon experience in choosing the implanted stem size is fundamental to achieve good fixation. However, especially in the complicated cases, it still has the risk that the stem size chosen might be unsuitable. To solve the problems, this system proposes the level of stability by analyzing ultrasonic wave measurements, and indicates the indexes in order to judge how degree the stem fits

in the clinical treatment. This chapter suggests the ultrasonic system with a single ultrasonic probe. This experiment makes a knock to the upper point of the stem inserted with a hammer, which has the trigger signals. It is detected the acoustic signals with the knocking signals. An ultrasonic probe is fixed in the upper side of the stem with a built-in magnet. A personal computer got the acoustic data. In the surgery, the surgeon tries to adapt for the patient from the small size stem to the larger size stem in turn. There is a correlation between the degree of tightening and the attenuation time of acoustic signal for the knocked sound by a hammer when inserting the stem. The higher tightened degree implies shorter attenuation period. At the present time, the surgeon's experience chooses the suitable stem. Therefore, this chapter suggests the stem determination system, which selects the suitable stem by fuzzy inference, which dynamically corresponds for each patient. Moreover, in order to do more quantitative evaluation and analysis, it is proposed how to select the most suitable stem for the patients by using the ultrasonic system in this study. The result successfully determines the suitable stem in comparison to the results obtained from the practical surgery.

Chapter 4 presents "Diagnosis System for Human Brain Imaging". The transcranial sonography imaging device visualizes blood flow and tissue, and substantially shortens diagnosis time. The research goal is the portable and real time brain diagnosis under the thick-skull. The choice of ultrasonic frequency is a trade-off between spatial image resolution and imaging depth. This study shows the diagnosis systems, which penetrate the skull, and consists two parts: the trans-skull brain imaging system and the trans-skull ultrasonic doppler system. First, data synthesis methods and data analysis methods of two ultrasonic waves for visualizing brain image under skull. The choice of frequency is a trade-off between spatial resolution of the image and imaging depth. Lower frequency produces less resolution but image deeper into the body. Higher frequency sound waves have a smaller wavelength and thus are capable of reflecting or scattering from smaller structures. In the bone, the ultrasound causes large absorption and scattering, so the ultrasonic device is rarely used to the bone. The bone tissue has higher attenuation than the other tissue. Therefore, the general ultrasonic devices are not available for transmitting bone tissue. However, it can transmit the low frequency under 1.0 MHz to bone tissue. In clinical practice, the ultrasonic device with the center frequency of 0.5 MHz is performed to diagnose osteoporosis. Therefore, it is employed 0.5 MHz and 1.0 MHz ultrasonic array probes. This study synthesizes and analyzes in frequency domain, and visualizes the sulcus and skull. It is performed the experiment with a cow scapula as a skull and a steel sulcus as a cerebral sulcus, and calculated the thickness of the bone from the synthesized waves. The thickness is determined from the surface and bottom points determined from the wave. The surface point is easily determined from the wave. The bottom point is determined by fuzzy inference. The sulcus surface was extracted from a B-mode image made from the synthesized waves. This study successfully determines the skull depth and visualizes the sulcus from the synthesized waves, and showed the usability to synthesize the respective ultrasonic wave of the different frequency. Lastly, this ultrasonic technology is applied mobile health care managements in smart medical system with implementation of iPhone/iPad. This study develops the total system with mobile phone application for medical ultrasonic system. It is meaningful for ultrasound-mediated diagnosis in emergency medicine and health care in the near future.

Chapter 5 concludes with discussing the usability of ultrasound and intelligent computing for secure and accurate medical diagnosis. The ultrasonic devices are noninvasive, and enable dynamic imaging. It is needed the development and technical improvement for new ultrasonic medical diagnosis system in the future. Lastly, this dissertation represents the scientific significance and contribution contents as the advanced study.

Chapter 2

Cellular Quantity Measurement System in Bone Marrow Stromal Cells

This chapter describes an ultrasonic system that estimates the cell quantity of an artificial culture bone, which is effective for appropriate treat with a composite of this material and Bone Marrow Stromal Cells. For this system, three approaches are examined for analyzing the ultrasound waves transmitted through the cultured bone, including stem cells to estimate cell quantity: multiple regression, fuzzy inference, and neural network. It is employed two characteristics from the obtained wave for applying each method. These features are the amplitude and the frequency; the amplitude is measured from the obtained wave, and the frequency is calculated by the cross-spectrum method. The results confirmed that fuzzy inference yields the accurate estimates of cell quantity, and neural network yields the accurate estimates of cell rank. Using this ultrasonic estimation system, the orthopaedic surgeons can choose the composites that contain favorable number of cells before the implantation.

2.1 Introduction

The large bone defects caused by bone tumor and fracture are treated by using conventional filling materials of autogeneous bone, allograft bone, and artificial bone, for example, autogeneous bone has problems of quantitative limitation [11]-[13] and imposes significant surgical damage on the patients. The compensation with allograft bone has to find a compatible donor and is highly susceptible to infection.

The artificial bone does not have an affinity for human bone. Thus, it is required to find a novel material without these problems. Recently, the composite of artificial culture bone and Bone Marrow Stromal Cells (BMSCs) has become an anticipated solution to these defects [14]-[22]. The artificial culture bone is commercially available, and its filling material is highly compatible with human bone [23]-[25]. The BMSCs are mesenchymal stem cells, which can differentiate into a variety of cell types, osteoblast myogenic, adipogenic cells and more [26]-[28]. In addition, this cell has no ethical problem [29]. However, this composite has seldom been studied for clinical application. In order to measure the cell quantity, the composite must be crushed and the cells count with an electro microscope [30]. However, the measured composite is not used for a future study and clinic. Additionally, the only approximate quantity to treat large bone defects is needed.

In order to detect objects and measure distances, X-rays and microwave of high frequency are used, but they destroy some tissue of the products or the cells. Therefore, it is proposed an ultrasonic system that estimates the cell quantity of artificial culture bone. The ultrasound device has many advantages, including real time scanning, smart and compact, low cost, and producing no tissue damage [31]. This system employs the ultrasound wave transmitted into these composites. It is known that the low frequency ultrasonic wave of approximately 1.0 MHz can be transmitted through bone tissue [32]-[35]. This study employs two features: amplitude and frequency in order to construct the system and calculate the predictive value. The amplitude is measured from the obtained wave, and the frequency is calculated from the frequency spectrum of transfer function using cross-spectrum [36]-[38]. The conventional method shows that the ultrasound amplitude

effectively responded to the quantity composites and was well correlated to the actual cell value [39]. This study estimates cell quantity by two approaches: multiple-regression as a linear analysis method, fuzzy inference, and neural network. Moreover, on the frequency domain, it was confirmed the attenuation in the immediate vicinity of 1.0 MHz, which is the center frequency of the probe. In order to demonstrate this attenuation, this study proposes two approaches using ultrasonic cell quantity determination on the frequency domain: the peak and the center of gravity (COG). As the results, COG frequencies were absolutely found less than peak frequencies on all composites. This study showed the ability of intervention to produce the desired effect. This study certified the superiority of the frequency data analysis.

These approaches are constructed based on the relation between cell quantity and two features; amplitude and frequency, which are high correlation coefficient with cell quantity. The results showed that fuzzy inference and neural network estimated cell rank with the highest accuracy.

2.2 Experimental Environments

2.2.1 Artificial Culture Bone

It is employed BMSCs, which are an Embryonic Stem (ES) cell, as an artificial culture bone. BMSCs change into some type of cell and are obtained from marrow of patients. In contrast to ES cell, BMSCs cause no rejection and have no problem of ethical issues [40]. This experiment employs animal-derived BMSCs. The artificial culture bone used in this study is Osferion (Olympus Terumo Biomaterials Corp.) as shown in Fig. 2-1 [41]. The dimension of the culture bone is a 10mm cube. Osferion is a macroporous ceramic with 75% porosities based on β -TCP (beta-tricalcium phosphate). Fig. 2-2 shows the porosity of Osferion. Average pore size is 100-400 μm in diameter. These culture bones are sterilized in a dry heater at 180 degree for 4 hours. This study uses the BMSCs in accordance with Japanese Government guidelines for the care and use of laboratory animals, and obtains the cells by the bone marrow of 15-week-old Sprague-Dawley rats. The average diameter of BMSCs is about 40 μm .



Fig. 2 - 1 Artificial Culture Bone.

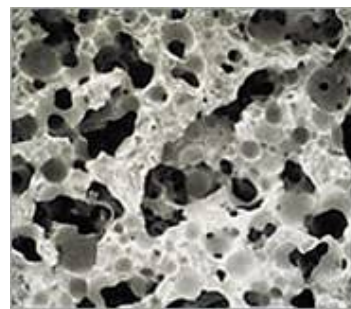


Fig. 2 - 2 Porosity of *Osferion*.

BMSCs are not able to grow in the atmosphere, and the raw artificial culture bone contains air because of macroporosity. Therefore, it is performed a preprocessing for raw artificial culture bone. Preprocessing includes degassing process for the artificial culture bone, and soaked the artificial culture bone in culture medium as shown in Fig. 2-3, and decrease pressure to remove air from this culture bone as shown in Fig. 2-4. Degassed culture bone is filled by medium and facilitates the penetration of BMSCs into this bone. Additionally, this process increases the intensity of the transparent wave because the acoustic wave transmits into liquid like medium faster than gas.

It is seeded BMSCs in the degassed bone, where the seeded BMSCs have 4 kinds of cell quantity: 1.0×10^6 , 1.5×10^6 , 2.0×10^6 , 1.0×10^7 [cells/ml]. This study employs 24 artificial culture bones, and takes four of each kind. Ref. [42] and [43] describe that mesenchymal stem cells cultured in vitro can differentiate into osteoblast cells immediately. Thus, it is cultivated all seeded culture bone for 24 hours.

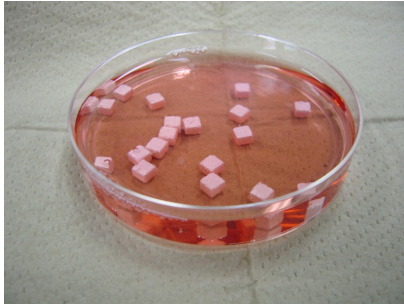


Fig. 2 - 3 Soak Artificial Culture Bone

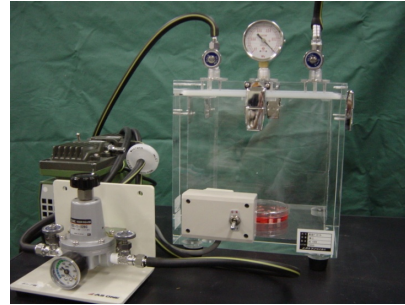


Fig. 2 - 4 Decrease Pressure

In the case of including BMSCs or not in soaked artificial culture bone, it is measured the velocity of sound for culture medium. The velocity of sound for artificial culture bone with BMSCs is 2324.61 [m/s], and the one without BMSCs is 2094.34 [m/s]. As this result, the velocity of sound for artificial culture bone with BMSCs is lower than the one without BMSCs. Therefore, it is said that the ultrasonic wave transmits into artificial culture bone.

The Sound travels through materials under the influence of sound pressure. The acoustic impedance is important in the determination of acoustic transmission at the materials having different acoustic impedances. The higher the product of its density is, the higher the transmitted signal intensity appears. Therefore, this study focused on the transmitted signal. From the obtained ultrasonic data, it is extracted the feature: frequency.

2.2.2 Ultrasonic Device

This estimation system consists of an ultrasound caliper probe, a pulsar receiver, an oscilloscope and a personal computer as shown in Fig. 2-5. This experiment uses the ultrasound caliper probe (NSI Corp.) as an ultrasound device as shown in Fig. 2-6.

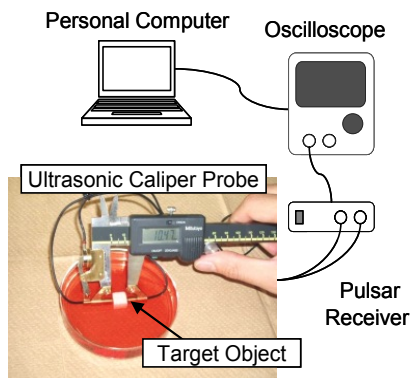


Fig. 2 - 5 Ultrasound Estimation System

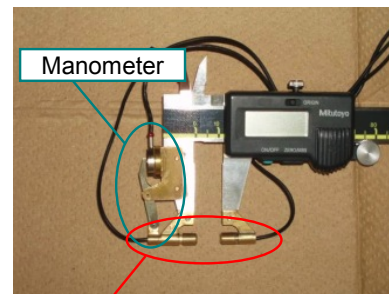


Fig. 2 - 6 Ultrasound Caliper Probe

The transmitting probe and receiving probe are attached to the portions of outside jaws of the

electronic caliper, respectively. This caliper probe transmits the ultrasound wave while holding a target object. At this time, the caliper probe holds the object with constant pressure by using a manometer, which is a component of the caliper probe. The center frequency of the probes is 1.0 MHz. Figure 2-7 shows a frequency spectrum of the ultrasound acquired by connecting the probes directly. Sampling interval of oscilloscope is 5 ns. The ultrasound wave is transmitted into the culture bone from three directions for three times each (nine in total) as shown in Fig. 2-8. From the obtained wave, it is extracted two characteristics; the amplitude and the frequency, which are the average characteristics acquired from nine waves. This study was based on other 5 experiments. In detail, the differences for the experimental condition are block size and cultivating time. Because these results have the even quality of artificial culture bone, the experimental values consists high reproducibility.

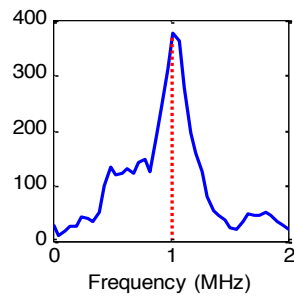


Fig. 2 - 7 Frequency Spectrum of Ultrasound Wave

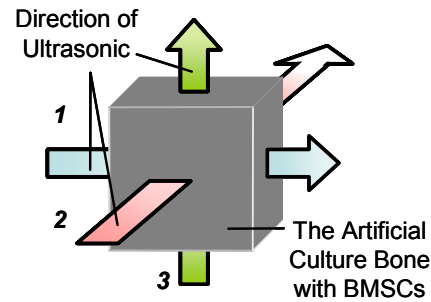


Fig. 2 - 8 Direction of Ultrasound Wave

2.3. Experimental Measurement

2.3.1 Ultrasonic Measurement

The conventional method shows that the ultrasound amplitude effectively responded to the quantity composites and was well correlated to the actual cell value number. This study focuses on the attenuation due to viscosity, which is proportional to the squares of the frequency [44]. This paper proposed the ultrasonic estimation method by using two features, amplitude and frequency.

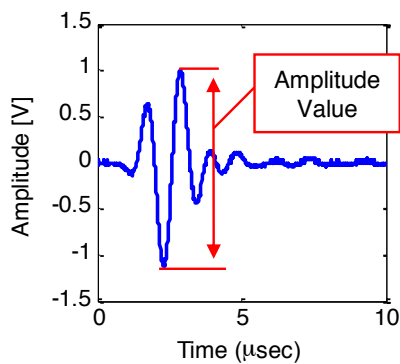


Fig. 2 - 9 Extraction of Amplitude

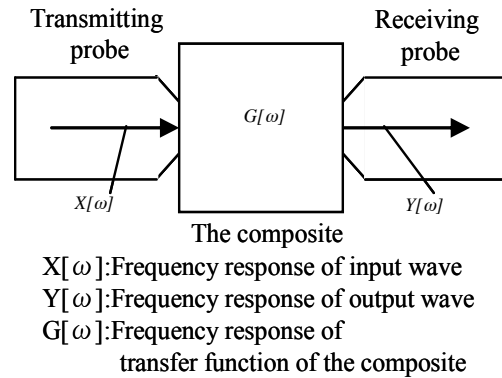


Fig. 2 - 10 Transfer Function Model

The first characteristic, the amplitude is the value of peak to peak in the obtained wave as shown in

Fig. 2-9. The ultrasound amplitude through homogeneous material is larger than the one through heterogeneous material, because of effects such as scattering and reflection, which can cause attenuation of ultrasound amplitude occur at the boundaries of the heterogeneous material. The second characteristic is obtained by applying the techniques; transfer function using Cross-Spectrum of the received waves. In Eq. 2-1 and Fig. 2-10, $G[\omega]$ denotes transfer function, $X[\omega]$ and $Y[\omega]$ denote frequency response of input and output respectively, $\bar{X}[\omega]$ denotes conjugate of $X[\omega]$. The transfer function using Cross-Spectrum is calculated by Eq. 2-1.

$$|G[\omega]| = |\bar{X}[\omega]Y[\omega]| / |X[\omega]\bar{X}[\omega]|. \quad (2-1)$$

An example of transfer function $G[\omega]$ is shown in Fig. 2-11. The frequency, ω_g , is defined as the frequency with the center of gravity (COG) on $G[\omega]$. The frequency is calculated as the average of ω_g of the obtained nine waves of artificial culture bone.

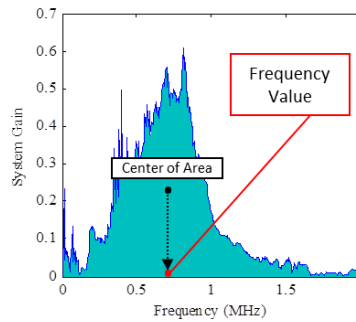


Fig. 2 - 11 Frequency Value using COG

2.3.2 Scanning Electron Microscopy Observation

After ultrasonic measurement, the cell proliferation was observed by scanning electron microscopy (SEM) for defining cell quantity. SEM obtains the true values of cell quantity. The image of the artificial culture bone is obtained by an electron microscope of 800 magnifications. Therefore, the truth cell quantity is obtained by multiplying 800. The cell value of cell quantity ranged from 145^(×800) to 836^(×800) cells/ml.

2.3.3 Relationship between Features

This section shows the relationship between three features: amplitude, frequency, and cell quantity, respectively. As shown in Fig. 2-12, the correlation coefficient of amplitude and cell quantity is 0.750 and one of frequency and cell quantity is 0.766. The frequency has a higher correlation coefficient to cell quantity than the amplitude. Therefore, this study estimates cell quantity by using two features, amplitude and frequency.

On the image obtained by an electron microscope of the artificial culture bone, there are 800 blocks. This experiment measured amount of cells in one block by the electron microscope. Therefore, the true cell quantity is obtained by multiplying 800, and ranged from 145^(×800) to 836^(×800) cells/ml. The cell quantity ranges from 0 to 1,000^(×800) cells/ml. For evaluation of the proposed methods, this system employs three ranks (“Low” / “Middle” / “High”) based on the measured cellular quantity as shown in Table 2-1.

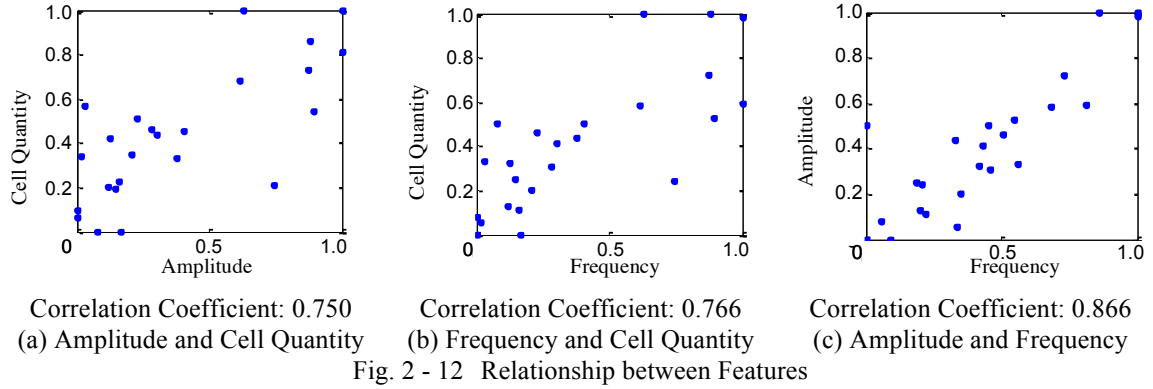


Table 2 - 1. CELL QUANTITY RANK TABLE

Cell Quantity [cells/ml] ^{.800 *1}	Rank	Count
$0 \leq \text{Cell} < 333$	Low	9
$333 \leq \text{Cell} < 666$	Middle	10
$666 \leq \text{Cell}$	High	5

*1 measured one block in 800 blocks with the artificial culture bone

2.4. Cell Quantity Estimation

2.4.1 Fuzzy Inference

This study proposes a fuzzy estimation system with the amplitude and frequency features. These features have high correlation coefficients with cell quantity, and obtain the following Knowledge 1 and 2.

Knowledge 1: An artificial culture bone with large cell quantity has high amplitude.

Knowledge 2: An artificial culture bone with large cell quantity has high frequency.

It is converted Knowledge 1 and 2 to the following fuzzy if-then rules. The notations X_{amp} and X_{freq} denote amplitude and frequency for composite X . The notation Y_{cells} denotes cell number variable.

Rule 1-1: If X_{amp} is Low, then Y_{cells} is Low.

Rule 1-2: If X_{amp} is Middle, then Y_{cells} is Middle.

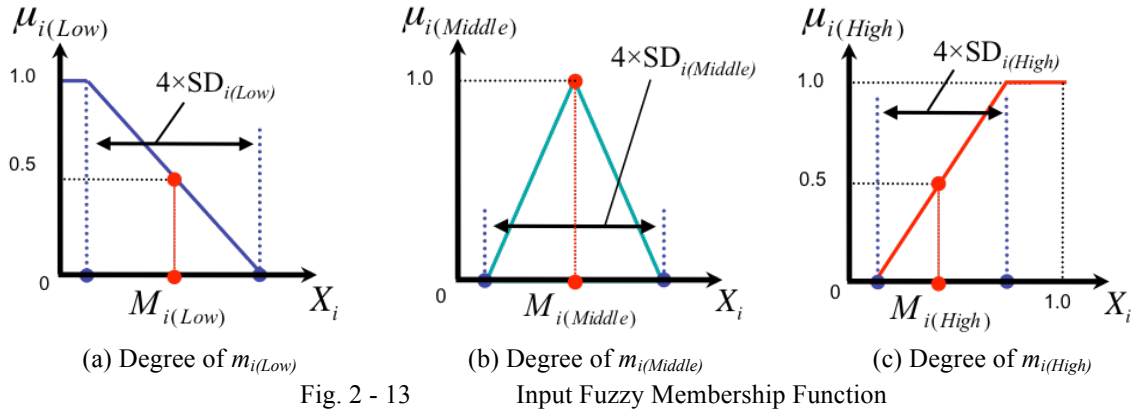
Rule 1-3: If X_{amp} is High, then Y_{cells} is High.

Rule 2-1: If X_{freq} is Low, then Y_{cells} is Low.

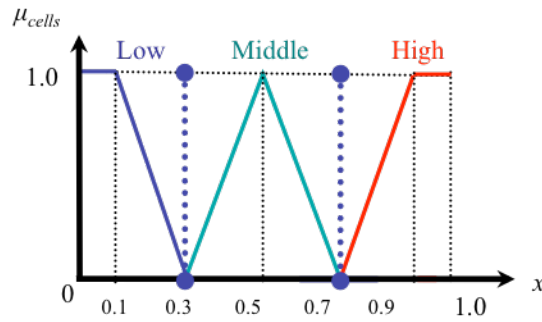
Rule 2-2: If X_{freq} is Middle, then Y_{cells} is Middle.

Rule 2-3: If X_{freq} is High, then Y_{cells} is High.

As shown in Fig. 2-13, these features are normalized between 0 and 1. Two features have high correlation coefficient with cell quantity. The input fuzzy membership functions are defined by the means and the standard deviations (SD) of amplitude and frequency in a group data for evaluating the other group. Two evaluation methods are employed. The first one is leave-one-out cross-validation. The second one divides 24 samples into two groups; each of them consists of 12 samples. One group is used for the parameter optimization and the other is used for the evaluation.



The notation $SD_{i(Low, Middle, High)}$ ($i=amp, freq, cells$) denotes the standard deviation of each class for each feature. The notation $M_{i(Low, Middle, High)}$ ($i=amp, freq, cells$) denotes the average of each class for each feature. The membership functions of “Low” and “High” are trapezoidal function aligned by standard deviation and the average of the data set: the width of oblique is $4 \times SD_{i(Low, High)}$, the midpoint of the oblique is $M_{i(Low, High)}$. The membership function of “Middle” is triangular function, the length of bottom of isosceles triangle is $SD_{i(Middle)}$, the middle point of this bottom is $M_{i(Middle)}$.



The results for applying the other width and bottom of $3 \times SD_{i(Low, Middle, High)}$ or $5 \times SD_{i(Low, Middle, High)}$ thereby obtained the similar results as $4 \times SD_{i(Low, Middle, High)}$. A fuzzy singleton function $S_{X_i}(X)$ is defined as following Eq. 2-2. The width and function's shapes in membership function with the experimental decided the results. The notations \wedge and \vee denotes fuzzy minimum and maximum operations, respectively. The output fuzzy membership function is defined as Fig. 2-14.

$$S_{X_i}(X) = \begin{cases} 1 & \text{if } X = X_i \\ 0 & \text{otherwise} \end{cases} \quad (2-2)$$

In the case of Low and High, it was employed the trapezoidal functions, which are the popular shapes of fuzzy membership functions. All function's shapes and widths in membership function were decided with the experimental results. The fuzzy inference is done in the min-max center-of-gravity method. The inference mechanism is shown in Fig. 2-15. This figure shows the fuzzy degrees $m_{(amp, freq)}(Low, Middle, High)$. The equations 2-3, 2-4, and 2-5 calculate the degrees, w_{Low} , w_{Middle} and w_{High} .

$$w_{Low} = \mu_{amp_Low}(X_{amp}) \wedge \mu_{freq_Low}(X_{freq}). \quad (2-3)$$

$$w_{Middle} = \mu_{amp_Middle}(X_{amp}) \wedge \mu_{freq_Middle}(X_{freq}). \quad (2-4)$$

$$w_{High} = \mu_{amp_High}(X_{amp}) \wedge \mu_{freq_High}(X_{freq}). \quad (2-5)$$

Equation 2-6 obtains the inference result.

$$\begin{aligned} M_t(X_{cell}) &= (w_{Low} \wedge M_{t_Low}(X_{cells})) \\ &\vee (w_{Middle} \wedge M_{t_Middle}(X_{cells})) \\ &\vee (w_{High} \wedge M_{t_High}(X_{cells})) \end{aligned} \quad (2-6)$$

The center of gravity, \hat{X}_{cells} , is calculated by Eq. 2-7.

$$\hat{X}_{cells} = \frac{\int M_t(X_{cells}) X_{cells} dX_{cells}}{\int M_t(X_{cells}) dX_{cells}}. \quad (2-7)$$

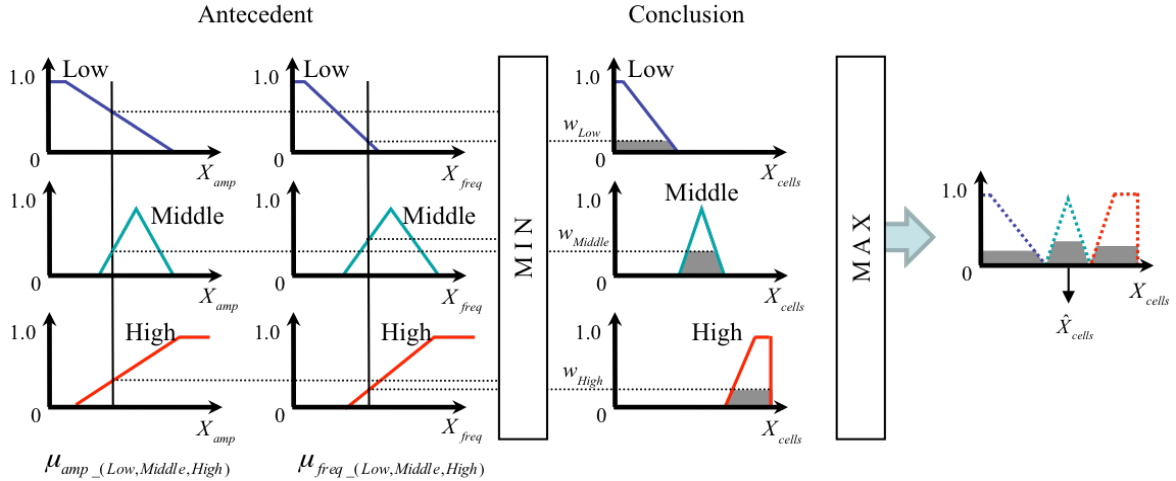


Fig. 2 - 15 Fuzzy MIN-MAX center of gravity methods

2.4.2 Neural Network

This study develops a neural network system as shown in Fig. 2-16. The Back Propagation (BP) learning is one of the typical models of neural networks. The neural network is composed of an input layer, a hidden layer and an output layer. For the input layer, $x_{i,p}$ ($i=1,2\dots l$) denote the input data. For each units in the hidden layer, $y_{j,p}$ ($j=1,2\dots m$) denote the output data. For each units in the output layer, $z_{k,p}$ ($k=1,2\dots n$) denote the output data. u_{ij} denote the weights between the input layer and the hidden layer. v_{jk} denote the weights between the hidden layer and the output layer.

In this experiment, there are 2 neurons in the input layer which are two features; amplitude value and frequency value, 10 neurons in the hidden layer, 23 neurons in the output layer. The parameter “ i ” denotes the number of the input layer: 2. The parameter “ j ” denotes the number of the hidden layer: 10. The parameter “ k ” denotes the number of the output layer: 23. The parameter “ p ” denotes the pattern number: 24. The total sum, $X_{j,p}$, of the input data for each units in the hidden layer in the neural network is defined by Eq. 2-8. The output data of the hidden layer is defined by Eq. 2-9.

$$X_{j,p} = \sum_i u_{ij} x_{i,p} \cdot \quad (2-8)$$

$$y_{j,p} = f(X_{j,p}) = \frac{1}{1 + \exp(-X_{j,p})} \quad (2-9)$$

The total sum, $Y_{k,p}$, of the input data for each units in the output layer in the neural network is defined by Eq. 2-10. The output data of the output layer is defined by Eq. 2-11.

$$Y_{k,p} = \sum_j u_{jk} y_{j,p} \cdot \quad (2-10)$$

$$z_{k,p} = f(Y_{k,p}) = \frac{1}{1 + \exp(-Y_{k,p})} \cdot \quad (2-11)$$

Accordingly, the error, $E_{k,p}$, of each output units is defined by Eq. 2-12. The goal of learning is to set weights between all layers of the neural network to minimize the total error $E_{k,p}$.

$$E_{k,p} = \frac{1}{2} (\hat{z}_{k,p} - z_{k,p})^2. \quad (2-12)$$

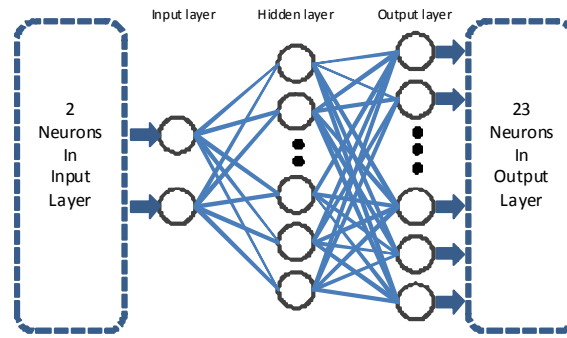


Fig. 2 - 16 Neural Network

In order to minimize this error, the weights u_{ij} and v_{jk} are adjusted. All the feature values are normalized, and fed into the neural network. This system employs 24 patterns and Leave-One-Out (LOO) Cross Validation. LOO makes a model with the remains excluded one sample. This constructed model applies the excluded sample. LOO performs this process for all samples. After 5,000 times of training the neural network of teaching patterns, the output of each neuron will approximate to one of the teaching patterns.

2.4.3 Multiple Linear Regression Model

The general purpose of multiple-linear regression is to learn more about the relationship between several independent or predictive variables and a dependent or criterion variable. Multiple-linear regression is a linear method to build a model constructed with relationship among multiple independent variables, X_i ($i=1,2,\dots,n$) and a dependent variable, Y . In this study, the linear model in Eq. 2-8 calculates the predictive variable Y_{cells} . The regression coefficients b_j ($j=0, 1, 2$) are defined so as to involve the minimum of the notation Q . In Eq. 2-9, the notation Q denotes the error sum of squares between Y_{cells} and \hat{Y}_{cells} . Here, b_0 , b_1 , and b_2 are 0.403, 0.538, and -0.006, respectively.

$$Y_{cells} = \beta_0 + \beta_1 X_{amp} + \beta_2 X_{freq}. \quad (2-8)$$

$$Q = \sum_{i=1}^{24} (Y_{cells} - \hat{Y}_{cells})^2. \quad (2-9)$$

The regression coefficients are calculated by solution to normal equation 2-10. The notation $S_{i,j}$ ($i,j=amp, freq, cells$) is variation covariation matrix. The notations, \bar{Y}_{cells} , \bar{X}_{amp} , and \bar{X}_{freq} , denote averages of the characteristics.

$$\begin{cases} \beta_1 S_{amp,amp} + \beta_2 S_{amp,freq} = S_{amp,cells} \\ \beta_1 S_{freq,amp} + \beta_2 S_{freq,freq} = S_{freq,cells} \\ \beta_0 = \bar{Y}_{cells} - \beta_1 \bar{X}_{amp} - \beta_2 \bar{X}_{freq} \end{cases} \quad (2-10)$$

Table 2 - 2. CELL QUANTITY ESTIMATION RESULTS

Cell No.	Amplitude X_{amp}	Frequency X_{freq}	True Quantity (cells/ml)	Estimated Quantity (cells/ml) \times 800			True Rank	Estimated Rank		
				Neural Network	Fuzzy Inference	Multiple Regression		Neural Network	Fuzzy Inference	Multiple Regression
1	1.128	0.678	215	199	266.7	227.5	Low	Low	Low	Low
2	0.856	0.661	145	185	181.6	157.0	Low	Low	Low	Low
3	1.248	0.687	240	185	304.1	262.0	Low	Low	Low	Low
4	0.994	0.671	199	271	220.3	192.9	Low	Low	Low	Low
5	0.968	0.672	185	440	212.6	193.4	Low	Mid	Low	Low
6	0.758	0.704	171	481	271.9	319.6	Low	Mid	Low	Low
7	1.819	0.746	481	470	447.8	448.9	Mid	Mid	Mid	Mid
8	1.532	0.723	439	488	378.3	364.5	Mid	Mid	Mid	Mid
9	1.105	0.698	271	171	266.6	265.1	Low	Low	Low	Low
10	1.672	0.748	440	514	413.0	440.6	Mid	Mid	Mid	Mid
11	0.958	0.683	195	185	210.3	215.6	Low	Low	Low	Low
12	1.237	0.704	281	185	317.0	294.8	Low	Low	Low	Low
13	1.674	0.735	680	836	796.4	845.1	High	High	High	High
14	1.229	0.678	430	418	627.7	604.7	Mid	Mid	Mid	Mid
15	0.716	0.656	418	439	463.8	445.9	Mid	Mid	Mid	Mid
16	0.864	0.670	728	836	466.5	486.3	High	High	Mid	Mid
17	1.210	0.695	792	728	656.0	617.4	High	High	Mid	Mid
18	1.084	0.677	470	440	609.0	562.9	Mid	Mid	Mid	Mid
19	0.996	0.654	426	488	547.7	495.8	Mid	Mid	Mid	Mid
20	1.350	0.699	676	680	691.1	659.8	High	High	High	Mid
21	0.656	0.650	488	514	463.8	404.1	Mid	Mid	Mid	Mid
22	1.481	0.700	836	728	707.9	656.5	High	High	High	Mid
23	1.096	0.685	544	470	625.1	581.7	Mid	Mid	Mid	Mid
24	1.173	0.689	514	440	651.0	607.8	Mid	Mid	Mid	Mid
R				0.869	0.874	0.869	-	-	-	-
Mean \pm SD ^{*1}				76.1 \pm 74.6	78.4 \pm 65.0	71.5 \pm 71.4	-	-	-	-
Accuracy (%)				-	-	-	-	91.67	91.67	83.33

2.5. Estimation Results

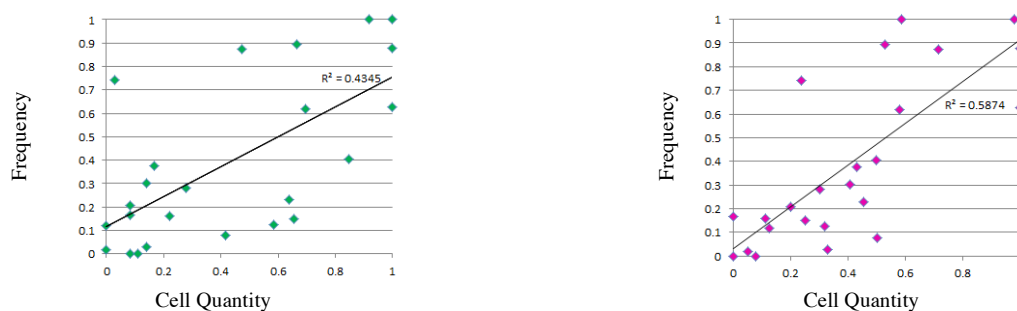
In order to identify the exact cell number in the artificial culture bones, it is applied the 24 bones to three methods: neural network, fuzzy inference and multiple linear regression, and employed Leave-One-Out Cross validation. The result is shown in Table 2-2. The notation “R” indicates the correlation coefficient between true cell quantities and estimated quantities. The notation “Mean \pm SD” is a quantity used to measure how close forecasts or predictions are to the eventual outcomes. From this table, the multiple regression system determines cell number with lower Mean Absolute Error in comparison with the neural network and fuzzy inference method. These results show that the better methods for identifying cell number of artificial culture bone the fuzzy inference and multi regression.

On the other hand, it is important to choose composites containing appropriate number of cells before implanting them to patients in clinical setting. Therefore, it should be estimated rough quantity of the artificial culture bone. For evaluation of the proposed methods, this study employed three ranks (“Low” / “Middle” / “High”) based on the measured cellular quantity. In Table 2-2, “True Rank” is the true value obtained by an electron microscope, and “Rank” shows the identified ranks. The “Accuracy” means success rate of how well the method correctly identifies the rank. From this table, neural network and fuzzy inference identified the rank of cellular quantity with higher accuracy with comparison to multiple regression.

2.6. Discussion on Frequency Feature

This section discussed on frequency feature. When obtaining the frequency values, it was applied two techniques, the frequency response $Y[\omega]$ of output wave and the transfer function $G[\omega]$ obtained by Cross-Spectrum. The results are shown in Fig. 2-17. These figures show the relation of the normalized data of frequency and cell quantity. The correlation coefficient of frequency and cell quantity using $Y[\omega]$ is 0.659 ($R^2=0.435$) in Fig. 2-17(a) and the correlation coefficient of frequency and cell quantity using $G[\omega]$ is 0.766 ($R^2=0.587$) in Fig. 2-17(b).

When the coefficient of determination (R^2) is more than 0.50, two data are considered highly correlated. Cross-Spectrum is superior to analyze the frequency of the Bone Marrow Stromal Cells/ β -tricalcium phosphate. Therefore, this study applied Cross-Spectrum for frequency.



(a) Frequency response of output wave, $Y[\omega]$ (b) Transfer function obtained by Cross-Spectrum, $G[\omega]$

Fig. 2 - 17 Correlation Coefficient of Frequency and Cell Quantity

In order to demonstrate the attenuation of frequency, this study proposes two approaches using ultrasonic cell quantity determination on the frequency domain: the peak (PEAK) and the center of

gravity (COG) on $G[\omega]$. For defining as cell quantity, the cell proliferation was evaluated by scanning electron microscopy (SEM) observation. The frequency values were defined with peak and center of gravity as shown in Fig. 2-18. The center frequency of the ultrasound is 1.0 MHz, thus the frequency response in more than 2.0 MHz is no longer. Therefore, the center of gravity is calculated from 0 to 2.0 MHz. This study focuses on the attenuation due to viscosity, which is proportional to the squares of the frequency [35], and has a discussion about the attenuation of frequency. According to this law attenuation of sound α is proportional to the dynamic viscosity η , square of the sound frequency ω , and reciprocally proportional to the fluid density ρ and cubic power of sound speed V :

$$\alpha = \frac{2 \eta \omega^2}{3 \rho V^3}. \quad (2-11)$$

This experiment employs the ultrasonic waves with the center frequency of 1.0 MHz. As given Eq. 2-11, the attenuation is proportional to the squares of the frequency. Therefore, the frequency range of approximate 1.0 MHz value attenuates. As the results, COG frequencies were absolutely found less than peak frequencies on all composites. Correlation coefficient between cell quantity and peak frequency is 0.672 (coefficient of determination is 0.452), and correlation coefficient between cell quantity and COG frequency is 0.766 (coefficient of determination is 0.587). COG is considered highly correlated, because coefficient of determination is more than 0.50.

The frequency features were obtained by 24 composites. Because the number of them is small, it is some problems for the validity of this analysis. The future studies are applying to more samples.

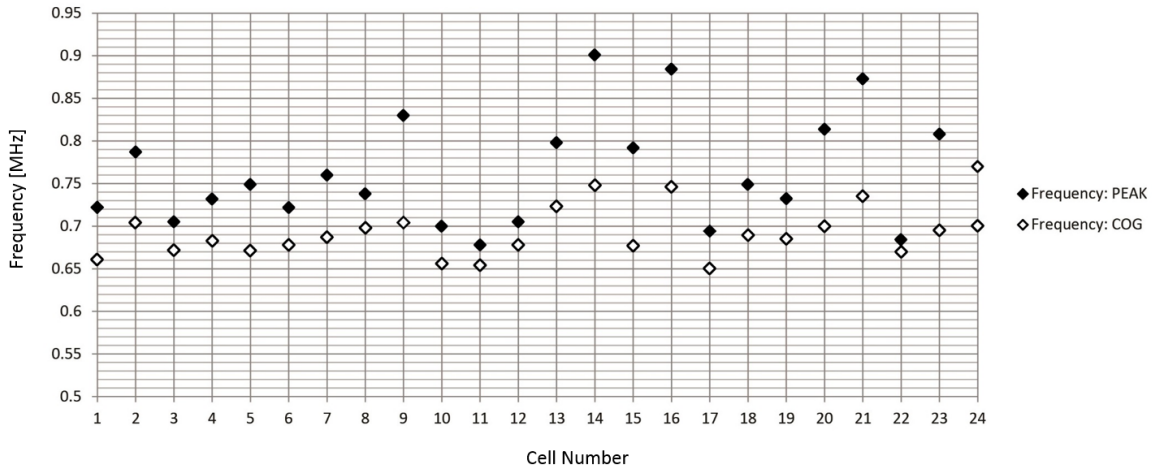


Fig. 2 - 18 PEAK and COG

2.7. Conclusion

This chapter proposed an ultrasonic method that can estimate the cell quantity using the ultrasound caliper probes, which are a transmitting probe and a receiving one. These probes have appropriate center frequency 1.0 MHz for passing through human bone.

It was introduced this estimation method by proposing the ultrasound estimation system, and acquired two features, “Amplitude” and “Frequency”, from the ultrasonic waves. Based on the relation between two features and cell quantity, it is constructed three approaches, “Multiple

Regression”, “Neural Network”, and “Fuzzy Inference”. Multiple-regression model has the possibility of multicollinearity. Multicollinearity is the case that a regression analysis overestimates the effect of one parameter, and underestimates the effect of the other. The variance inflation factor (VIF) is the metric widely used in the investigations of multicollinearity. *VIF* of regression models is 3.999 which is lower than 10, thus this model is free of multicollinearity. In conclusion, the fuzzy inference approach determines cell quantity with the highest correlation coefficient. On the other hand, the neural network and fuzzy inference systems identified the rank of cellular quantity with highest accuracy. These systems enable to choose composites that contain favorable number of cells before implantation. This fact demonstrates that soft computing approaches are valuable for identifying cell quantity in the artificial culture bones by using two features obtained by the ultrasonic waves. On the frequency domain, this study confirmed the attenuation in the immediate vicinity of 1.0 MHz, which is the center frequency of the probe. Moreover, to demonstrate this attenuation, it was proposed two approaches using ultrasonic cell quantity determination on the frequency domain: the peak and the COG. For defining as cell quantity, the cell proliferation was evaluated by SEM observation. As the results, COG frequencies were absolutely found less than peak frequencies on all composites. This study showed the ability of intervention to produce the desired effect, and certified the superiority of the frequency data analysis. Moreover, it was established the validity for measuring the cell quantity in BMSCs by using the feature of frequency with Cross-Spectrum focusing on the attenuation.

The number of samples is small, so this study divided them into three ranks (Low, Middle, High) with respect to cell quantity. Therefore, it is some problems for the validity of the estimation results. It remains as the future studies to apply this system and evaluate in detail to more samples.

Chapter 3

Stem Determination System for Total Hip Arthroplasty

This chapter describes a fuzzy system of stem implantation on Total Hip Arthroplasty by an ultrasonic device. The system can perform automatic and accurate assessment in the surgery. This system employs a single ultrasonic probe whose center frequency is 1,000Hz, and detects the acoustic signals when knocking the inserted stem with a hammer. It has a correlation between the degree of tightening and the attenuation time of acoustic signal. That is, the higher tightened degree implies shorter attenuation period. The support system selects the most suitable stem size by fuzzy inference with respect to the attenuation time and its difference time from correct stem to one larger size stem, which dynamically adapts to each patient. As the results, this study successfully determined the suitable stem in comparison to the results of the practical surgery.

3.1 Introduction

Total Hip Arthroplasty (THA), which is surgical replacement of the hip joint with an artificial prosthesis, is a reconstructive procedure that has improved the management of those diseases of the hip joint that have responded poorly to conventional medical therapy. It is an orthopedic procedure that involves the surgical excision of the head and proximal neck of the femur and removal of the acetabular cartilage and subchondral bone. This joint replacement consists in replacing a damaged joint with prosthesis. In the orthopedic surgery, the arthritic or dysfunctional joint surface is replaced with an orthopaedic prosthesis [45]. THA rebuilds the damaged hip joint with some implants and is operated to treat the hip joint diseases such as osteoarthritis. The THA implants mainly consist of cup, liner, head and stem, which play a role of acetabulum, hip cartilage, head of femur, and femur, respectively. The principal complication after THA is dislocation [46]. The primal mechanisms of dislocation are impingement of the femoral neck on the cup liner, impingement of the femur on the pelvis, and spontaneous dislocation due to excessive external force against muscular force. For example, a hip joint that is affected by osteoarthritis may be replaced entirely with a prosthetic hip. This would involve replacing both the acetabulum, hip socket, and the head and neck of the femur. The purpose of this procedure is to relieve pain, to restore range of motion and to improve walking ability, thus leading to the improvement of muscle strength.

A joint replacement surgery is becoming a more common practice [47], [48]. The prosthetic implant used in hip replacement consists of different parts, the acetabular cup, the femoral component and the articular interface. The femoral component is the component that fits in the femur. The use of cementless femoral implants for total hip arthroplasty has increased in popularity over the last few decades [49]. Numerous implant designs based on different views concerning implant fixation are currently available. Bone is removed and the femur is shaped to accept the femoral stem with attached prosthetic femoral head or ball. Options exist for different patients and indications. Correct selection of the prosthesis is important [50], [51]. The selection of the optimum size and type of implant to fit the anatomical characteristics of the individual patient is important in order to avoid postoperative complications such as dislocation or loosening [52]-[54]. Regardless of implant design, primary stability of the cementless femoral implants in the femoral canal must be achieved at the time of operation and is really important for osseointegration, long-term fixation

and clinical success [55]-[57].

The surgeon experience in choosing the stem size to be implanted is fundamental to achieve good fixation. However, especially in the complicated cases, it still has the risk that the stem size chosen might be unsuitable. To solve the problems, it is described the mechanical stability at the time of implantation. It is difficult to predict the precise size of the implant during the preoperative plan especially when the stem implantation is planned. Thus, this system estimates the level of stability by analyzing ultrasonic wave measurements. In order to perform more quantitative measurement and more reasonable assessment based on Reference [58], [59], this paper proposes a fuzzy system of more reasonable assessment for the stem implantation on Total Hip Arthroplasty by an ultrasonic device. In the surgery, the size of the implanted stem is decided to the surgeon after adapting to the patient from the small size stem to the larger size one in turn. It depends on the surgeon skill, and do not have a quantitative decision measures. Therefore, it is proposed a system, which can perform automatic and accurate assessment in the surgery. It is valuable for both surgeons and patients. This system employs a single ultrasonic probe whose center frequency is 1,000Hz, and detects the acoustic signals when knocking the inserted stem with a hammer. It has a correlation between the degree of tightening and the attenuation time of acoustic signal. That is, the higher tightened degree implies shorter attenuation period. The stem determination support system selects the most suitable stem by fuzzy inference, which dynamically adapts for each patient. As the results, it was successfully determined the suitable stem in comparison to the results of the practical surgery. Consequently, this study indicated the indexes in order to judge how degree the stem fits in the clinical treatment for Total Hip Arthroplasty, and indicated how to select the most suitable stem for the patients by using the ultrasonic system. The fuzzy inference which dynamically adapts for each patient solved some problems of the individual difference. As the results, this system selected the suitable stem with higher accuracy.

3.2. Total Hip Arthroplasty

Hip fractures occur as a result of major or minor trauma. In elderly patients with bones weakened by osteoporosis, relatively little trauma, even walking, may result in a hip fracture. The hip is made of a ball and a socket joint, linking the dome at the head of the femur and the cup in the pelvic bone as shown in Fig. 3-1. A total hip prosthesis is surgically implanted to replace the damaged bone within the hip joint. Then a metal ball and a metal stem are inserted in the femur and a plastic socket is placed in the enlarged pelvis cup. The artificial components are fixed in place. The muscles and tendons are then replaced against the bones and the incision is closed. Each patient has each various bone in the hip. So, the surgeon has to find the most suitable stem for the patient while operating. In the present situation, there are some differences of selecting the suitable stem. Therefore, this system proposes the determination system of selecting the suitable stem for the patient.

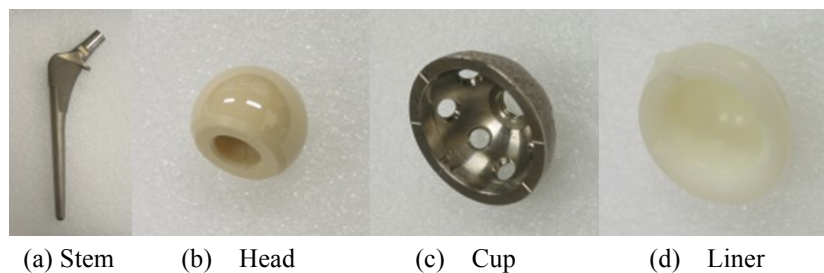


Fig. 3 - 1. Parts for Total Hip Arthroplasty

3.3. Preliminary Experiment

This experiment performed a preliminary experiment to analyze the degree of tightening the stem clinically measured, and confirmed a correlation between the degree of tightening and the attenuation time of acoustic signal. Fig. 3-2 shows the preliminary experiment system. The vise fixes the stem and a buffer material is a 20mm thick sponge. This system compared the difference of degree when the stem is loose and tight fixing. Fig. 3-3 shows some sizes of stems, which the stem number is in proportion to the stem size.

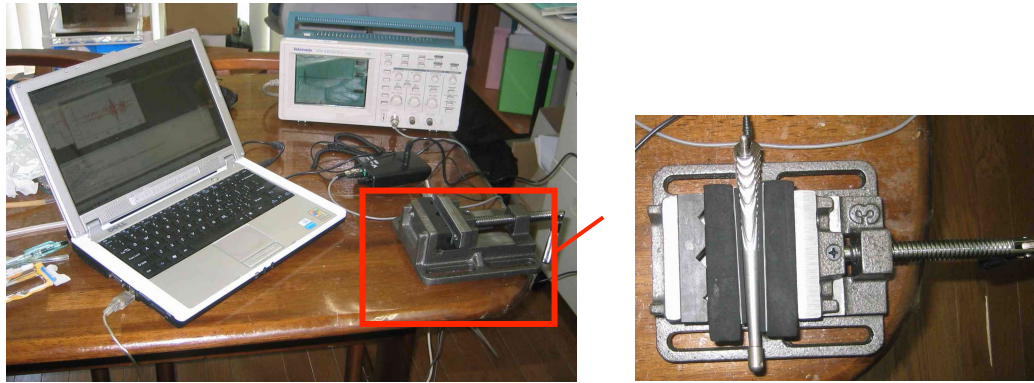


Fig. 3 - 2. Preliminary Experiment System



Fig. 3 - 3. Stem

As shown in Fig. 3-4, the higher tightened degree implies shorter attenuation period. Therefore, the tightened degree controls the attenuation time of amplitude. This experiment uses three sizes of stems with #6, #8, and #10. By using a pressure perception film, this system quantifies the fixed pressures with 60N, 80N, and 100N as shown in Fig. 3-5.

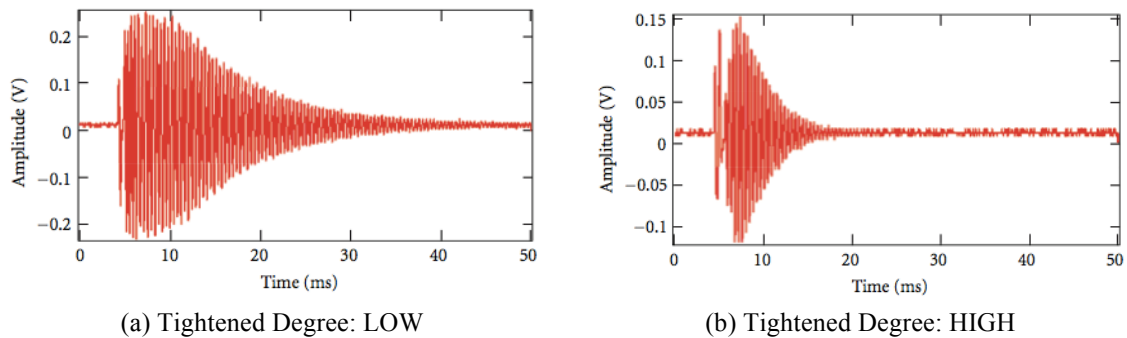


Fig. 3 - 4. Attenuation Time (STEM #8)

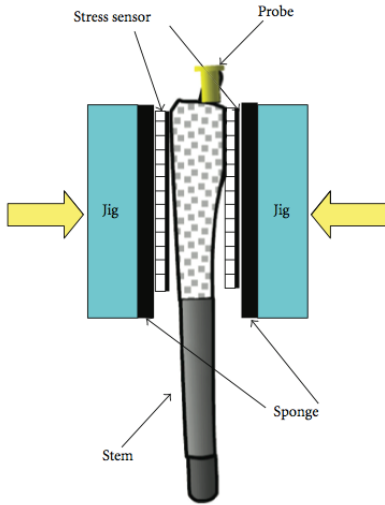


Fig. 3 - 5. Pressure Testing

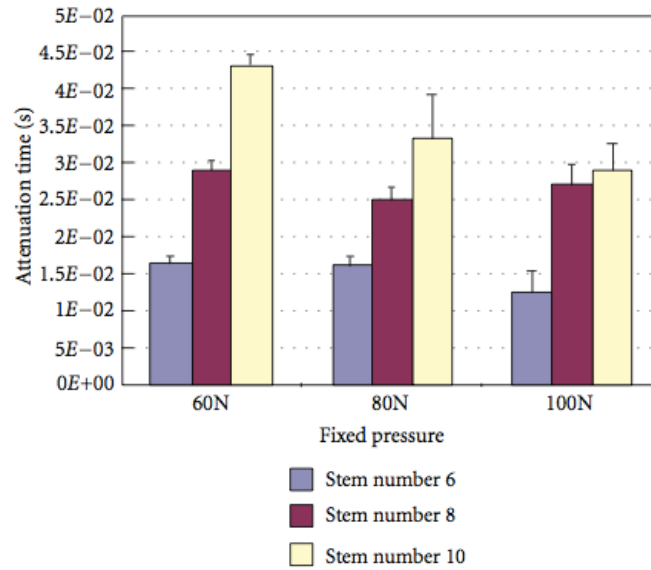


Fig. 3 - 6. Relationship between Attenuation Time and Pressure

As the results, the changes of attenuation time in each stem are shown in Fig. 3-6. This figure shows that the attenuation time of STEM #6 (light blue bar) and STEM #10 (light yellow bar) becomes to shorten as the fixed pressure is stronger from 60N to 100N. As for STEM #8, the attenuation time shorten only when changing fixed pressure from 60N to 80N. In the case of the same fixed pressure, the attenuation time tends to be longer as the stem size is larger. In the surgery, the surgeon tries to adapt for the patient from the small size stem to the larger size stem in turn. In clinical practice, the decrease of the attenuation time as the stem size being larger means that the fixed pressure of the stem becomes to strengthen. Consequently, the stem adapts better for the patient.

3.4. Measurement System

This system employs a single ultrasonic probe whose center frequency is 1,000Hz. The acquired ultrasonic waveform is analyzed by a personal computer.

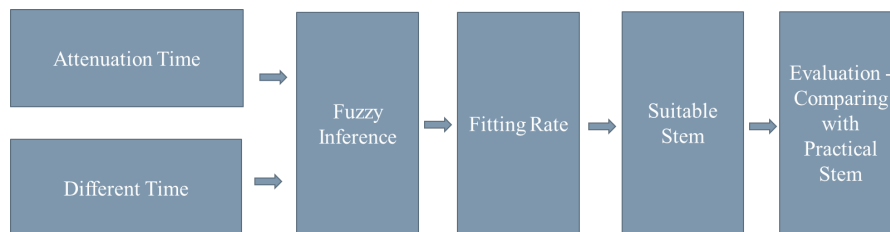


Fig. 3 - 7. Framework of this system

Figure 3-7 shows the framework of this measurement system. The obtained data, attenuation time and different time, are used in fuzzy inference. After calculating the fitting rate, this system selects the suitable stem. By comparing it and the practical stem, it is evaluated the results.

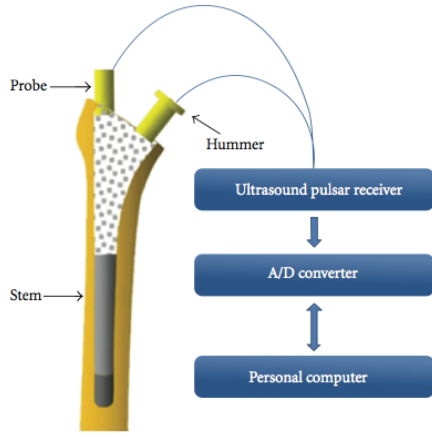


Fig. 3 - 8. Measurement System

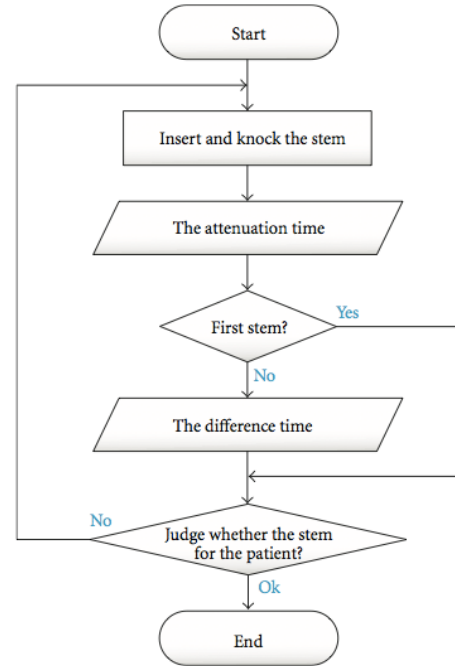


Fig. 3 - 9. Flowchart

At first, this experiment made a knock to the upper point of the stem inserted with a hammer, which is used as the trigger signal as shown in Fig. 3-8. By using the knocking signals, it is measured the acoustic signals. The microphone for measuring (10mmΦ) is fixed in the upper side of the stem with a built-in magnet. The acoustic data is changed to the digital data by the AD converter (Picoscope ADC-212/100), and is sent to the personal computer. In the clinical treatment, an index to judge how degree the stem fits for the patient is the knocked sound by a hammer when inserting the stem. The surgeon recognizes that the dull knocked sound means the loose fixed. From the physical opinion, in the case of loose fixing, the attenuation time of amplitude is long because the acoustic energy continues to transmit into the stem. On the other side, in the case of tight fixing, the attenuation time of amplitude is short because the acoustic energy transmits from the stem to the external fixed object and is absorbed on the early stage.

The flowchart of this system is shown in Fig. 3-9. In the surgery, the surgeons adapt the patient from the small size stem to the larger size one in turn. This system obtains the attenuation time when inserting the smallest stem, and the attenuation time and calculate the different time by using the attenuation time of the first inserted stem and one of the second inserted stems. The fuzzy inference judges whether the inserted stem is most suitable or not so.

3.5 Attenuation Time

The raw wave in Fig. 3-10 performed envelope processing to the positive area of the acoustic wave as shown in Fig. 3-11. It is defined that X as stem size (STEM # X) and the maximum of the attenuation value as $A_{\max}(X)$ and the time at that time as $T_{\max}(X)$. $A_{10}(X)$ is defined as $A_{\max}(X) / 10$, and the time $T_{10}(X)$ at the value $A_{10}(X)$.

The attenuation time $T_{\text{ATT}}(X)$ of STEM # X is calculated by Eq. 3-1. This system estimates the degree of fixing by using this attenuation time.

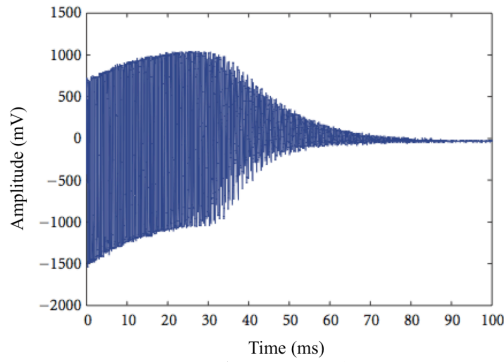


Fig. 3 - 10. Raw Data of Acoustic Wave

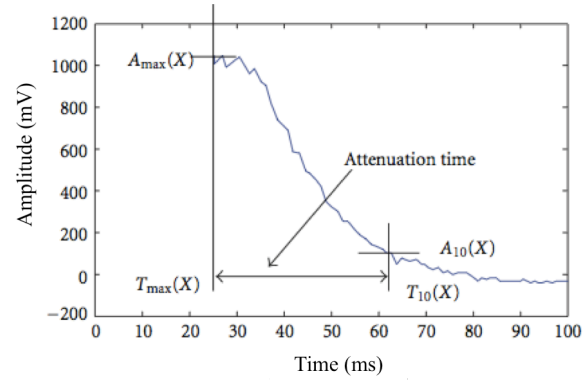


Fig. 3 - 11. Attenuation Time

$$T_{ATT}(X) = T_{10}(X) - T_{max}(X). \quad (3-1)$$

The attenuation times of STEM #4 and #6 are shown in Fig. 3-12. The $A_{max}(4)$ and $A_{max}(6)$ are of the same values. As shown in this figure, the notation $T_{ATT}(4)$ is shorter than the notation $T_{ATT}(6)$. This result means that STEM #4 is fixed tighter than STEM #6.

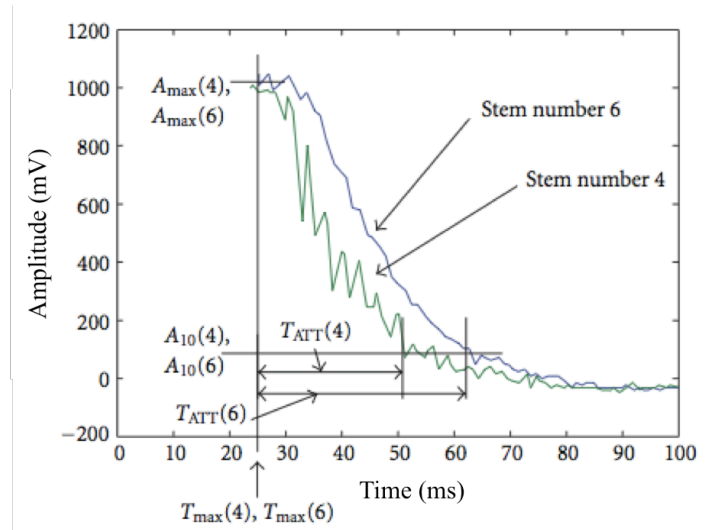


Fig. 3 - 12. Attenuation Time of STEM #4 and #6

3.6. Fuzzy Inference

This system proposes a fuzzy evaluation system with two features, the attenuation time $T_{ATT}(X)$ and difference time for STEM #X. The difference time $T_{DIF}(X)$ is calculated by Eq. 3-2.

$$T_{DIF}(X) = T_{ATT}(X) - T_{ATT}(X-1). \quad (3-2)$$

The difference time defines as the time between the attenuation time of the stem and that of the one size smaller stem. From the obtained coefficients, Knowledge 1, 2, 3, and 4 are derived.

Knowledge 1: The tight fixing has the short attenuation time.

Knowledge 2: The tight fixing has the short difference time.

Knowledge 3: The attenuation time depends on the fixed degree.

Knowledge 4: The difference time depends on the fixed degree.

These are converted to the following fuzzy if-then rules.

Rule 1: IF *Attenuation time* is *Short* THEN the degree of fixing is *High*.

Rule 2: IF *Difference time* is *Short* THEN the degree of fixing is *High*.

The fuzzy if-then rules are represented by the fuzzy membership functions as shown in Fig. 3-13. In this figure, the notations, Th_a and Th_d , denote thresholds of the attenuation time and difference time, respectively.

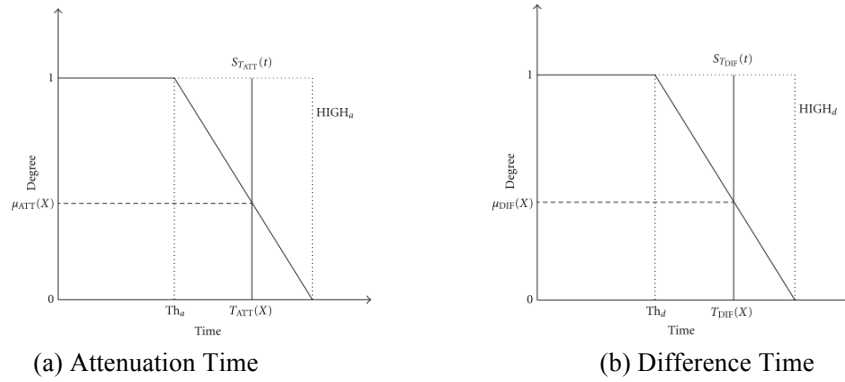


Fig. 3 - 13. Fuzzy Membership Function Fuzzy Membership Function

The input fuzzy membership functions are defined by the means and the standard deviations (SD) of the attenuation time and the difference time, respectively. The notation Th_a is determined as the time which is the standard deviation being shorter than the mean of the attenuation time. The notation Th_d is determined as the time which is the standard deviation being shorter than the mean of the difference time. Two fuzzy degrees, μ_{att} and μ_{diff} , are calculated by Eq. 3-3 and 3-4.

$$\mu_{ATT}(X) = \min(S_{T_{ATT}}(t), HIGH_a). \quad (3-3)$$

$$\mu_{DIF}(X) = \min(S_{T_{DIF}}(t), HIGH_d). \quad (3-4)$$

The fuzzy singleton functions, $S_{T_{ATT}}(t)$ and $S_{T_{DIF}}(t)$, are defined by Eq. 3-5 and 3-6.

$$S_{T_{ATT}}(t) = \begin{cases} 1 & \text{if } t = T_{ATT}(X) \\ 0 & \text{otherwise} \end{cases}. \quad (3-5)$$

$$S_{T_{DIF}}(t) = \begin{cases} 1 & \text{if } t = T_{DIF}(X) \\ 0 & \text{otherwise} \end{cases}. \quad (3-6)$$

Equation 3-7 calculates the fix degree $\mu_{FIX}(x)$ of STEM #X.

$$S_{T_{ATT}}(t) = \begin{cases} 1 & \text{if } t = T_{ATT}(X) \\ 0 & \text{otherwise} \end{cases}. \quad (3-7)$$

Where the notation, r , is the ratio, it is experimentally decided.

3.7. Experimental Results

Under consideration of the thresholds on Table 3-1 and 3-2, the threshold of the attenuation time, Th_a , is more adaptable than that of the difference time, Th_d . Therefore, it is calculated the adaptable ratio ($r=0.823$) and put the adaptable ratio to the fuzzy membership functions. The total degree $\mu_{FLX}(x)$ is calculated by Eq. 3-8.

$$\mu_{FLX}(X) = \mu_{ATT}(X) \times 0.823 + \mu_{DIF}(X) \times (1 - 0.823). \quad (3-8)$$

Table 3 - 1. THRESHOLD OF FUZZY MEMBERSHIP FUNCTION (ATTENUATION TIME)

Th_a	Subject number 1	Subject number 2	Subject number 3	Subject number 4	Subject number 5	Subject number 6	Subject number 7	Subject number 8
Stem number 4	30.61	—	—	—	28.44	27.50	30.94	27.50
Stem number 5	23.22	—	23.19	—	25.48	24.58	28.42	23.19
Stem number 6	18.91	—	18.53	18.60	21.88	20.51	22.59	19.13
Stem number 7	18.91	20.13	19.41	20.52	—	20.64	23.04	19.82
Stem number 8	14.75	17.42	17.30	15.74	—	16.39	16.65	—
Stem number 9	18.51	20.79	—	—	—	19.72	—	—
Stem number 10	—	—	—	—	—	—	—	—

Table 3 - 2. THRESHOLD OF FUZZY MEMBERSHIP FUNCTION (DIFFERNT TIME)

Th_d	Subject number 1	Subject number 2	Subject number 3	Subject number 4	Subject number 5	Subject number 6	Subject number 7	Subject number 8
Stem number 4	—	—	—	—	—	—	—	—
Stem number 5	2.21	—	—	—	2.17	2.15	2.01	6.04
Stem number 6	4.73	—	2.95	—	2.93	3.00	3.80	2.95
Stem number 7	-1.73	—	-2.09	-0.38	—	-0.27	-0.62	-1.27
Stem number 8	-0.41	-0.08	-0.13	0.73	—	0.19	2.69	—
Stem number 9	-2.57	-2.45	—	—	—	5.28	—	—
Stem number 10	—	—	—	—	—	—	—	—

This proposed system applied to 8 total hip arthroplasty patients. The result of the fixed stem size and the analyzed stem size was shown in Table 3-3. The attenuation time measured in the practical surgery is showed in Fig. 3-14. In this figure, the horizontal-axis means the size of the stem and the vertical-axis means the attenuation time.

Table 3 - 3. RESULT OF STEM SIZE

	Determined size	Used size
Subject number 1	9 or 10	10
Subject number 2	N/A	9
Subject number 3	8	8
Subject number 4	8	8
Subject number 5	5 or 6	6
Subject number 6	9	9
Subject number 7	7 or 8	8
Subject number 8	7	7

By using this proposed method, it was selected the suitable stem of 7 patients. As concerns Subject #1 and #7, two sizes of the determined stem were selected. Because these subjects have the fixed stem which is one size larger than the stem with the shortest attenuation time, it is left out of

consideration that the determined stem has two types which are the fixed size stem and the one size smaller stem. As concerns Subject #2 and #5, it was not selected the suitable stem because the difference time is relatively large as shown in Fig. 3-14. As the results, the effectiveness of selecting the suitable stem was 87.5%.

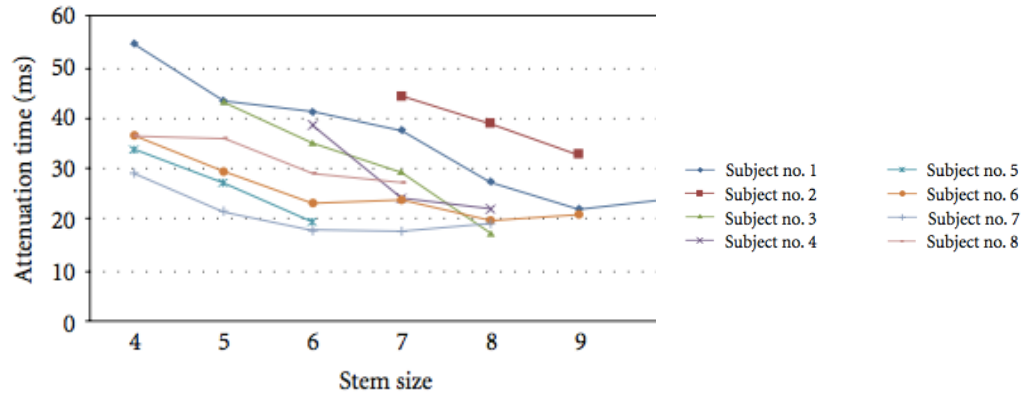


Fig. 3 - 14. Selected Stem Size in Practical Surgery

3.8. Conclusion

This chapter proposed a stem determination system for total hip arthroplasty patients. The acquired ultrasonic waveform with the single ultrasonic probe with the center frequency 1,000Hz is analyzed by a personal computer. At first, this system made a knock to the upper point of the stem inserted with a hammer, which has the trigger signals. By using the knocking signals, it was measured the acoustic signals. The ultrasonic probe for measuring is fixed in the upper side of the stem with a built-in magnet. The acoustic data is changed to the digital data by the AD converter and is sent to the personal computer. In the surgery, the surgeon tries to adapt for the patient from the small size stem to the larger size stem in turn. Therefore, this system, which selects the best suitable stem by using the attenuation time, is valuable for surgeons and patients of total hip arthroplasty.

As the results, this study successfully determined the suitable stem in comparison to the results obtained from the practical surgery. It became an index in order to judge how degree the stem fits in the clinical treatment for Total Hip Arthroplasty. It remains as future works to consider the much better effective method and to apply the method to total hip arthroplasty patients.

Chapter 4

Diagnosis System for Human Brain Imaging

This paper describes ultrasonic diagnosis system for human brain imaging. The research goal is the portable and real time brain diagnosis under the thick-skull. The choice of ultrasonic frequency is a trade-off between spatial image resolution and imaging depth. This study shows the usability of data synthesis by employing two different frequency ultrasounds. In this chapter, the first section proposes the trans-skull ultrasonic doppler system, whose target is blood flow, and the second section proposes the trans-skull brain imaging system. This approach is particular interest for the design of further study intending to visualize any defects by ultrasound methods. The last section designs the mobile medical system to review data prior to patient access. Improved communication can also ease the process for patients, clinicians, and caregivers. As one of the implementations for smart medical system, the ultrasonic diagnosis and mobile communication system are proposed. In summary, this chapter indicates that the ultrasonic image is useful to visualize the imitated brain area. This observation is encouraging for further studies of evaluating brain in patients.

4.1 Trans-skull Ultrasonic Doppler System

4.1.1 Introduction

The cerebrovascular accident is one of the worst diseases for Japanese. Recently, about one and half million patients had cerebrovascular accident of a year and, 10% of them cause death in Japan [60]. The cause of cerebrovascular accident is lack of the oxygen by a blood vessel being clogged up, an obstruction of the blood vessel by the blood clot. If having the cerebrovascular accident, it is needed prompt treatment. It is important to use tissue plasminogen activator (t-PA) that helps to dissolve blood clots. The t-PA time limit is about 3 hours. It is needed the quick search of blood clot.

The imaging of the human brain is essential to diagnose the brain. Magnetic Resonance Imaging (MRI) and X-ray Computed Tomography (CT) are widely used for the brain disease diagnosis. These systems can obtain the detailed image of the brain. However, they need at least 20 minutes for imaging and it is high cost for patients. Therefore, a noninvasive and real-time diagnosis system is needed. An ultrasonic system has several advantages such as low cost, bedside usage and dynamic imaging and so on. As the noninvasive system, the ultrasonic devices are widely used. In clinical practice, the ultrasonic devices with the center frequency of 2-10 MHz are used to visualize internal organs in the human body [61]. However, the ultrasound attenuates by the reasons of absorption and dispersion when the ultrasound transmits and receives the object. In particular, it is difficult to receive the echo passing through the bone. However, it is known that the low frequency ultrasound approximately 1.0 MHz can transmit and receive the bone tissue. Therefore, the study intended the bone is performed with the low frequency ultrasound. The transcranial sonography has been proposed using two linear array probes, which consists of 128 elements. However, it is difficult to transmit ultrasound from any position because the two array probes are set up on both sides of human brain. In References [62], [63], the imaging system of the skull and brain surface has been proposed using a single ultrasonic probe whose center frequency is 1.0 MHz. In this system, a target object is scanned with 1.0 mm scanning interval using a 3-D

scanner. It is difficult to apply it to clinical practice because this scanner is too large to perform in clinical practice. A simple and unrestrained system without the large mechanical scanner is needed. Transcranial Doppler (TCD) is used for brain diagnosis. TCD is a technique for measuring the blood flow by placing an ultrasonic probe at the anterior and superior attachment site of the upper ear (posterior temporal windows) in adults [64], [65]. However, TCD frequently cannot obtain enough data for thick skull width of the adults, because ultrasonic waves cannot transmit/receive the blood flow data by the large attenuation from the skull bone. A few studies were done for free-placement systems [66], [67]. The transcranial sonography has been proposed using 2.5 MHz 2D array probes. However, it is difficult to transmit ultrasound from the random position.

This study proposes a free-placement trans-skull Doppler imaging system with a 1.0 MHz array ultrasonic probe. This study extended the works in [68], [69]. The experimental results showed that the system detected the flow velocity by Doppler effect, and it confirmed the useful method.

4.1.2 Experimental Devices

This section shows the experimental devices about the 1.0 MHz ultrasonic array probe as shown in Fig. 4-1, the target object, and the water flow pump.



Ultrasound transducer size: 24 mm×1.5 mm×32 mm
External size: 30 mm×60 mm×40 mm

Fig. 4 - 1. 1.0 MHz (ISL1938) Ultrasonic Array Probe.

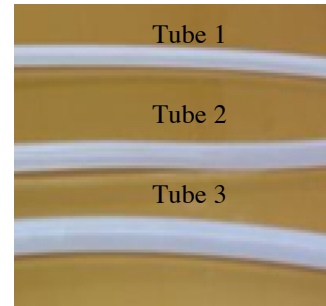


Fig. 4 - 2. Silicon Tubes.

4.1.2.1 Target Object

This experiment imitated the blood vessel under the skull. The inside and outside diameter of the silicon tubes are shown in Table 4-1. In this experiment, it is employed three silicon tubes shown in Fig. 4-2.

Table. 4 - 1. Colored Pixels.

	Inside Diameter	Outside Diameter	Thickness
Tube 1	4.0 mm	5.5 mm	1.5 mm
Tube 2	5.0 mm	7.5 mm	2.5 mm
Tube 3	6.0 mm	9.0 mm	3.0 mm

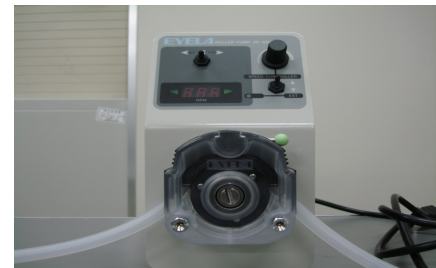


Fig. 4 - 3. Water Flow Pump.

4.1.2.2 Water Flow Pump

This experiment employs a fixed quantity water flow pump (Tokyo Rikakikai Co., LTD. RP-10000) in Fig. 4-3. This system changes the direction of water stream by changing the rotation direction of a roller, and sets turning speed of a roller with 300 or 400 rpm, and the current speed in the tube for about 50 or 70 cm/s. This speed is almost equivalent to the speed of the cerebrum artery in the human brain, 50-70 cm/s.

4.1.3 Proposed Method

Fig. 4-4 shows the experimental system. The system is composed of array ultrasonic probe, two water tanks, ultrasonic flow detection equipment and a personal computer. The ultrasonic data are provided to a personal computer through an ultrasonic array probe. The sampling interval of A/D converter is 3 MHz. The ultrasonic pulse repetition frequency (PRF) is 50 Hz. These are the equipment specification.

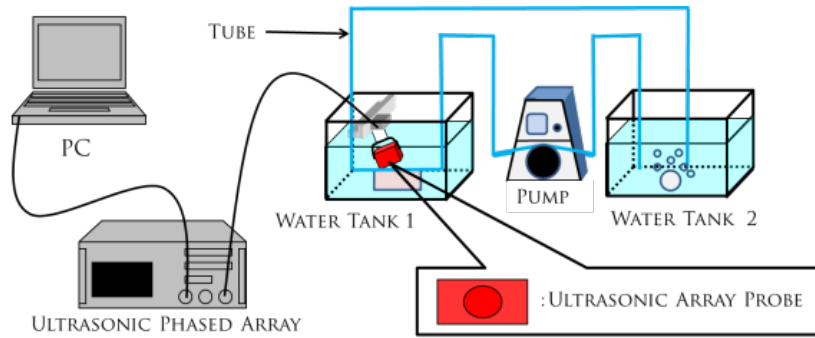


Fig. 4 - 4. Experimental System.

4.1.3.1 Data Acquisition System

The notation θ is the angle between an ultrasonic array probe and the water current, which is fixed at 45 degree as shown in Fig. 4-5. The water including bubble is imitated as Levovist, which is ultrasonic contrast agent. The scapula of cow is employed as a skull in Fig. 4-6, the pork meat is employed instead of skin to cover skull in Fig. 4-7. The thickness of the scapula is 0.16-0.27 mm.

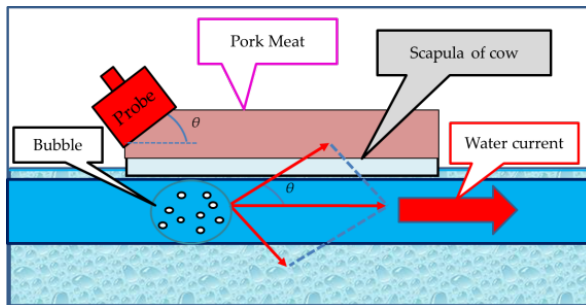


Fig. 4 - 5. Data Acquisition System.

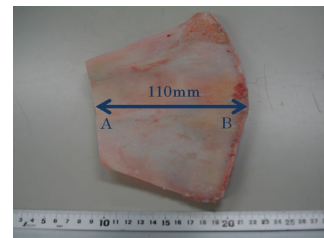


Fig. 4 - 6. Cow Scapula.

Figure 4-8 shows the procedure of this method. Firstly, this system acquires the waveforms from the probes, and divides the waveform data in order to remove the overlap. In this study, the

waveform data consists of $32 \text{ channels} \times 3,500 \text{ pixels}$. It is divided every 3,500 pixels to 64 pixel set data by shifting 32 pixels, sequentially, and applied FFT to the divided waveform data for confirming Doppler effect. Lastly, the study calculates the center of gravity (COG) in frequency domain, and compares COG of the acquired data and the standard frequency. The standard frequency was determined as the mean of COGs of three ultrasonic waveforms from silicon tubes with no water current. It is calculated the degree of frequency transition by Doppler effect, and made imaging of Doppler effect from the calculated data based on the fuzzy inference.



Fig. 4 - 7. Pork Meat.

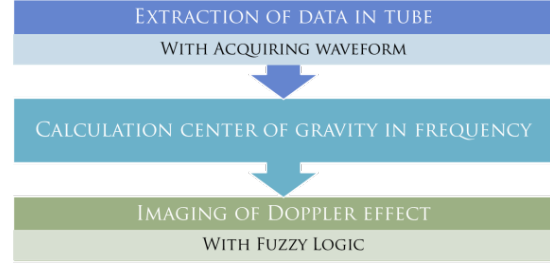


Fig. 4 - 8. Procedure of this method.

4.1.4 Doppler Effect and COG in Frequency Domain

The notation f denotes the frequency. The notations P , f_{\max} , and f_{\min} denote the power spectrum density, the max frequency ($=2.0 \text{ MHz}$), and the minimum frequency, respectively. The center of gravity (COG) in frequency domain, f_g , is calculated by Eq. 4-1.

$$f_g = \left(\sum_{f=f_{\min}}^{f_{\max}} P(f) \times f \right) / \sum_{f=f_{\min}}^{f_{\max}} P(f). \quad (4-1)$$

Figure 4-9 shows the frequency transitions, which is the distribution map in frequency domain. The blue and red lines show no water current and water current, respectively. The green line means the peak in frequency, which is same frequency value in the case of no water current and water current. However, the power spectrum density of the low frequency becomes lower, and that of the high frequency becomes higher. Thus, the COG in the frequency domain is calculated.

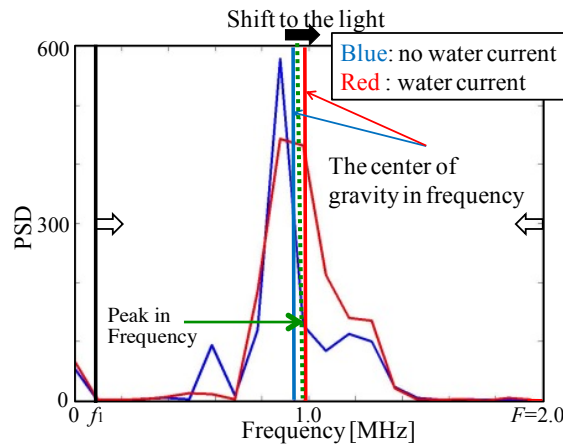
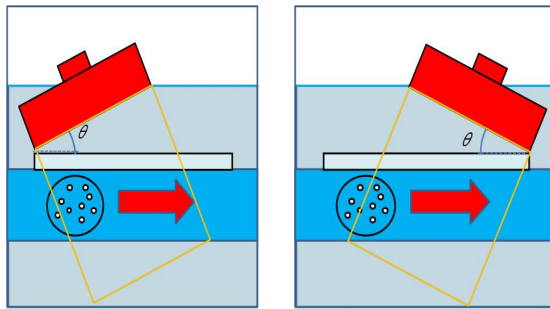


Fig. 4 - 9. Frequency Transitions.

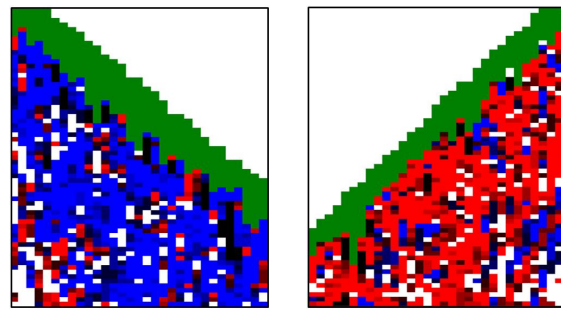
The COG shifted clearly to higher frequency direction when compared with the peak. This study focuses on the law attenuation due to viscosity, which is proportional to the squares of the frequency [44], and has a discussion about the attenuation of frequency. According to this law attenuation of sound α is proportional to the dynamic viscosity η , square of the sound frequency ω , and reciprocally proportional to the fluid density ρ and cubic power of sound speed V :

$$\alpha = \frac{2 \eta \omega^2}{3 \rho V^3}. \quad (4-2)$$

This experiment employs the ultrasonic waves with the center frequency of 1.0 MHz. As given Eq. 4-2, the attenuation is proportional to the squares of the frequency. The frequency range of approximate 1.0 MHz value attenuates. This study suggests that this attenuation causes that the peak becomes lower than the COG, and the frequency of the COG can be considered highly correlated. Therefore, the COG of the spectrum is employed for measuring the flow direction. The standard frequency was determined as the mean of COGs of three ultrasonic waveforms from silicon tubes with no water current. The standard frequency was 0.980 MHz. Fig. 4-10 (a), (b) show the water current measurement.



(a) Going Away (b) Approaching
Fig. 4 - 10. Water Current Measurement.



(a) Going Away (b) Approaching
Fig. 4 - 11. Extracted Images.

As the results, the images are simply extracted the bone and water current in order to confirm the frequency shift as shown in Fig. 4-11. This experiment confirmed the water current directions under the bone. The green pixels mean the bone; the blue pixels mean water current going away, and the red pixels mean water current approaching. The black pixels mean the unidentified object, and the white pixels mean others. In addition, the Doppler frequency was given in Table 4-2. The standard frequency was 0.980 MHz. When the water current direction is going away, the frequency shift has negative values. On the other hand, when the water current direction is approaching, the frequency shift has positive values. This system perfectly confirmed the Doppler effect under the bone, and the frequency shift by using three kinds of tubes and the water current speed, respectively.

Table. 4 - 2. Doppler Frequency.

Going Away [MHz]					Approaching [MHz]				
Tube	50.0 cm/s		70.0 cm/s		Tube	50.0 cm/s		70.0 cm/s	
	Mean \pm SD	Shift	Mean \pm SD	Shift		Mean \pm SD	Shift	Mean \pm SD	Shift
1	0.958 \pm 0.006	-0.022	0.950 \pm 0.002	-0.030	1	1.003 \pm 0.004	0.023	1.012 \pm 0.002	0.032
2	0.953 \pm 0.002	-0.028	0.946 \pm 0.002	-0.035	2	1.003 \pm 0.004	0.022	1.013 \pm 0.003	0.033
3	0.951 \pm 0.003	-0.029	0.946 \pm 0.004	-0.034	3	1.004 \pm 0.003	0.024	1.015 \pm 0.002	0.035

4.1.5 Evaluation System

This system proposes the fuzzy evaluation system with the amplitude, and obtains the knowledge as follows.

- Knowledge 1:* The moving object has flow direction of Doppler Effect.
Knowledge 2: The amplitude of boundary echo is large.
Knowledge 3: The maximum amplitude of object echo does not change in the condition.

The waveform data consists of $32 \text{ channels} \times 3,500 \text{ pixels}$, and divides 3,500 pixels to 64 pixel set by shifting 32 pixels, sequentially. Then, it is obtained total 109×64 pixel set data. This pixel set data is denoted by the notation x . The notation $f_d(x)$ denotes the frequency after Doppler shift in each 64 pixel set data. The notations $A_o(x)$ and $A_d(x)$ denote the maximum amplitude, and the difference between the current amplitude data and the previous one. The acoustic impedance of bone is the highest in this experiment, and the most of ultrasonic power is reflected there. The silicon tube is the second highest. This study introduces the attenuation coefficient in order to enhance the signal level. The notations x_1 and x_2 denote the number of times passed bone and silicon tube, respectively. The notations α_1 and α_2 denote the attenuation coefficient of bone and silicon tube, which are determined as 0.40 and 0.95. All the parameters are determined by the preliminary experimental results. The notation $A(x)$ denotes maximum amplitude with the attenuation coefficient by Eq. 4-3.

$$A(x) = \alpha_1^{-x_1} \times \alpha_2^{-x_2} \times A_o(x) . \quad (4-3)$$

The notations $\mu_{flow}(x)$, $\mu_{boundary}(x)$, and $\mu_{object}(x)$ denote the fuzzy degree of water current vector, one of boundary point, and one of object point, respectively. They mean the fuzzy degrees of $f_d(x)$, $A(x)$, and $A_d(x)$, respectively. The notations f_l , f_c , and f_n denote the mean of the COGs obtained by water current going away from the probe, the mean of COGs obtained by water current approaching to the probe, and the COG by noise in 64 pixel set data, respectively. The notations A_w , A_b , A_t , and A_s denote the maximum amplitude of the water, the water bubble, the silicon tube, and the scapula of cow, respectively. The following fuzzy IF-THEN rules are derived from them and represented by three fuzzy membership functions.

- Rule 1:* IF $f_d(x)$ is close to one of f_l, f_c and f_n , THEN $\mu_{flow}(x)$ is high.
Rule 2: IF $A_d(x)$ is high, THEN $\mu_{boundary}(x)$ is high.
Rule 3: $A(x)$ is close to one of A_w, A_b, A_t , and A_s , THEN $\mu_{object}(x)$ is high.

Figure 4-12 shows the fuzzy membership function for the flow direction, which is defended by Eq. 4-4, 4-5, 4-6. The f_l , f_c , and f_n are determined as 0.030, 0.028, and 0.010. All the parameters are determined by the preliminary experimental results.

$$\mu_l(f_d(x)) = \min(LEAVE, S_{f_d}(f_d(x))) . \quad (4-4)$$

$$\mu_c(f_d(x)) = \min(COME, S_{f_d}(f_d(x))) . \quad (4-5)$$

$$\mu_n(f_d(x)) = \min(NOT, S_{f_d}(f_d(x))) . \quad (4-6)$$

Equation 4-7 defines the fuzzy degree for flow direction.

$$\mu_{flow}(x) = \mu_l(f_d(x)) + \mu_c(f_d(x)) + \mu_n(f_d(x)) . \quad (4-7)$$

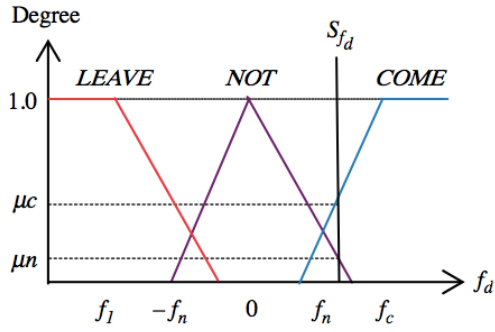


Fig. 4 - 12. Membership Functions
- Flow Direction -.

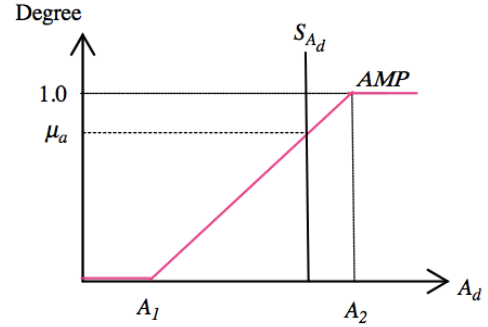


Fig. 4 - 13. Membership Functions
- Difference of Amplitude -.

Figure 4-13 shows the fuzzy membership function for the difference of amplitude, which is defined by Eq. 4-7. The notations A_1 and A_2 denote the difference of the amplitude value among water area and that between bone and water in 64 pixel set data, respectively. The A_1 and A_2 are experimentally determined as 40 and 100. All the parameters are determined by the preliminary experimental results. Equation 4-8 defines the fuzzy degree for the boundary point.

$$\mu_{boundary}(x) = \alpha_1^{-x_1} \times \alpha_2^{-x_2} \times \mu_a(A_d(x)) \quad (4-8)$$

Figure 4-14 shows the fuzzy membership function for the amplitude, which is defined by Eq. 4-9, 4-10, 4-11, and 4-12. The A_w , A_b , A_t , and A_s are determined as 30, 70, 100, and 180, respectively. All the parameters are determined by the preliminary experimental results.

$$\mu_w(A(x)) = \min(WATER, S_A(A(x))) \quad (4-9)$$

$$\mu_b(A(x)) = \min(BUBBLE, S_A(A(x))) \quad (4-10)$$

$$\mu_t(A(x)) = \min(TUBE, S_A(A(x))) \quad (4-11)$$

$$\mu_s(A(x)) = \min(SCAPULA, S_A(A(x))) \quad (4-12)$$

Equation 4-13 defines the fuzzy degree for the amplitude.

$$\mu_{object}(A) = \mu_w(A(x)) + \mu_b(A(x)) + \mu_t(A(x)) + \mu_s(A(x)) \quad (4-13)$$

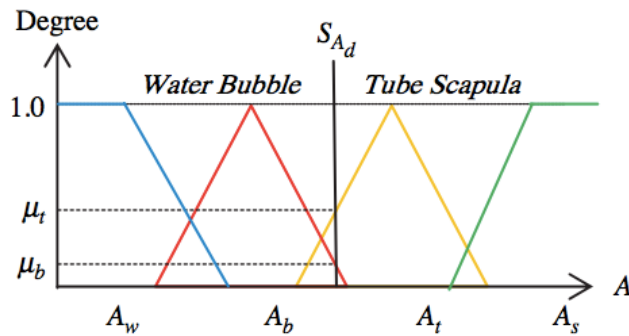


Fig. 4 - 14. Membership Functions - Amplitude -.

4.1.6 Experimental Results

This study applied the proposed method to the brain model with the scapula of cow and silicon tubes. The standard frequency was determined as the mean of COGs of three ultrasonic waveforms from three silicon tubes with no water current. The standard frequency was determined as the mean of COGs of three ultrasonic waveforms from silicon tubes with no water current. The standard frequency was 0.980 MHz. With employing water current, it is acquired the ultrasonic waves by 32 elements of the ultrasonic array probe, and calculated the COGs from the echo data. Figure 4-15 shows the experimental environment.

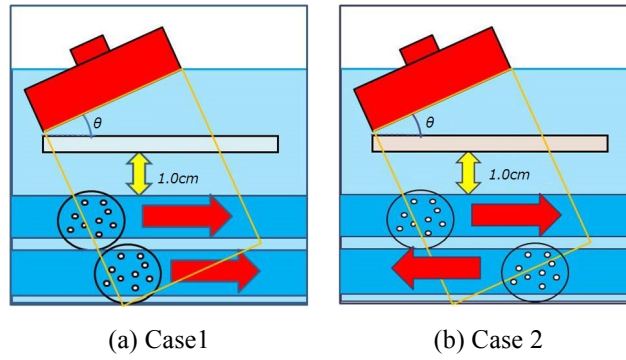
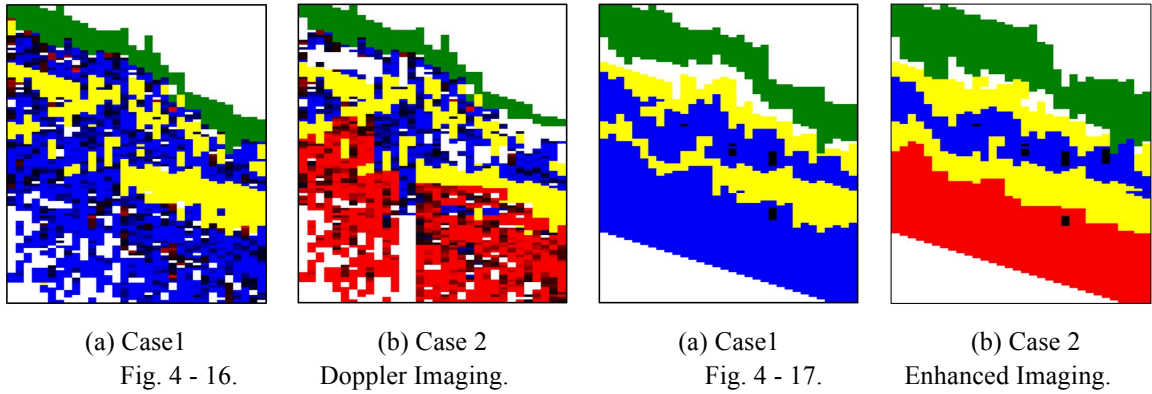


Fig. 4 - 15. Experimental Environment.

Table. 4 - 3. Doppler Frequency.

Rules			Portions	Colored Pixel
$\mu_{boundary}$	Object	Flow		
$\geq th$	$\mu_s \geq \mu_b$	$\mu_n \geq \mu_l + \mu_c$	Bone	Green
	$\mu_b \geq \mu_w + \mu_l$	$\mu_l + \mu_c \geq \mu_n$	Unidentified object	Black
	$\mu_l \geq \mu_s + \mu_b$	N/A	Silicon tube	Yellow
$< th$	$\mu_w > \mu_b$	$\mu_l \geq \mu_n$	Going away	Blue
	$\mu_w > \mu_b$	$\mu_c \geq \mu_n$	Approaching	Red
	N/A	$\mu_n > \mu_l + \mu_c$	Other	



To evaluate the COG transition, it is acquired the ultrasonic waves from three type silicon tubes with water current, and taken the data 10 times for each tube and water speeds of 50 and 70 cm/s.

This study extracted the mean of COG under the bone from the ultrasonic echo data. Table 4-3 shows the rule table to image bone, tube and water current. The notation th denotes the threshold of $\mu_{boundary}$. It is perfectly confirmed the Doppler effect under the bone, and the frequency shift according to water current speed. Figure 4-16 shows the experimental results of Doppler imaging for two cases in Fig. 4-15. This system confirmed the green pixels, which mean the bone area, and recognized all water current directions going away and approaching the array probe. Figure 4-17 shows the enhanced images obtained by the standard image processing procedure. These images clearly show the bone, silicon tubes and flow direction.

4.1.7 Conclusion

This section proposed a portable trans-skull Doppler system with 1.0 MHz array ultrasonic probe, and employed a cow scapula as a skull and three silicon tubes as the blood vessel. It is identified the Doppler effect from an ultrasonic data. This experiment confirmed the Doppler effect irrespective of the thickness of the silicon tube, and the frequency transition of the Doppler effect for 50 and 70 m/s water current speed under the bone, and provided automated imaging of Doppler effect. Thus, the current image processing techniques can easily clarify the image. Consequently, this study recognized Doppler effects of 1.0 MHz under the bone by using bubble in water.

The experimental results were evaluated by Doppler imaging. Under the conditions with 0.16-0.27 mm thickness bone and the equipment specification, it is confirmed to enable to diagnose the blood flow under the bone. The system determined the fuzzy degree and detected the flow direction by Doppler effect under skull and visualized the skull and flow direction. To determine the blood flow and locate blood vessel, the COG in the frequency domain was calculated. The COG shifted clearly to higher frequency direction when compared with the peak. This study focused on the law attenuation due to viscosity, which is proportional to the squares of the frequency, and had a discussion about the attenuation of frequency. The attenuation is proportional to the squares of the frequency. The frequency range of approximate 1.0 MHz value attenuates. This study suggested that this attenuation causes that the peak becomes lower than the COG, and the frequency of the COG can be considered highly correlated. Therefore, the COG of the spectrum was employed for measuring the flow direction. This approach was superior for this experiment.

In the portable system, it is important to flow direction by Doppler effect under skull, and automatically extract the region of skull and blood vessel simply. That is, the experimental results showed the superiority to measure the blood flow from any part of the adult human skull.

The future works is to develop a human brain disease diagnosis system by applying Doppler effects, which means the frequency and the intensity of the ultrasonic waves, and the ubiquitous ultrasonic system available in home and an ambulance.

4.2 Trans-skull Brain Imaging System

4.2.1 Introduction

Ultrasound has been used to image the human body and has become one of the most widely used diagnostic tools in modern medicine. The technology is relatively inexpensive and portable, especially when compared with other modalities, such as magnetic resonance imaging (MRI) and computed tomography (CT), which are time-consuming, and require radioactive tracers.

Ultrasound is also used to visualize tissue during routine and emergency prenatal care. As currently applied in the medical field, properly performed ultrasound poses no known risks to the patient. Moreover, it has been shown that it is possible to visualize and measure changes in ultrasound intensities with the use of harmonic gray-scale ultrasound imaging.

Though the frequency up to 50-100 MHz has been experimentally used in a technique known as biomicroscopy in special regions, typical diagnostic sonographic scanners operate in the frequency range of 2-18 MHz [70]. In the bone, the ultrasound causes large absorption and scattering, so the ultrasonic device is rarely used to the bone. The bone tissue has higher attenuation than the other tissue. Therefore, the general ultrasonic devices are not available for transmitting bone tissue. In previous study, the transcranial sonography has been proposed using two linear array probes. These ultrasonic array probes consist of 128 elements. However, it is difficult to transmit ultrasound from the random position because the two array probes are set up on both sides of human head. On the other hands, they employ the spherical array probe that consists of the 448 elements. However, they only described a signal processing. It is proposed an imaging system of the skull and brain surface using a 1.0 MHz single ultrasonic probe. In this system, it was scanned a target object at the interval of 1.0mm with a 3-D scanner. It is difficult to apply to clinical practice because this scanner is too large to use and constrains human head. Therefore, a simple and unrestrained system without the large mechanical scanner is strongly required. It is proposed the transcranial brain imaging system by using ultrasonic array probe [71]. On the other hand, in the case of employing wideband ultrasound, it is difficult to make a sector scan system on structural design. Thus, the frequency analysis is useful using multiple ultrasonic waves.

This study proposes ultrasonic image registration for multi-frequency analysis, and uses a cow scapula as a skull and a steel sulcus as a cerebral sulcus. To obtain the high-quality image by taking each advantage of two alternative frequency waves, it is proposed some synthesizing methods using statistic resonance [72]-[78], YURAGI, Fourier Transform, and Wavelet Transform. The results obtained the clearest ultrasonic image when synthesizing with Wavelet transform, and are superior to the other synthesized ones.

4.2.2 Experimental Environments

The most defective point of the ultrasonic wave is impossible to pass through the bone. Thus far, the brain diagnosis had not used the ultrasonic devices. But currently, the ultrasonic performance have improved, the ultrasonic wave passing through the temple enables the brain diagnosis. This study describes an imaging method for the human cerebral sulcus using two ultrasonic array probes with the center frequency of 0.5 MHz and 1.0 MHz to extract the surface of the bone and the sulcus.

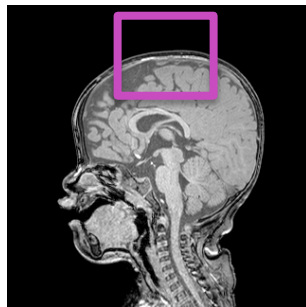


Fig. 4 - 18. Target - Human Brain.

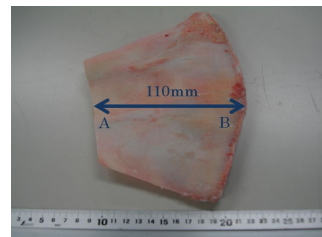


Fig. 4 - 19. Cow Scapula.

This experiment indicates with a pink square in Fig. 4-18. This study employs a cow scapula as a skull and a steel sulcus as a cerebral sulcus. Because the average thickness of human skull is about 3.0mm, it is employed the part of the cow scapula about 2.6 mm.

4.2.2.1 Experimental Materials

The cow scapula is shown in Fig. 4-19. The thickness of the point A is 2.64 mm and the thickness of the point B is 11.18 mm. The width is 110.0 mm. This experiment employs the point “A”. A steel sulcus is employed as a cerebral sulcus as shown in Fig. 4-20. Table 4-4 shows the specification of the steel sulcus. This experiment employs the steel sulcus of No. 2.

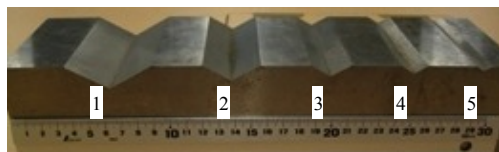


Fig. 4 - 20. Steel Sulcus.

Table. 4 - 4. Specification of Steel Sulcus.

Sulcus	1	2	3	4	5
Width [mm]	51.96	34.64	24.25	17.32	10.39
Depth [mm]	15.00	10.00	7.00	5.00	3.00

4.2.2.2 Ultrasonic Device

This experiment employs 1.0 MHz array probe (ISL Inc., ISL1938) 0.5 MHz array probe (ISL Inc., ISL2022) as shown in Fig. 4-21 (a) and (b). The center frequency of ISL1938 is 1.0 MHz and that of ISL2022 is 0.5 MHz. Figure 4-5 shows the system of these array probes. Both array probes consist of 32 elements at intervals of 1.5 mm.



Ultrasound transducer size: 24 mm×1.5 mm×32 ch
External size: 30 mm×60 mm×40 mm

(a) 1.0 MHz (ISL1938)



Ultrasound transducer size: 30 mm×1.5 mm×32 ch
External size: 50 mm×70 mm×50 mm

(b) 0.5 MHz (ISL2022)

Fig. 4 - 21. Ultrasonic Array Probe.

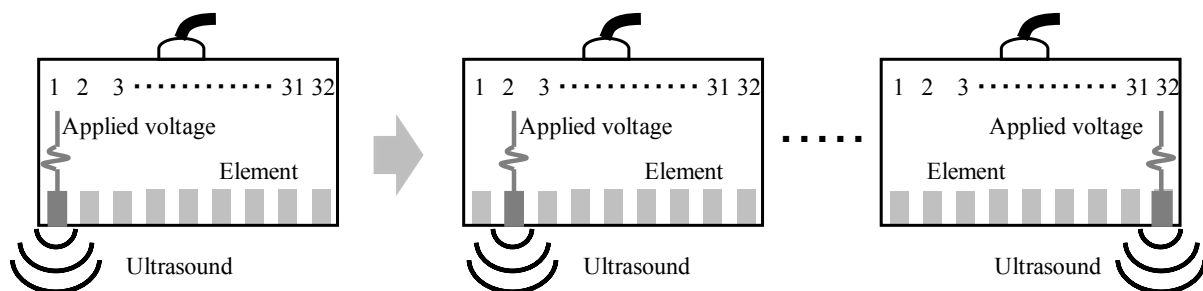


Fig. 4 - 22. System of Array Probe (Electronic control shift).

On the other hand, the ultrasound transducer size of 1.0 MHz is $24 \text{ mm} \times 1.5 \text{ mm} \times 32 \text{ ch}$, and the one of 0.5 MHz is $30 \text{ mm} \times 1.5 \text{ mm} \times 32 \text{ ch}$. If a wideband ultrasonic transducer is employed, it is difficult to make a sector scan system on structural design. The voltage is applied to the element and the ultrasound is generated from the element. The applied voltage shifts by one element and the ultrasound is generated. The array probe can obtain 32 ultrasonic waveforms inline in Fig. 4-22.

4.2.2.3 Data Acquisition System

The ultrasonic data acquisition system is shown in Fig. 4-23 (a). The cow scapula and the steel sulcus are placed in a thermostat water bath. In this experiment, water temperature is adjusted to 20°C by a thermostat water bath (Thomas Kagaku Co. Ltd., T-22L). The distance between the array probe and the cow scapula is about 25 mm. The distance between the cow scapula and the steel sulcus is about 10 mm. The ultrasonic phased array (Eishin Kagaku Co. Ltd., MC-64) transmits and receives ultrasonic waves via the array probe. The pulse repetition frequency (PRF) is 50 MHz. This experiment obtains the ultrasonic waves from the random position by manual scanning of the ultrasonic array probe, and 32 data at once.

Fig. 4-23 (b) and (c) are the B-mode images which are ultrasonic images by using 1.0 MHz and 0.5 MHz ultrasonic array probes.

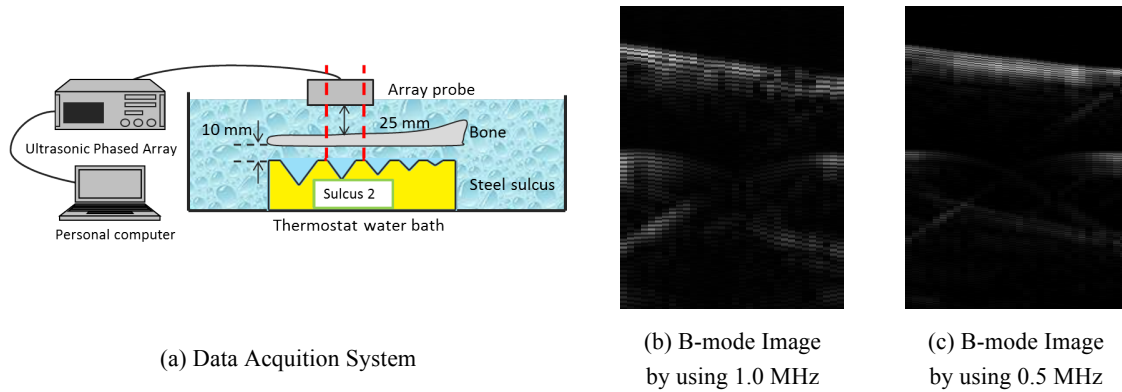


Fig. 4 - 23. Ultrasonic Data System.

4.2.3 Data Synthesis

To improve the ultrasonic image quality, this study proposes the ultrasonic data synthesis, and employs the ultrasonic data which both the bone and the sulcus are set as shown in Fig. 4-23 (b) and (c). The flowchart of the proposed system is shown in Fig. 4-24. This method consists of two types data synthesis. It is synthesized the acquisition waves of 1.0 MHz and 0.5 MHz. On the other hand, it is added the waves of 1.0 MHz and Gaussian noise as the YURAGI.

4.2.3.1 Statistic Resonance

This method synthesizes the waves of 1.0 MHz and 0.5 MHz by employing statistic resonance. It is added the waves obtained by the 1.0 MHz array probe to the waves by the 0.5 MHz array probe using Eq. 4-14. In this study, the value 'ratio' is 0.5. The notations $f(x,y)$ and $g(x,y)$ denote the

amplitudes of ultrasonic waves obtained by the array probe of 1.0 MHz and those of 0.5 MHz, respectively, where (x,y) denotes the coordinate of ultrasonic B-mode image.

$$h(x,y) = \text{ratio} \times f(x,y) + (1 - \text{ratio}) \times g(x,y). \quad (4-14)$$

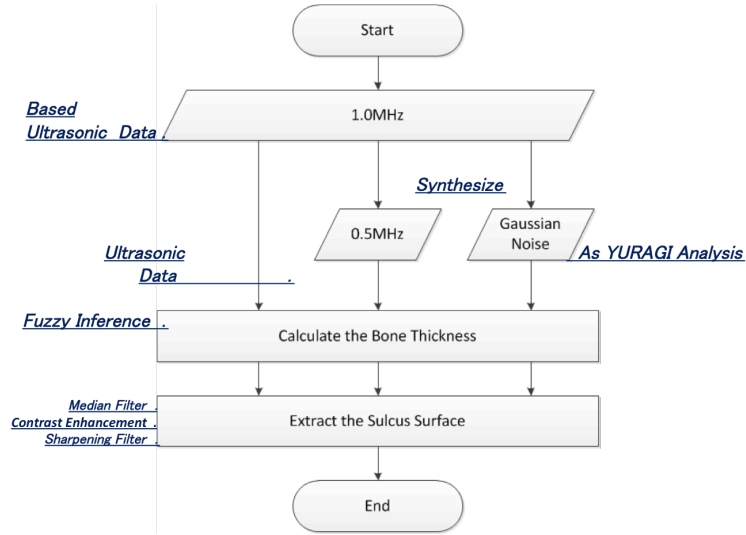


Fig. 4 - 24. Flowchart of Data Synthesis.

4.2.3.2 YURAGI

In linear information theory, electrical engineering, and neurobiology, noise has traditionally been viewed as being detrimental to information transmission. Stochastic resonance (SR) is a nonlinear phenomenon in statistical dynamics, whereby information flow in a multistate system is enhanced by the presence of optimized noise. Some biology-inspired techniques are known to provide the optimal search framework. In various engineering aspects, a Japanese term YURAGI denotes biological fluctuation. Generally, $1/f$ -Yuragi is defined as the noise whose power spectral density yields the $1/f$ curve, i.e., pink noise. YURAGI introduces a novel, noise utilizing, and aspect to biological signal processing. Therefore, this paper proposes a synthesis of YURAGI as a novel method for human brain imaging by using the ultrasonic array probes to synthesize the waves of 1.0 MHz and Gaussian noise. In addition, YURAGI synthesis does not need image registration. As YURAGI synthesis, the Gaussian noise was added to the 1.0 MHz waves, as is described by Eq. 4-2. The function $h_I(x,y)$ denotes the YURAGI synthesized waves. The function $f(x,y)$ denotes the ultrasonic waves that were obtained using the 1.0 MHz array probe. The function $g_I(x,y)$ denotes Gaussian noise as YURAGI.

$$h_I(x,y) = f(x,y) + g_I(x,y). \quad (4-15)$$

Gaussian noise is added to the 1.0 MHz waves. YURAGI is a phenomenon in which noise enhances the response of a nonlinear system to a weak signal. To find the optimal response, the synthesizing rate of $g_I(x,y)$ was varied from 0 to 0.01 in steps of 0.001. As the results, the synthesizing rate was fixed as 0.003.

4.2.4 Data Analysis

The most defective point of the ultrasonic wave is impossible to pass through the bone. Thus far, the brain diagnosis had not used the ultrasonic devices. But currently, the ultrasonic performance have improved, the ultrasonic wave passing through the temple enables the brain diagnosis. This method describes an imaging method for the human cerebral sulcus using two ultrasonic array probes with the center frequency of 1.0 MHz and 0.5 MHz to extract the surface of the bone and the sulcus.

4.2.4.1 Fourier Transform

The Fourier transform is the useful tool to analyze the frequency components of the signal and decomposes a signal into its constituent frequencies. The original signal depends on time, and therefore it is called the time domain representation of the signal, whereas the Fourier transform depends on frequency and is called the frequency domain representation of the signal. The term Fourier transform refers both to the frequency domain representation of the signal and the process that transforms the signal to its frequency domain representation. It is also possible to generalize the Fourier transform on discrete structures such as finite groups. The efficient computation of such structures, by the Fourier transform, is essential for high-speed computing. This study employs the Fourier transform for the purpose of fast processing.

In order to improve the ultrasonic raw image, this study proposed the ultrasonic data synthesis method. As preliminary experiment, it is synthesized the images which are measured the bone and the sulcus, individually. Firstly, it was measured the bone by using 1.0 MHz ultrasonic probe in Fig. 4-25 (a). Secondly, it was measured the sulcus by using 0.5 MHz ultrasonic probe in Fig. 4-25 (b). The ultrasonic images of the bone and the sulcus are Fig. 4-25 (c) and (d), respectively.

With these ultrasonic images, this study proposed the ultrasonic data synthesis by applying the Fourier transform. The Fourier transform is a mathematical operation that decomposes a signal into its constituent frequencies. The original signal depends on time, and therefore it is called the time domain representation of the signal, whereas the Fourier transform depends on frequency and is called the frequency domain representation of the signal. The term Fourier transform refers both to the frequency domain representation of the signal and the process that transforms the signal to its frequency domain representation. It is also possible to generalize the Fourier transform on discrete structures such as finite groups. The efficient computation of such structures, by fast Fourier transform, is essential for high-speed computing. This study employs fast Fourier transform for the purpose of fast processing, and applies the fast Fourier transform to 1.0 MHz ultrasonic data of the bone image and 0.5 MHz ultrasonic data of the sulcus image using Eq. 4-16, respectively.

$$f_j = \sum_{k=0}^{N-1} x_k e^{-\frac{2\pi i j k}{N}}. \quad j = 0, \dots, N-1 \quad (4-16)$$

After applying fast Fourier transform, it is synthesized the ultrasonic data of 1.0 MHz and 0.5 MHz on complex number, and applied the inverse Fourier transform to the synthesized data using Eq. 4-17.

$$x_k = \frac{1}{N} \sum_{j=0}^{N-1} f_j e^{\frac{2\pi i j k}{N}}. \quad k = 0, \dots, N-1 \quad (4-17)$$

Figure 4-25 (e) shows the image obtained by the inverse Fourier transform data. It is defined this image as the FFT synthesized image. Judging from this synthesized image, it was demonstrated the ultrasonic data synthesis by fast Fourier transform. On the other hand, it is applied the FFT

method to tofu as biological phantom in Fig. 4-26 (a) and (b). In this study, the raw images of the bone and the tofu are obtained respectively as shown in Fig. 4-26 (c) and (d). The image of the bone is obtained by 1.0 MHz ultrasonic array probe. The other one of the tofu is obtained by 0.5 MHz ultrasonic array probe. Figure 4-26 (e) shows the synthesized image.

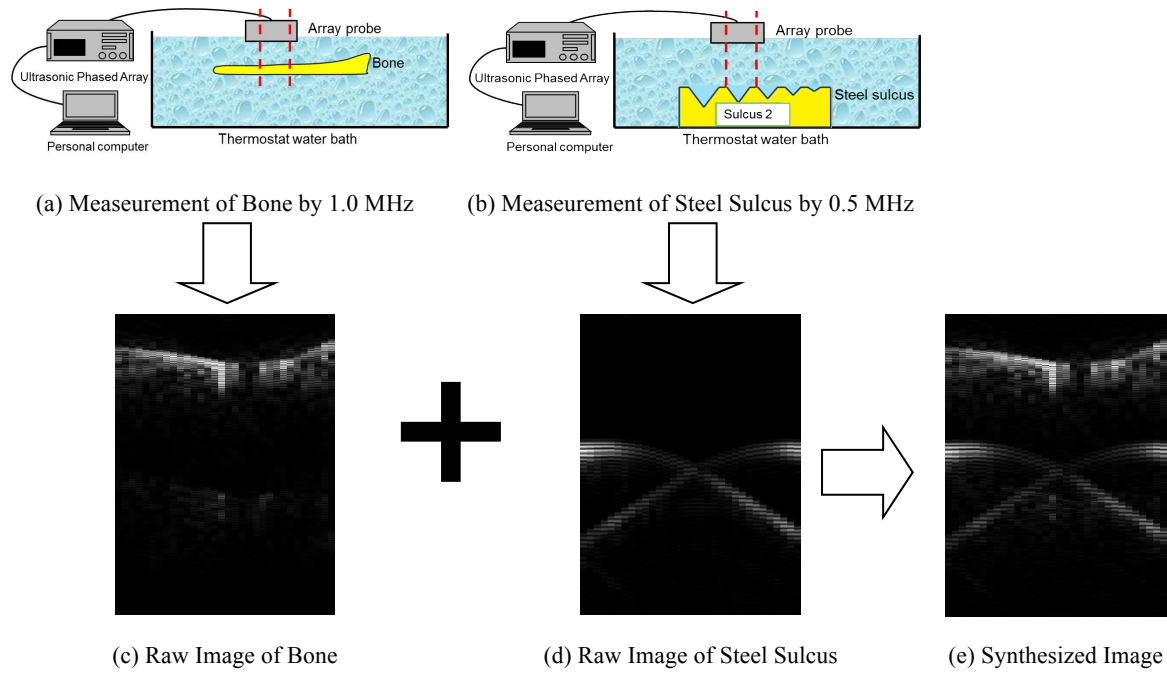


Fig. 4 - 25. FFT Synthesized Image of Bone and Steel Sulcus.

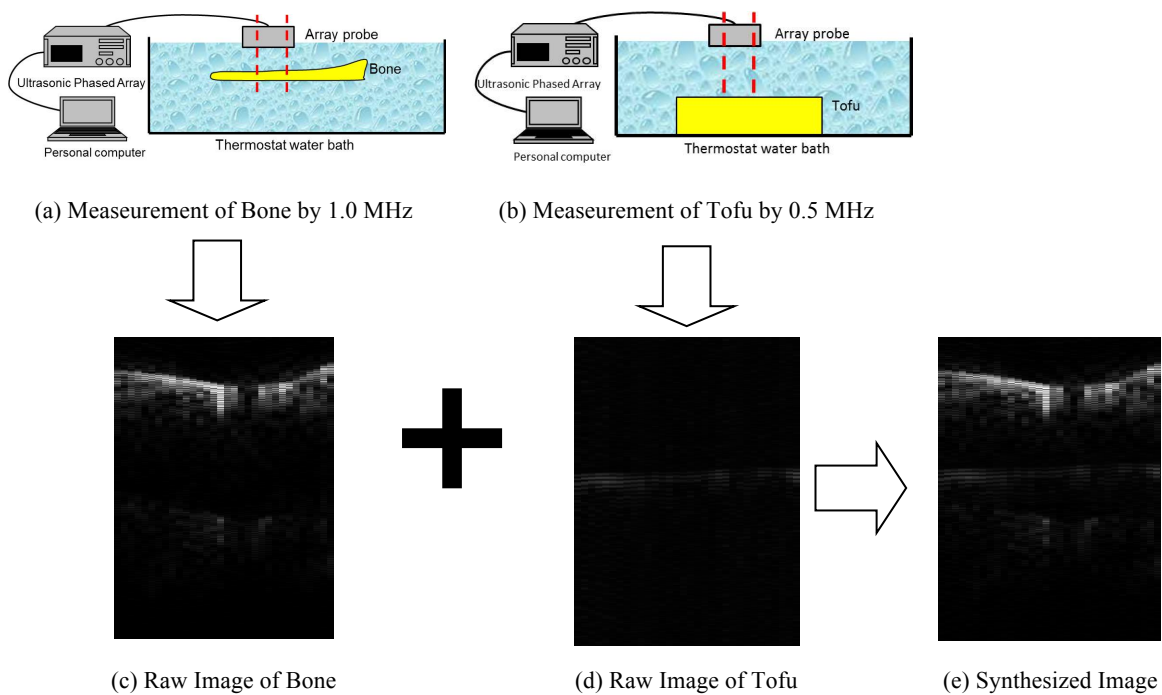


Fig. 4 - 26. FFT Synthesized Image of Bone and Tofu.

As the results, this study obtained the clearer images synthesized using Fourier transform. These results are superior to the results which are normally synthesized the images of 0.5 MHz and 1.0 MHz. The Fourier transform is useful to synthesize the respective ultrasonic wave of the different frequency. Therefore, this system proposes the data analysis in frequency domain as shown in Fig. 4-27. The first method was synthesizing the data of 1.0 MHz and 0.5 MHz by using arithmetic mean. The second method was synthesizing the data of 1.0 MHz and 0.5 MHz by using the Fourier transform which never changes each frequency component. Lastly, it is synthesized the data of 1.0 MHz and 0.5 MHz by using Wavelet transform, which is also never, changes each frequency component.

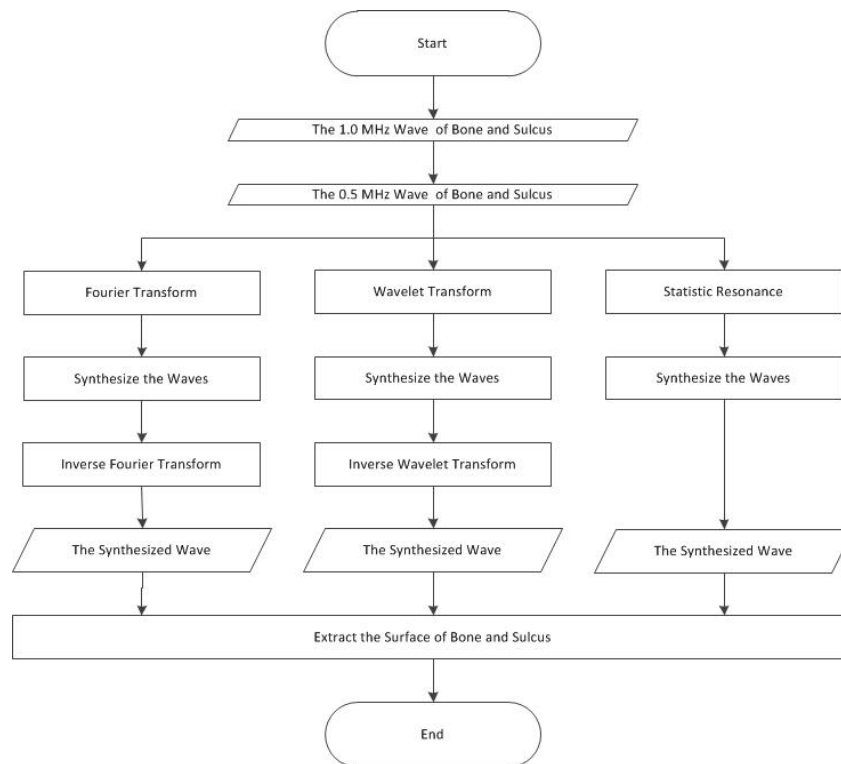


Fig. 4 - 27. Flowchart of Data Analysis.

4.2.4.2 Wavelet Transform

The Wavelet transform is a computational tool for a variety of signal and image processing applications. For example, the Wavelet transform is useful for the compression of digital image files; smaller files are important for storing images using less memory and for transmitting images faster and more reliably. The Wavelet transform covers the problems which the Fourier transform has as follows. If taking the Fourier transform over the whole time axis, it cannot be defined at what instant a particular frequency rises. The Short-time Fourier transform (STFT) uses a sliding window to find spectrogram, which gives the information of both time and frequency. Another problem exists that the length of window limits the resolution in frequency. The Wavelet transform is based on small wavelets with limited duration and allow us to analyze the signal in different scale.

By using two ultrasonic waves for the center frequency of 1.0 MHz and 0.5 MHz, it is applied

the Wavelet transform using Eq. 4-18 and 4-19.

$$\psi_{jk}(x) = 2^{j/2} \psi(2^j x - k). \quad (4-18)$$

$$WA(x) = \sum_{j,k=-\infty}^{\infty} c_{jk} \psi_{jk}(x). \quad (4-19)$$

Equation 4-20 then gives the wavelet coefficient c_{jk} .

$$c_{jk} = (W_{\psi} f)(2^{-j}, k2^{-j}). \quad (4-20)$$

Passing through the Wavelet transform, it is obtained the outputs giving the detail coefficients from the high-pass filter and approximation coefficients from the low-pass filter as shown in Fig. 4-28.

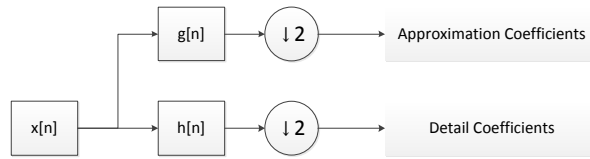


Fig. 4 - 28. Block diagram of filter analysis.

4.2.5 Data Extraction

4.2.5.1 Bone Thickness Determination

This method extracts the thickness of the skull from the synthesized waves, and easily determines the surface echo position of the bone from the synthesized waves. It is determined the bottom echo position of the bone using fuzzy logic technique, and calculated the bone thickness from the surface and bottom echo positions. The notations $f(x,y)$ and $g(x,y)$ denote the amplitudes of ultrasonic waves obtained by the array probe of 0.5 MHz and that of 1.0 MHz, respectively, where (x,y) denote the coordinate of ultrasonic B-mode image. The coordinate system is shown in Fig. 4-29.

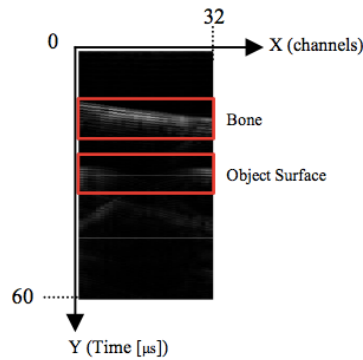


Fig. 4 - 29. Ultrasonic B-mode Image.

For calculating the thickness of the cow scapula, it is necessary to determine the surface and bottom points of the cow scapula. First, this study describes a determination method of the surface point of the bone. The reflection echo from the bone surface is first received. It is determined the surface echo by extracting the first received echo manually. Figure 4-30 (a) shows the acquisition

waveform and the detected surface echo, $s(x, y)$. In Fig. 4-30 (b), the detected echo was ranged from 22 μ s to 25 μ s.

The notation, m , denotes the end point of the detected echo from the start point (denoted by 0). This method calculates a correlation coefficient between the acquisition waveform and the detected surface echo in order to determine the surface point of the bone. The correlation coefficient is calculated using Pearson's product-moment correlation coefficient in Eq. 4-21.

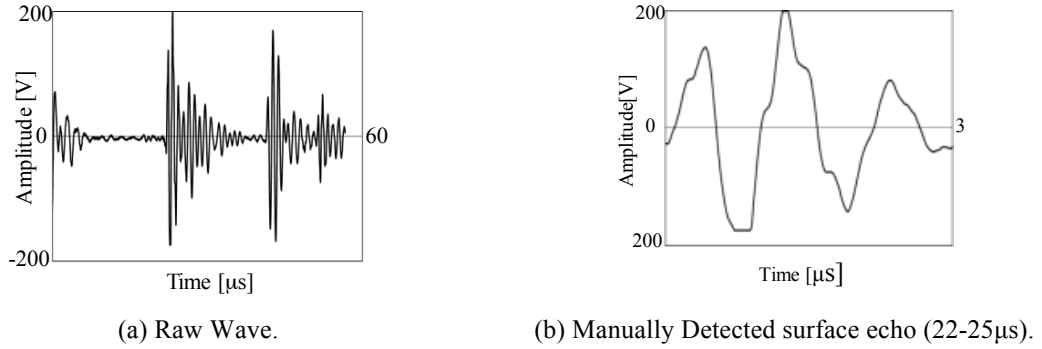


Fig. 4 - 30. Acquisition Waveform.

$$r(x, y) = \frac{\frac{1}{m-1} \sum_{y=l}^{m+i} (h(x, y) - \overline{h(x, y)}) (s(x, y) - \overline{s(x, y)})}{\sqrt{\frac{1}{m-1} \sum_{y=l}^{m+i} (h(x, y) - \overline{h(x, y)})^2} \sqrt{\frac{1}{m-1} \sum_{y=0}^m (s(x, y) - \overline{s(x, y)})^2}}, \quad (4-21)$$

for every i ($1 \leq i \leq n-m$)

The notation $\overline{h(x, y)}$ denotes the average of the amplitudes of $h(x, y)$. The notation $\overline{s(x, y)}$ denotes the average of the amplitudes of $s(x, y)$. Figure 4-31 shows the correlation coefficient waves. In the correlation coefficient waves, it is determined the highest correlation coefficient point as the surface point of the bone, and the bottom point of the bone and calculate the bone thickness using the surface and bottom points of the bone.

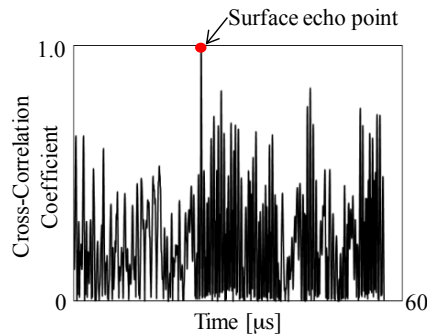


Fig. 4 - 31. Correlation Coefficients.

This study determines the bottom echo point using fuzzy inference. The ultrasound reflects at the boundary between water and the bone because the cow scapula acoustic impedance is quite different from the water acoustic impedance. Therefore, the amplitude of reflection echo enlarges in proportion to the difference of the acoustic impedance. The phase and frequency of the bottom

and surface echoes are approximately similar because these echoes are parts of the ultrasonic transmission echo. Therefore, the correlation coefficient between the bottom echo and the surface echo is high. Moreover, the distance between the surface echo and the bottom echo is proportional to the thickness of the bone. These facts obtain the knowledge as follows.

Knowledge 1: The amplitude of the bottom echo of the bone is large.

Knowledge 2: The correlation coefficient between the surface echo and the bottom echo of the bone is high.

Knowledge 3: The interval distance between the surface echo and the bottom echo depends on the thickness.

The following fuzzy if-then rules are derived from these knowledge.

Rule 1: IF *Amplitude* is *High* THEN the degree of bottom is High.

Rule 2: IF *Correlation* is *High* THEN the degree of bottom is High.

Rule 3: IF *Thickness* is *Close* to the assumed thickness THEN the degree of bottom is High.

The fuzzy if-then rules are formed by the fuzzy membership functions as shown in Fig. 4-32. The notations, Th_a , Th_c and Th_t denote thresholds of *Amplitude*, *Correlation* and *Thickness*, respectively. The Th_a is determined as the maximum of the amplitudes of $h(x, y)$. The Th_c is determined as 1.0. The Th_t is the assumed thickness. Three fuzzy degrees μ_{amp} , μ_{cor} and μ_{thi} are calculated by Equations 4-22, 4-23 and 4-24, respectively.

$$\mu_{amp}(x, y) = \min(S_{y_a}(a), HIGH_a). \quad (4-22)$$

$$\mu_{cor}(x, y) = \min(S_{y_c}(c), HIGH_c). \quad (4-23)$$

$$\mu_{thi}(x, y) = \min(S_{y_t}(t), CLOSE). \quad (4-24)$$

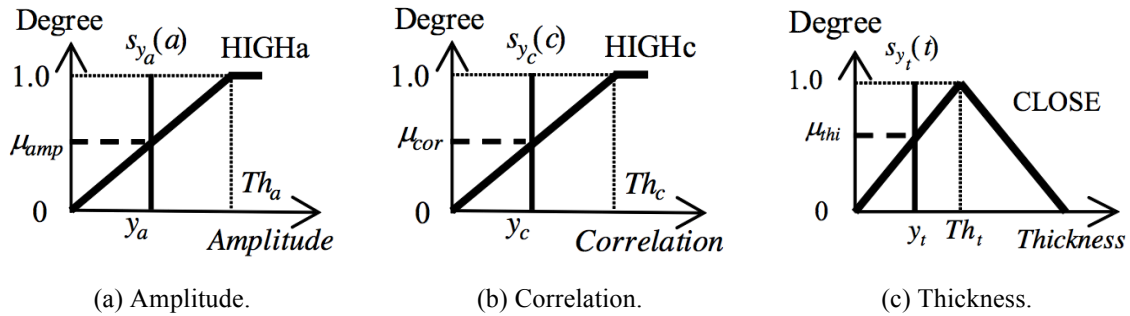


Fig. 4 - 32. Fuzzy Membership Function.

This method calculates μ_{thi} for every Th_t from 3.0 mm to 5.0 mm at the interval of 0.2 mm. The fuzzy singleton functions $S_{y_a}(a)$, $S_{y_c}(c)$ and $S_{y_t}(t)$ are defined by Eqs. 4-25, 4-26, and 4-27, respectively. Equation 4-28 calculates the total degree $\mu_{bottom}(x, y)$.

$$S_{y_a}(a) = \begin{cases} 1 & \text{if } a = y_a \\ 0 & \text{otherwise} \end{cases}. \quad (4-25)$$

$$S_{y_c}(c) = \begin{cases} 1 & \text{if } c = y_c \\ 0 & \text{otherwise} \end{cases} \quad (4-26)$$

$$S_{y_t}(t) = \begin{cases} 1 & \text{if } t = y_t \\ 0 & \text{otherwise} \end{cases} \quad (4-27)$$

$$\mu_{bottom}(x, y) = \mu_{amp}(x, y) \times \mu_{cor}(x, y) \times \mu_{thi}(x, y). \quad (4-28)$$

The $\mu_{bottom}(x)$ denotes the fuzzy degree of the bottom of the bone. The point with the highest degree is determined as the bottom point, y , for all x . The notations t_b and t_s denote the surface and bottom points, respectively. The notation v_m denotes the velocity of the bone. In this study, the velocity of the bone is 4,000 (m/s). Equation 4-29 calculates the bone thickness with the surface and bottom points.

$$Thickness = \frac{1}{2} \times (t_b - t_s) \times v_m. \quad (4-29)$$

4.2.5.2 Sulcus Surface

This method extracts the sulcus surface shape from the synthesized B-mode image $h(x, y)$. Figure 4-33 shows the flowchart for the extraction method of the sulcus surface shape. This method consists of five steps. First, it is made a B-mode image from the synthesized waves $h(x, y)$. Second, it is applied the Median Filter to remove the random noise. Third, it is applied the contrast enhancement to the image in order to increase the part of low intensity because the raw sulcus surface has low intensity. The tone curve between the input and output of the intensity is shown in Fig. 4-34. This method manually determines the threshold, Th ($= 40$). Fourth, it is applied the Sharpening Filter to the image in order to emphasize the change of the intensity because the sulcus surface is indistinct.

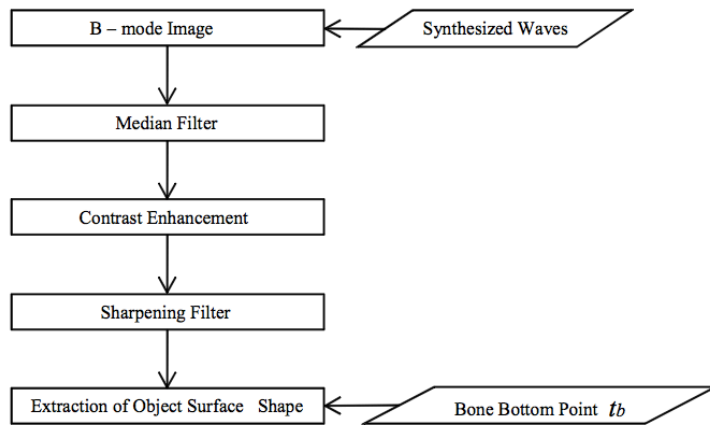


Fig. 4 - 33. Flowchart of Extraction Method of Sulcus Surface Shape.

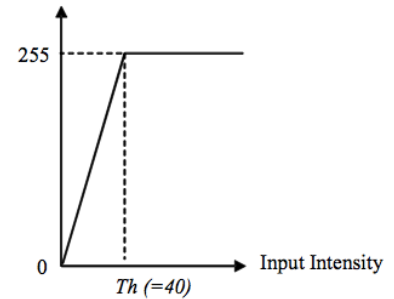


Fig. 4 - 34. Polygonal Line Tone Curve.

Finally, the sulcus surface shape is extracted from the image. Fig. 4-35 shows the extraction algorithm of the sulcus surface shape, which consists of three steps. Fig. 4-36 shows the extraction method from the sharpened image.

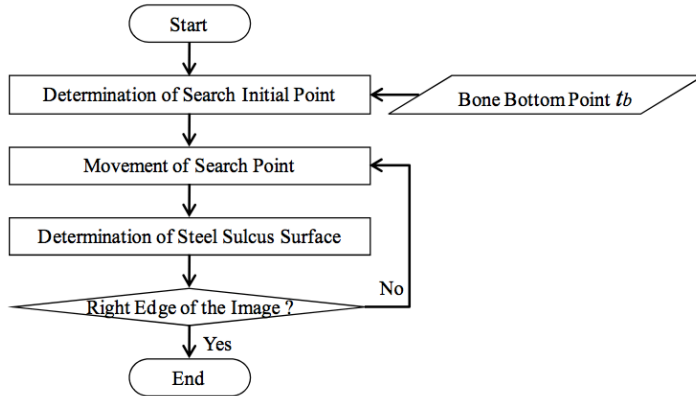


Fig. 4 - 35. Extraction Algorithm of Steel Sulcus Surface.

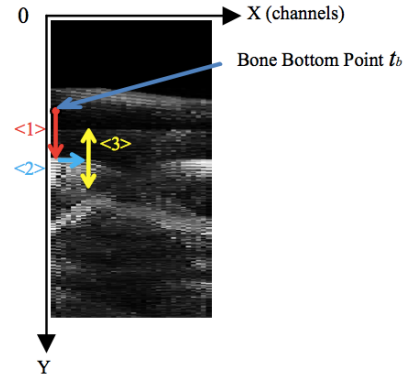


Fig. 4 - 36. Extract Sulcus Surface Shape from Sharpened Image.

- Step 1:** From the pixel point, $(0, 0)$, it is determined the first largest intensity pixel, $h(0, q)$, with higher intensity than a threshold ($=150$) as the sulcus surface point.
- Step 2:** This step moves the interest pixel to one pixel right $h(1, q)$ from the determined pixel obtained in Step 1. It is determined the largest intensity pixel being larger than the threshold in the range $q-10 < y < q+10$ as the sulcus surface point.
- Step 3:** This step repeats Step 2 until $x = 32$.

4.2.6 Experimental Results

The proposed method was applied to a cow scapula used as a skull and a steel sulcus used as a cerebral sulcus. The sulcus was placed in the thermostat water bath. The cow scapula was set between the array probe and the steel sulcus of No. 2. The obtained B-mode image width was 48 mm ($= 32 \times 1.5$ mm, acquisition data = 32 channels, separation between elements = 1.5 mm). The authors evaluated the accuracy of experimental results.

On data synthesis, the proposed method was applied to calculate the thickness of the cow scapula from the synthesized waves. In this experiment, the thickness of the cow scapula was about 2.6 mm. Table 4-5 lists the measurement results of the cow scapula thickness. As is given in this table, the measured thickness of the cow scapula was measured with the approximate truth value. The best results for the measured cow scapula thickness were obtained when only the 1.0 MHz data and the YURAGI synthesis data were employed. Moreover, the proposed method was applied to the steel sulcus. Fig. 4-37 shows the results for the extracted image of the steel sulcus shape. The image shown in Fig. 4-37 (a) defines the true image, and it was obtained from the acquisition data of 1.0 MHz without the cow scapula.

Table 4-6 lists the results of the steel sulcus depth and width measurement. In the case of the best results, the steel sulcus width error was 1.36 mm and the steel sulcus depth error of 0.07 mm. These results were obtained using the synthesized the 1.0 MHz and 0.5 MHz waves. As shown in this table, for the most part, the synthesized data are superior to the data obtained using only 1.0 MHz wave.

Table 4-7 provides the details of the colored pixels in these figures. The white pixels show the steel part and are contained in both the truth image and the extracted image. The blue pixels show the over extracted pixels, which are not present in the truth image. On the other hand, the red pixels show the absent pixels, which are present in the truth image.

Table. 4 - 5. Measurement Results of Bone Thickness.

Element No.	Thickness [mm]		
	1.0 MHz	1.0 MHz + 0.5 MHz	1.0 MHz + YURAGI
ch01	2.86	2.45	2.89
ch02	2.32	2.36	2.32
ch03	2.35	2.35	2.35
ch04	2.29	2.27	2.29
ch05	2.77	2.62	2.77
ch06	2.23	2.55	2.23
ch07	2.73	2.87	2.73
ch08	2.61	2.62	2.61
ch09	2.64	2.60	2.64
ch10	2.58	2.52	2.58
ch11	2.54	2.50	2.54
ch12	2.51	2.46	2.51
ch13	2.48	2.45	2.48
ch14	2.45	2.46	2.45
ch15	2.42	2.12	2.42
ch16	2.10	2.03	2.10
ch17	2.07	2.01	2.07
ch18	2.48	2.26	2.48
ch19	2.00	2.21	2.00
ch20	2.45	1.99	2.45
ch21	2.45	2.34	2.45
ch22	2.42	2.26	2.42
ch23	2.51	2.44	2.51
ch24	2.42	2.40	2.42
ch25	2.04	2.02	2.04
ch26	2.04	2.02	2.04
ch27	2.35	2.29	2.35
ch28	2.45	2.67	2.45
ch29	2.48	2.40	2.48
ch30	2.39	2.55	2.39
ch31	2.35	2.91	2.35
ch32	2.32	2.54	2.32
Average	2.41	2.39	2.41
Standard Deviation	0.19	0.24	0.19

*Truth Value: Thickness = 2.60 mm



(a) True



(b) 1.0 MHz



(c) 1.0 MHz + 0.5 MHz



(d) 1.0 MHz + YURAGI

Fig. 4 - 37.

Extracted Image.

Table. 4 - 6. Measurement Results of Steel Sulcus.

		1.0 MHz	1.0 MHz + 0.5 MHz	1.0 MHz + YURAGI
Width	Length [mm]	36.00	36.00	40.50
	Difference [mm]	1.36	1.36	5.86
	Error [%]	4.05	4.05	17.05
Depth	Length [mm]	7.08	9.93	11.70
	Difference [mm]	2.92	0.07	1.70
	Error [%]	29.20	0.70	17.0

Table. 4 - 7. Colored Pixels.





		True Image	Extracted Image
TP (True-Positive)		object	object
TN (True-Negative)		background	background
FP (False-Positive)		background	object
FN (False-Negative)		object	background

Figure 4-38 shows the compared image and Fig. 4-38 (a) shows the truth image. Table 4-8 gives the results of FP and FN for the compared image with the true image.

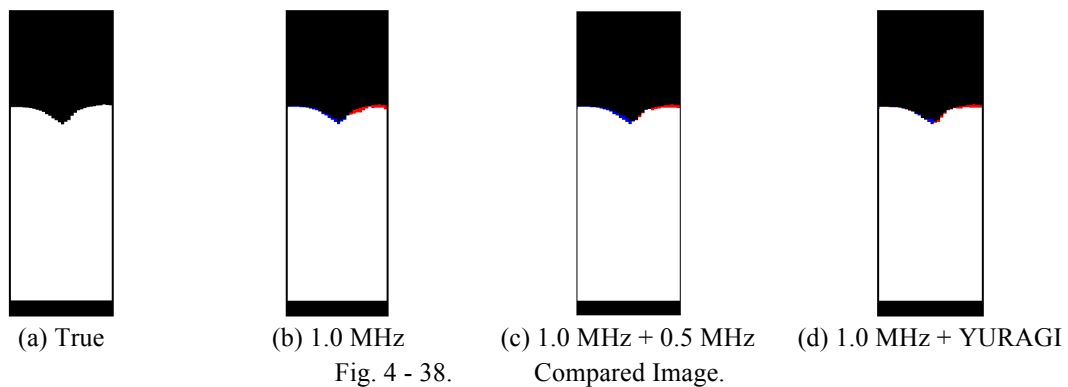


Fig. 4 - 38.

Compared Image.

Table. 4 - 8. Results of FP and FN for Compared Image.

	FP (False-Positive)	FN (False-Negative)	FP + FN (Error Rate)
1.0 MHz	1.79 %	2.43 %	4.22 %
Statistic Resonance	1.99 %	1.71 %	3.70 %
YURAGI	0.39 %	2.46 %	2.85 %

Figure 4-39 shows the effectiveness of the images. The effectiveness is defined as the percentage of conformed pixels between the true image and the extracted image; i.e., it is the sum of the red and blue pixels divided by the number of the truth pixels. As shown in this figure, the YURAGI synthesized waves have the higher effectiveness of 97.15 % when the synthesizing rate of YURAGI is 0.003, the normal raw waves of 1.0 MHz have the effectiveness of 95.78 %, and the synthesized waves of 1.0 MHz and 0.5 MHz has the effectiveness of 96.30%. Thus, YURAGI synthesis is more useful in this study.

On data analysis, it was applied the synthesized methods to the ultrasonic images and indicated the validity of synthesizing the waves of two alternative frequencies using ultrasonic data of a cow scapula as a skull and a steel sulcus as a cerebral sulcus. This experiment performed three analysis methods. After applying each method, it is extracted the sulcus surface of the image in Fig. 4-40.

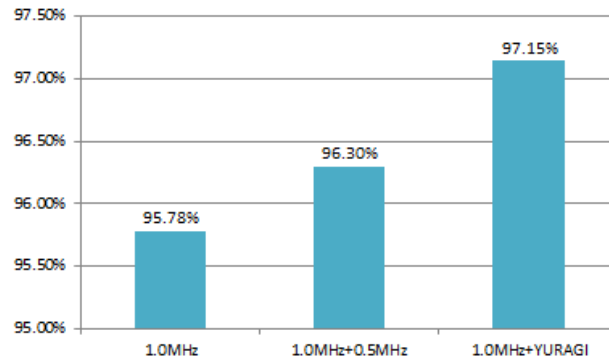
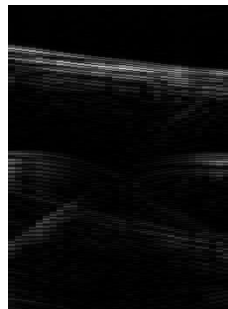
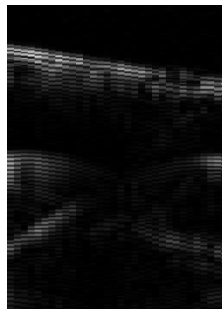


Fig. 4 - 39. Effectiveness of Images.

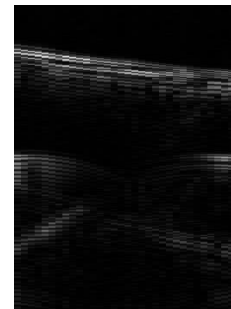
As the results, it was compared each image with the only sulcus image, which is defined as the true image. Figure 4-41 is the results with the extracted images. The light-blue bars show the pixel numbers of FP and FN, and the blue bars show the pixel numbers of FP. The rate of FP and FN is approximate 5% or less. Judging from this figure, it is indicated that the synthesizing method using the Wavelet transform is superior to the other methods. The image of the bone and the sulcus with the Wavelet transform was the clearest for all the images. The Wavelet transform has the basis function with automatic scaling, and thus enables to analyze the wide range frequency. For synthesizing the ultrasonic images, the Wavelet transform is more effective synthesis method.



(a) Fourier Transform.



(b) Wavelet Transform.



(c) Statistic Resonance.

Fig. 4 - 40. Synthesized Images.

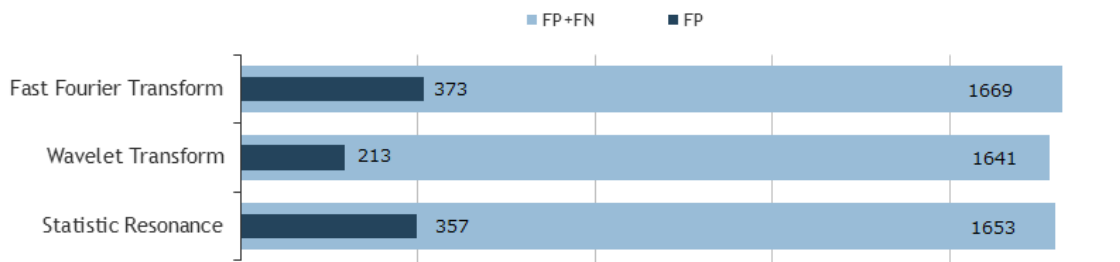


Fig. 4 - 41. Results with Extract Image.

4.2.7 Conclusion

This section proposed an ultrasonic image synthesis by using two ultrasonic array probes with the

each center frequency of 1.0 MHz and 0.5 MHz. In the preliminary experiment, the images of the individual objects were synthesized by using FFT. As biological phantom, the tofu was employed. With the synthesized images, the synthesis is useful for the ultrasonic images. This study performed the experiment using a cow scapula as a skull and a steel sulcus as a cerebral sulcus. As to data synthesis, this experiment extracted the sulcus width within the error of 5.86 mm and depth within the error of 1.94 mm. As for imaging the sulcus under the skull, the highest effectiveness of the synthesized wave is 96.30% when the weight of 0.5MHz waves is 0.60, and the one of YURAGI-Analysis wave is 97.15% when the weight is 0.003. Thus, YURAGI-Analysis is useful to this study. On the other hand, as to data analysis, it was obtained the clearest synthesized image using Wavelet transform. This result is superior to the results, which are the other synthesized images. The Wavelet transform will be useful for the ultrasonic waves.

The choice of frequency is a trade-off between spatial resolution of the image and imaging depth. Lower frequency produces less resolution but image deeper into the body. Higher frequency sound waves have a smaller wavelength and thus are capable of reflecting or scattering from smaller structures. In the bone, the ultrasound causes large absorption and scattering, so the ultrasonic device is rarely used to the bone. The bone tissue has higher attenuation than the other tissue. Therefore, the general ultrasonic devices are not available for transmitting bone tissue. However, it can be transmitted the low frequency under 1.0 MHz to bone tissue. In clinical practice, the ultrasonic device with the center frequency of 0.5 MHz is performed to diagnose osteoporosis. This work indicated the superiority to synthesize the ultrasonic images of different frequencies.

In the future, the sparse decoding and PCA will apply to this system. It will be meaningful for human brain ultrasound-mediated diagnosis in the near future. On the other hands, the sparse coding is available to learn the basis function for each tissue. The component is incorporated and computed the coefficient of the basis function. When this system is achieved, it is so useful for human brain ultrasound-mediated diagnosis.

4.3 Mobile Healthcare Management System

This section describes mobile health care managements in smart medical system. The transformation of electricity grids into smart grids has been widely remarked as a key for sustainable growth around the globe. The trend to smart grids comes at a time in which information and communication technologies have revolutionized personal communications and turned wireless communications into a commodity. Thus, it is no coincidence that communications technology will play an essential role in the implementation of smart grids. This study designs the mobile medical system to review data prior to patient access. Improved communication can also ease the process for patients, clinicians, and caregivers. As one of the implementations for smart medical system, the ultrasonic diagnosis and mobile communication system are proposed.

4.3.1 Introduction

Mobile health care managements grant patients access to health information, best medical practices, and health knowledge. Moreover, it helps clinicians to make better treatment decisions by providing more continuous data and to identify health threats and improvement opportunities based on drug information or current medical practices and care plans. The medical support system also makes it easier for clinicians to care for their patients by facilitating continuous communication. Eliminating communication barriers and allowing documentation flow between

patients and clinicians can save time consumed by face-to-face meetings and telephone communication. Improved communication can also ease the process for patients, clinicians, and caregivers to ask questions, to set up appointments, and to report problems. Additionally, the smart medical system can quickly provide critical information to proper diagnosis or treatment in the case of an emergency. The software development and implementation is the ease with which customizations may implement and refine some advantages. For example, the features of the care notebook component were initially developed for health specific requirements. By expanding the types of data, this tool supports for specific needs and care plans, overlapping data points can help best practices across implementations.

The final goal for this research is to contract the smart medical system by using ultrasonic device and mobile communication technology. A medical diagnosis system using ultrasonic device is widely used in the medicine. Recently, a simple and unrestrained system without the large mechanical scanner is strongly required. This study proposed the transcranial brain imaging system by using ultrasonic array probe. This study suggested mobile health care system with smart phone application. Moreover, this system proposed that it is important for physicians and patients to use mobile technology in order to assist with clinical decision-making.

4.3.2 Mobile System Implementation

The linking of patient information with medical systems makes it possible to increase the efficiency of health care innovation. The smart care needs simple to operate on both desktop and mobile. With integrated telecommunication, voice recording, and direct dictation into the record, clinical governance is needed. The decision support leads the self-designed clinical way by inputting screens. This system applied the ultrasonic smart medical system by using iPhone/iPad as shown in Fig. 4-42. After processing for analyzing ultrasonic images, the detail data will be sent to the mobile items. The smart medical care is a comprehensive iPhone/iPad application for clinicians, social care workers, and family to record their interactions with patients and clients. It is developed this application as shown in Fig. 4-43.

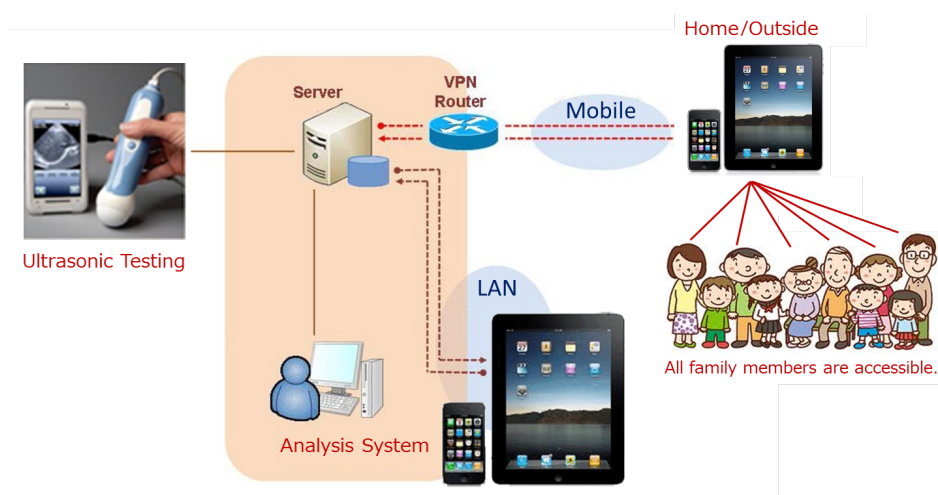


Fig. 4 - 42. Ultrasonic Smart Medical System.

Fig. 4-44 (a) and (b) are the screens 'Start screen'. Fig. 4-44 (a) shows the ultrasonic image with the comments after the diagnosis. The received image will be stocked in the database. When

pushing the button ‘Share’ in this screen, the users can post the message on Facebook and share the information with their family as shown in Fig. 4-44 (b).

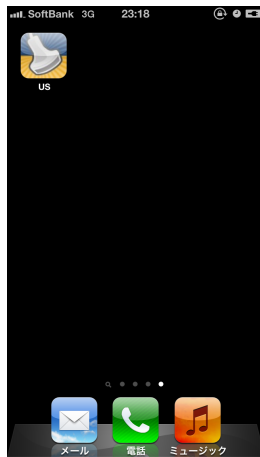
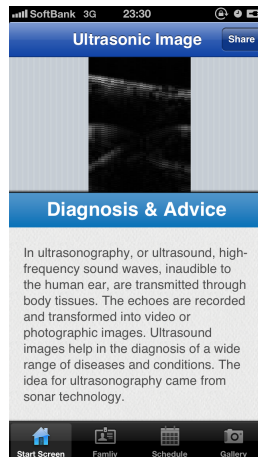
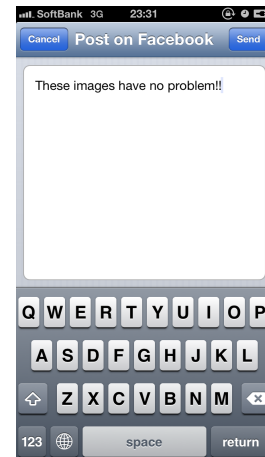


Fig. 4 - 43. Start Screen of Application.



(a) Ultrasonic Image



(b) Post on Facebook Screen

Fig. 4 - 44. Ultrasonic Image Screens.

Fig. 4-45 (a) and (b) are the screens ‘Family’. The users can manage the members who share the information as shown in Fig. 4-45 (a). When pushing the name bar, they can browse the detail for the selected members in Fig. 4-45 (b).

Fig. 4-46 (a) and (b) are the screens ‘Schedule’. The innovative smart medical care application connects to the patient management systems to be scheduled and care requirements distributed to appropriate resources. The access is gained with a secure login of username and password, where users can access their schedule, view family’ details with previous relevant history, record notes and clinical observations, and schedule further appointments as shown in Fig. 4-46 (a). When pushing the date bar, the users can browse the venue details as shown in Fig. 4-46 (b).



(a) Family Lists

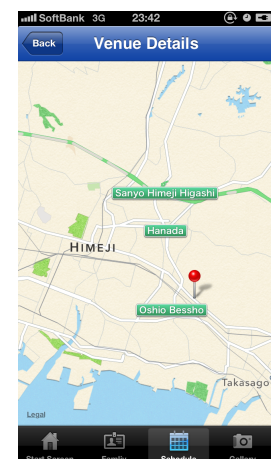


(b) Family Details

Fig. 4 - 45. Family List Screens.



(a) Schedule Lists



(b) Venue Details

Fig. 4 - 46. Schedule Screens.

Fig. 4-47 (a) and (b) are the screens 'Gallery'. The users can browse the ultrasonic images, which the members had already been diagnosed as shown in Fig. 4-47 (a). When pushing the image, they can browse the full screen image in Fig. 4-47 (b).

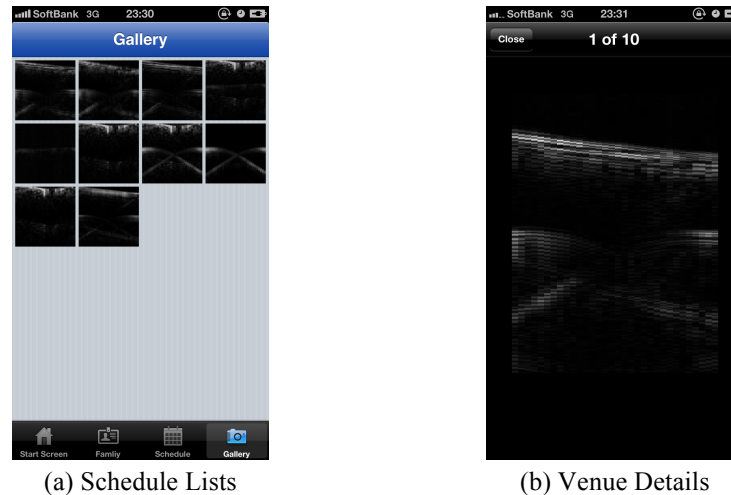


Fig. 4 - 47. Gallery Screens.

4.3.3 Discussion

This section applied the ultrasonic smart medical system by using iPhone/iPad. This system has some merits below.

Patients Merits:

1. Improvement of the medical quality by sharing the medical treatment information
2. Easy understanding for medical treatment contents
3. Disclosure of the medical treatment information
4. Waiting time shortening at the hospital
5. Cooperation by the electronic data with other medical institutions

Doctors/Nurses Merits:

1. Realization of a "readable" medical record
2. Support to informed consent
3. Immediate Reference for the medical record (information and test result)
4. Improvement of the medical quality by using the applications
5. Labor saving with electric communication technology

In addition to storing individual personal health information, some PHRs provide added-value services such as drug-drug interaction checking, electronic messaging between patients and providers, managing appointments, and reminders. However, it is by no means obvious which communication technologies will be integrated into electricity grids. Communication systems need to be seen as part of systems, including in particular health information processing systems. Therefore, this study is useful for mobile health care system.

4.3.4 Conclusion

The mobile smartphones and downloadable applications have become commonplace in the medical field as personal and professional tool. The medically related apps suggest that physicians use mobile technology to assist with clinical decision-making.

Physicians are quickly integrating the Smartphone apps, such as those available in Apple and Android, into clinical practice. Smartphone apps are self-contained software applications that can be downloaded by the advanced mobile phones. The appeal points of apps for the users are their ability to store reference information, save critical data, perform complex calculations, and access internet-based content.

The clinical use of smartphones and apps will continue to increase, and there is an absence of high-quality and popular apps despite a desire among physicians and patients. This information should be used to guide the development of future health care delivery systems. Moreover, the reliability and ease of use will remain major factors in determining the successful integration of apps into clinical practice.

This section proposed mobile health care managements in smart medical system. It is employed the ultrasonic images by using two ultrasonic array probes with the each center frequency of 1.0 MHz and 0.5 MHz, and performed the experiment using a cow scapula as a skull and a steel sulcus as a cerebral sulcus, and implementation of iPhone and iPad. As the results, it was developed the total system with mobile phone application for medical ultrasonic system. It will be meaningful for ultrasound-mediated diagnosis in emergency medicine and health care in the near future.

Chapter 5

Conclusion

This dissertation discussed intelligent computing in medical ultrasonic system with fuzzy logic, data synthesis, frequency analysis, and so on.

Chapter 2 proposed the noninvasive cellular quantity measurement method in BMSCs / β -tricalcium phosphate. In order to measure the cell quantity, up to now, the composite must be crushed and the cells count with an electro microscope. However, the measured composite is never used for a future study and clinic. This work developed the approach, which estimated the approximate cell quantity to treat large bone defects, and attempted to identify cellular quantity with an ultrasonic system. The ultrasonic waves reflect at boundaries where there is a difference in acoustic impedances of the materials on each side of the boundary. Therefore, this system focused on the reflected signal. From the obtained ultrasonic data, it was extracted two features: amplitude and frequency. Amplitude is obtained from the raw ultrasonic wave, and frequency is calculated from frequency spectrum obtained by applying cross-spectrum method. Therefore, this study suggested that the frequency features were valuable to analyze the BMSCs with the features of the frequency attenuations, and showed the ability of intervention to produce the desired beneficial effect. It was certified the superiority of the frequency data analysis. This study established the validity for measuring the cellular quantity in BMSCs by using the feature of frequency with Cross-Spectrum focusing on the attenuation.

Chapter 3 proposed a fuzzy system of stem implantation on total hip arthroplasty by an ultrasonic device. In the surgery, the surgeons try to adapt for the patient from the small size stem to the larger size stem in turn. Therefore, this system performed automatic and accurate assessment in the surgery. This experiment employed a single ultrasonic probe whose center frequency is 1,000 Hz, and detected the acoustic signals when knocking the inserted stem with a hammer. It had high correlation between the degree of tightening and the attenuation time of acoustic signal. That is, the higher tightened degree implied shorter attenuation period. The support system selected the most suitable stem size by fuzzy inference with respect to the attenuation time and its difference time from correct stem to one larger size stem, which dynamically adapts to each patient. As a result of applying to 8 total hip arthroplasty patients, the effectiveness of selecting the suitable stem was 87.5%, and this system successfully determined the suitable stem in comparison to the results of the practical surgery.

Chapter 4 proposed human brain ultrasound-mediated diagnosis in emergency medicine and home health care in the fields of data analysis and mobile item implementation. The ultrasonic simple operation to touch to the body surface diagnosis enables real-time visual recognition for heart beat and unborn baby moving, and so on. It is safety to human body and many repetitions. The goal of this study was the portable and real time brain diagnosis under the thick-skull. This experiment employed two ultrasonic array probes with the center frequency of 1.0 MHz and 0.5 MHz. The choice of ultrasonic frequency is a trade-off between spatial resolution of the image and imaging depth. By using some soft computing techniques, this system showed the validity of data synthesis and analysis for ultrasonic waves, and described mobile health care managements in smart medical system. First section proposed the trans-skull ultrasonic doppler system, whose target is blood flow. The experimental results were evaluated by Doppler imaging. Under the conditions with 0.16-0.27 mm thickness bone and the equipment specification, it is confirmed to enable to diagnose the blood flow under the bone. The system determined the fuzzy degree and

detected the flow direction by Doppler effect under skull and visualized the skull and flow direction. To determine the blood flow and locate blood vessel, the COG in the frequency domain was calculated. The COG shifted clearly to higher frequency direction when compared with the peak. This study focused on the law attenuation due to viscosity, which is proportional to the squares of the frequency, and had a discussion about the attenuation of frequency. The attenuation is proportional to the squares of the frequency. The frequency range of approximate 1.0 MHz value attenuates. This study suggested that this attenuation causes that the peak becomes lower than the COG, and the frequency of the COG could be considered highly correlated. Therefore, the COG of the spectrum was employed for measuring the flow direction, and this approach was superior for this experiment. Second section proposed the trans-skull brain imaging system. This approach was particular interest for the design of further study intending to visualize any defects by ultrasound methods. As to data synthesis, this experiment extracted the sulcus width within the error of 5.86 mm and depth within the error of 1.94 mm. As for imaging the sulcus under the skull, the highest effectiveness of the YURAGI synthesized wave is 97.15%, when the weight is 0.003. On the other hand, as to data analysis, it was obtained the clearest synthesized image using Wavelet transform. Therefore, data synthesis and analysis were useful for the ultrasonic waves. Last section designed the mobile medical system to review data prior to patient access. Improved communication eases the process for patients, clinicians, and caregivers. As one of the implementations for smart medical system, the ultrasonic diagnosis and mobile communication system were proposed. The mobile health care managements grant patients access to health information, best medical practices, and health knowledge. Moreover, it helps clinicians to make better treatment decisions by providing more continuous data and to identify health threats and improvement opportunities based on drug information or current medical practices and care plans. The medical support system also makes it easier for clinicians to care for their patients by facilitating continuous communication. Eliminating communication barriers and allowing documentation flow between patients and clinicians save time consumed by face-to-face meetings and telephone communication. The software development was customized and refined. Additionally, the smart medical system quickly provides critical information to proper diagnosis or treatment in the case of an emergency. This implementation indicated that the ultrasonic image is useful to emergency medicine and home health care. This observation is encouraging for further studies of evaluating brain in patients.

Medical diagnosis system using ultrasonic device is widely used in medicine. Comparing with CT and MRI, it is greatly different in point of usability. Taking advantages of ultrasonic devices, all systems were proposed in this dissertation employed intelligent computing. First, the cell quantity measurement method in BMSCs / β -TCP was represented and analyzed with fuzzy logic and neural network, and found out the attenuation of frequency. Second, the fuzzy stem determination method was represented. For the patients and surgeons of total hip arthroplasty, this system performed automatic and accurate assessment in the surgery. This study successfully determined the suitable stem in comparison to the results obtained from the practical surgery. It became an index in order to judge how degree the stem fits in the clinical treatment. Third, the ultrasonic human brain diagnosis method was represented. It consisted of blood vessel imaging system and trans-skull brain imaging system; both systems included the final goal for this ultrasonic research to construct the smart medical system by using ultrasonic device and mobile communication technology. All data synthesis and analysis served successful ultrasonic imaging. Moreover, the implementation for ultrasonic diagnosis with mobile smartphones and downloadable applications, which are becoming commonplace as personal and professional tool, assists mobile medical technology on clinical decision-making.

Last, the author hopes that this research will be of use for medical ultrasonic diagnosis system as the advanced study and scientifically contribute to future medicine.

Bibliography

- [1] K. A. Wear, "Autocorrelation and Cepstral Methods for Measurement of Tibial Cortical Thickness," *IEEE Transactions on Ultrasonics, Ferroelectrics, and Frequency Control*, Vol.50, No.5, pp.655-660, June 2003.
- [2] J. Krautkramer and H. Krautkramer, ed., "Ultrasonic Testing of Materials," Springer-Verlag, Berlin 1990.
- [3] S. S. Homaeigohar, M. A. Shokrgozar, A. Khavandi, and A. Y. Sad, "In vitro biological evaluation of beta-TCP/HDPE--A novel orthopedic composite: a survey using human osteoblast and fibroblast bone cells," *J Biomed Mater Res A*, vol. 84, pp. 491-499, 2008.
- [4] D. Wendt, A. Marsano, M. Jakob, M. Heberer, and I. Martin, "Oscillating perfusion of cell suspensions through three-dimensional scaffolds enhances cell seeding efficiency and uniformity," *Biotechnol Bioeng*, vol. 84, pp. 205-214, 2003.
- [5] L. Cristofolini, E. Varini, I. Pelgreffi, A. Cappello, A. Toni, "Device to measure intra-operatively the primary stability of cementless hip stems," *Med Eng Phys* 28, pp.475-482, 2006.
- [6] B. D. Lindsey, E. D. Light, H. A. Nicoletto, E. R. Bennett, D. T. Laskowitz, and S. W. Smith, "The Ultrasound Brain Helmet: New Transducers and Volume Registration for In vivo Simultaneous Multi-Transducer 3-D Transcranial Imaging," *IEEE Transactions on Ultrasonics, Ferroelectrics, and Frequency Control*, Vol. 58, No. 6, 2011.
- [7] F. Vignon, J. -F. Aubry, M. Tanter, A. Margoum, and M. Fink, "Dual-Arrays Brain Imaging Prototype: Experimental In Vitro Results," *IEEE International Ultrasonics Symposium*, pp. 504-507, 2005.
- [8] P.J. White, G.T. Clement, and K. Hynynen, "Transcranial Ultrasound Focus Reconstruction with Phase and Amplitude Correction," *IEEE Transactions on Ultrasonics, Ferroelectrics, and Frequency control*, pp.1518-1522, Vol. 52, No. 9, 2005.
- [9] R. Agarwal, C. M. Angst, "Technology-enabled transformations in U.S. health care: early findings on personal health records and individual use," *Human-Computer Interaction and Management Information Systems: Applications*, Vol. 5, pp. 357-378, 2006.
- [10] American Health Information Management Association, "The Role of the Personal Health Record in the HER," July 25, 2005.
- [11] E. D. Arrington, W. J. Smith, H. G. Chambers, Bucknell AL, Davino NA, "Complications of iliac crest bone graft harvesting," *Clin Orthop* 329:300-0.
- [12] J. C. Banwart, M. A. Asher, R. S. Hassanein, "Iliac crest bone graft harvest donor site morbidity," *A statistical evaluation. Spine* 1995, 20(9); 1050-60.
- [13] E. M. Younger, M. W. Chapman, "Morbidity at bone graft donor site," *J Orthop Trauma* 1989;3(3):192-5.
- [14] J. W. Calvert, L. E. Weiss, M. J. Sundine, "New frontiers in bone tissue engineering," *Clin Plast Surg*. 2003 Oct;30(4):641-8.
- [15] G. Jun, M. Victor, I. Arnold, "The Osteogenic Potential of Culture-Expanded Rat Marrow Mesenchymal Cells Assayed In Vivo in Calcium Phosphate Ceramic Blocks," *Clinical Orthopaedics & Related Research*, 262:298-311, January 1991.
- [16] C. Knabe, R. Gildenhaar, G. Berger, W. Ostapowicz, R. Fitzner, R. J. Radlanski, U. Gross, "Morphological evaluation of osteoblasts cultured on different calcium phosphate ceramics," *Biomaterials*, 1997 Oct;18(20):1339-47.
- [17] H. Mahesh. Mankani, Sergei A. Kuznetsov, Bruce Fowler, Albert Kingman, Pamela Gehron Robey, "In vivo bone formation by human bone marrow stromal cells: Effect of carrier particle size and shape," *Biotechnology & Bioengineering*, 9 Nov 2000, Pages 96-107.

- [18] J. Toquet, R. Rohanizadeh, J. Guicheux, S. Couillaud, N. Passuti, G. Daculsi, D. Heymann, "Osteogenic potential in vitro of human bone marrow cells cultured on macroporous biphasic calcium phosphate ceramic," *Journal of Biomedical Materials Research*, 3 Jan 1999, Pages 98-108.
- [19] Q. Zheng, T. Zhu, J. Du, H. Wang, S. Li, "Studies on the ossification of compound transplantation of porous TCP ceramics and bone marrow," *J Tongji Med Univ.* 1996; 16(4):236-40.
- [20] H. Ohgushi, M. Okumura, "Osteogenic capacity of rat and human marrow cells in porous ceramics. Experiments in athymic (nude) mice," *Acta Orthop Scand.* 1990 Oct; 61(5):431-4.
- [21] M. Kikuchi, S. Itoh, S. Ichinose, K. Shinomiya, J. Tanaka, "Self-organization mechanism in a bone-like hydroxyapatite/collagen nanocomposite synthesized in vitro and its biological reaction in vivo," *Biomaterials*, 2001 Jul;22(13):1705-1711.
- [22] J. Toquet, R. Rohanizadeh, J. Guicheux, S. Couillaud, N. Passuti, G. Daculsi, D. Heymann, "Osteogenic potential in vitro of human bone marrow cells cultured on macroporous biphasic calcium phosphate ceramic." *J Biomed Mater Res* 1999. 44:98-108.
- [23] M. Gebhart, J. Lane, "A radiographical and biomechanical study of demineralized bone matrix implanted into a bone defect of rat femurs with and without bone marrow," *Acta Orthop Belg.* 1991; 57(2):130-43.
- [24] E. Kon, A. Muraglia, A. Corsi, P. Bianco, M. Marcacci, I. Martin, A. Boyde, I. Ruspantini, P. Chistolini, M. Rocca, R. Giardino, R. Cancedda, R. Quarto, "Autologous bone marrow stromal cells loaded onto porous hydroxyapatite ceramic accelerate bone repair in critical-size defects of sheep long bones," *Journal of Biomedical Materials Research*, 15 Dec 1999, Pages 328-337.
- [25] M. Sous, R. Bareille, F. Rouais, D. Clément, J. Amédée, B. Dupuy, C. Baquey, "Cellular biocompatibility and resistance to compression of macroporous beta-tricalcium phosphate ceramics," *Biomaterials*. 1998 Dec; 19(23):2147-53.
- [26] L. F. William, "Tissue engineering and cell based therapies, from the bench to the clinic: The potential to replace, repair and regenerate," *Reproductive Biology and Endocrinology* 2003, 1:102.
- [27] K. Inoue, H. Ogushi, T. Yoshikawa, M. Okumura, T. Sempuku, S. Tamai, Y. Dohi, "The Effect of Aging on Bone Formation in Porous Hydroxyapatite: Biochemical and Histological Analysis," *Journal of Bone and Mineral Research*, June 1997:12:989-994.
- [28] P. A. Zuk, M. Zhu, H. Mizuno, J. Huang, J. W. Futrell, A. J. Katz, P. Benhaim, H. P. Lorenz, M. H. Hedrick, "Multilineage cells from human adipose tissue: implications for cell-based therapies." *Tissue Eng.* 2001 Apr; 7(2):211-28.
- [29] A. James, J. Itskovitz-Eldor, S. S. Shapiro, M. A. Waknitz, J. J. Swiergiel, V. S. Marshall, J. M. Jones, "Embryonic Stem Cell Lines Derived from Human Blastocysts", *Science* 6 Nov, 1998, Vol. 282. no. 5391, pp. 1145-1147
- [30] P. Kasten, R. Luginbuhl, M.V. Griensven, T. Barkhausen, C. Krettek, M. Bohner, U. Bosch, "Comparison of human bone marrow stromal cells seeded on calcium-deficient hydroxyapatite, beta-tricalcium phosphate and demineralized bone matrix." *Biomaterials* 2003. Jul.24:2593-2603
- [31] L. W. Schmerr, "Fundamentals of Ultrasonic Nondestructive Evaluation," *Plenum Press*, 1998.
- [32] K. Nagamune, S. Kobashi, K. Kondo, et al. "An Ultrasonic Evaluation for Degradation of Insulating Oil using Fuzzy Inferencel." *Proceedings of 2003 IEEE Symposium on Ultrasonics* 1:893-6.
- [33] M. Endo, K. Nagamune, N. Shibamura, S. Kobashi, K. Kondo, and Y. Hata, "Ultrasonography System for Finding Distal Transverse Screw Hole of Intramedullary Nail," *Proc. of the Fourth Int. Symposium on Human and Artificial Intelligence Systems*, pp. 229-234, 2004.
- [34] P. Ligier, B.Fournier and G. Berger, "Quantitative Ultrasound Parametric Images of Cancellous Bone Compared to X-Ray Computed Tomography", *Proc. Ultrasonic Symp.*, pp1479-1478, 1994.
- [35] R. Barkmann and C. Gluer, "Associations between Parameters of Ultrasound Transmission and Structure Parameters of Cortical Bone", *Proc. Ultrasonic Symp.*, pp1649-1652, 2002.
- [36] S. Yamaguchi, K. Nagamune, K. Oe, S. Kobashi, K. Kondo, and Y. Hata, "Fuzzy logic approach to identification of cellular quantity by ultrasonic system," *Proc. The 2007 IEEE Int. Conf. on Granular*

- Computing, pp. 636-639, 2007.
- [37] S. Yamaguchi, K. Nagamune, K. Oe, S. Kobashi, K. Kondo, and Y. Hata, "A fuzzy estimation system for cellular quantity of artificial culture bone," Proc. Of IEEE Int. Conf. on Complex Medical Engineering, 2007.(online)
 - [38] Y. Hata, S. Yamaguchi, S. Kobashi, and K. Oe, "Fuzzy ultrasonic system for identifying cellular quantity of artificial culture bone," Proc. 2008 IEEE Int. Conf. on Systems, Man and Cybernetics, pp. 3062-3066, 2008.
 - [39] K. Oe, M. Miwa, K. Nagamune, Y. Sakai, S. Y. Lee, T. Niikura, T. Iwakura, T. Hasegawa, N. Shibamura, Y. Hata, R. Kuroda, and M. Kurosaka, "Nondestructive evaluation of cell numbers in bone marrow stromal cells/beta-tricalcium phosphate composites using ultrasound," Tissue Engineering, Part C: Methods, Vol. 16, No. 3, pp.347-353, June 2010
 - [40] M. H. Mankani, S. A. Kuznetsov, B. Fowler, et al. "In vivo bone formation by human bone marrow stromal cells: effect of carrier particle size and shape." *Biotechnol Bioeng* 2001. 72:96-107.
 - [41] OLYMPUS TERUMO BIOMATERIALS CORP. <http://www.biomaterial.co.jp/en/index.html>
 - [42] O. Hajime, I. C. Arnold, "Stem cell technology and bioceramics: From cell to gene engineering," *Journal of Bone and Mineral Research*, 9 Nov 1999:913 – 927
 - [43] T. Yoshikawa, H. Ohgushi, S. Tamai, "Immediate bone forming capability of prefabricated osteogenic hydroxyapatite," *Journal of Bone and Mineral Research*, 6 Dec 1998:481-492.
 - [44] J. David and N. Cheeke, Fundamentals and Applications of Ultrasonic Waves, 2002
 - [45] A. Sansom, J. Donovan, C. Sanders, P. Dieppe, J. Horwood, I. Learmonth, S. Williams, R. Gooberman-Hill, "Routes to total joint replacement surgery: patients' and clinicians' perceptions of need," *Arthritis Care Res (Hoboken)*, vol. 62, no. 9, pp. 1252-1257, 2010.
 - [46] G. E. Lewinnek, J. L. Lewis, R. Tarr, C. L. Compere, and J. R. Zimmerman, "Dislocations after total hip-replacement arthroplasties," *J Bone Joint Surg Am*, vol. 60, no. 2, pp. 217-220, 1978.
 - [47] W. J. Maloney, T. Schmalzried, W. H. Harris, "Analysis of longterm cemented total hip arthroplasty retrievals," *Clin. Orthop. Relat. Res.*, pp. 70-78, 2002.
 - [48] E. Schneider, C. Kinast, J. Eulenberger, D. Wyder, G. Eskilsson, S. M. Perren, "A comparative study of the initial stability of cementless hip prostheses," *Clin. Orthop. Relat. Res.*, pp. 200-209, 1989.
 - [49] R. K. Sinha, D. S. Dungy, H. B. Yeon, "Primary total hip arthroplasty with a proximally porous-coated femoral stem," *J Bone Joint Surg Am*, vol. 86-A, pp. 1254-1261, 2004.
 - [50] M. Lannocca, E. Varini, A. Cappello, L. Cristofolini, E. Bialoblocka, "Intra-operative evaluation of cementless hip implant stability: A prototype device based on vibration analysis," *Medical Engineering & Physics* 29, pp. 886-894, 2007.
 - [51] E. Varini, L. Cristofolini, F. Traina, M. Viceconti, A. Toni, "Can the rasp be used to predict intra-operatively the primary stability that can be achieved by press-fitting the stem in cementless hip arthroplasty," *Clinical Biomechanics* 23, pp. 408-414, 2008.
 - [52] D. D. D'lima, A. G. Urquhart, K. O. Buehler, R. H. Walker, C. W. Colwell, "The effect of the orientation of the acetabular and femoral components on the range of motion of the hip at different head-neck ratios," *J Bone Joint Surg*, vol. 82-A, no. 3, pp. 315-321, 2000.
 - [53] S. L. Delp, A. V. Komattu, R. L. Wixson, "Superior displacement of the hip in total joint replacement: Effects of prosthetic neck length, neck-stem angle, and anteversion angle on the moment-generating capacity of the muscles," *J Orthopaedic Res*, vol. 12, no. 6, pp. 860-870, 1994.
 - [54] F. Pierchon, G. Pasquier, A. Cotton, C. Fontaine, J. Clarisse, A. Duquenois, "Causes of dislocation of total hip arthroplasty," *J Bone Joint Surg*, vol. 76-B no. 1, pp.45-48, 1994.
 - [55] T. Albrektsson, P. I. Branemar, H. A. Hansson, J. Lindstrom, "Osseointegrated titanium implants. Requirements for ensuring a long-lasting, direct bone-to-implant anchorage in man," *Acta Orthop Scand*, vol. 52, pp.155-170, 1981.
 - [56] J. J. Callaghan, C. S. Fulghum, R. R. Glisson, S. K. Stranne, "The effect of femoral stem geometry on interface motion in uncemented porous-coated total hip prostheses. Comparison of straight-stem

- and curved-stem designs,” *J Bone Joint Surg Am*, vol. 74, pp.839-848, 1992.
- [57] P. S. Nourbash, W. G. Paprosky, “Cementless femoral design concerns. Rationale for extensive porous coating,” *Clin Orthop Relat Res*, pp.189-199, 1998.
 - [58] N. Shibamura, K. Nagamune, Y. Hata, T. Nishiyama, H. Tateishi, and M. Kurosaka, “Evaluation of the stability of a femoral stem using ultrasound,” *Proc. of the 53rd Annual Meeting of the Orthopaedic Research Society*, p.1733, 2007.
 - [59] N. Shibamura, Y. Hata, T. Nishiyama, T. Fujishiro, H. Tateishi, and M. Kurosaka, “Determination of Total Hip Arthroplasty Stem Stability by Intraoperative Measurement Using an Acoustic Testing Technique,” *Proc. of the 54rd Annual Meeting of the Orthopaedic Research Society*, p.1842, 2008.
 - [60] Ministry of Health, Labour and Welfare’s HP, <http://www.mhlw.go.jp/index.shtml>.
 - [61] Thomas R. Nelson, etc, *Three-Dimensional Ultrasound*, Lippincott Williams and Wilkins, 1999.
 - [62] Y. Hata, S. Kobashi, K. Kondo, Y. T. Kitamura, and T. Yanagida, “Transcranial Ultrasonography System for Visualizing Skull and Brain Surface Aided by Fuzzy Expert System,” *IEEE Trans. on Systems, Man and Cybernetics*, pp. 1360-1373, Vol. 35, No. 6, 2005.
 - [63] M. Kimura, S. Kobashi, K. Kondo, Y. Hata, Y. T. Kitamura, and T. Yanagida, “Fuzzy Ultrasonic Imaging System for Visualizing Braine Surface under Skull Considering Ultrasonic Refraction,” in *Proc. 2006 IEEE International Conference on Systems, Man, and Cybernetics*, pp. 3790-3794, 2007.
 - [64] A. Rune, M. T. Marc, and H. Nornes, “Noninvasive Transcranial Doppler Ultrasound Recording of Flow Velocity in Basal Cerebral arteries,” *Journal of Neurosurgery*, vol. 57, pp. 769-774, 1982.
 - [65] P. C. Njemanze, “Cerebral Lateralization in Random Letter Task in the Visual Modality: A Transcranial Doppler Study,” *Brain and Language*, vol. 53, pp. 315-325, 1996
 - [66] N. M. Ivancevich, K. K. Chu, J. D. Dahl, E. D. Right, G. E. Trahey, S. F. Idriss, P. D. Wolf, E. D. Tulloch, and S. W. Smith, “Real Time 3D Ultrasound Imaging of the Brain,” *IEEE, Ultrasonics Symposium*, vol.1, pp. 110-113, Aug 2004.
 - [67] D. H. Evans, and W. N. McDicken, “*Doppler Ultrasound Second Edition*,” John Wiley and Sons, 2000.
 - [68] M. Nakamura, T. Ishikawa, S. Kobashi, K. Kuramoto and Y. Hata, "Blood flow detection under skull by doppler effect," *Proc. of 2011 IEEE Int. Conf. on Systems, Man, and Cybernetics*, pp. 758-763, 2011.
 - [69] M. Nakamura, Y. T. Kitamura, T. Yanagida, S. Kobashi, K. Kuramoto, and Y. Hata, "Free placement trans-skull doppler system with 1.0MHz array ultrasonic probe," *Proc. of 2010 IEEE Int. Conf. on Systems, Man and Cybernetics*, pp. 1370-1374, 2010.
 - [70] G. Seidel, C. Algermissen, A. Christoph, L. Claassen, M. Vidal-Langwasser, T. Katzer, “Harmonic imaging of the human brain: visualization of brain perfusion with ultrasound. *Stroke*,” Vol. 31, pp. 151–154, 2000.
 - [71] Y. Ikeda, S. Kobashi, K. Kondo and Y. Hata, “Fuzzy Ultrasonic Array System for Locating Screw Holes of Intramedullary Nail,” in *Proc. 2006 IEEE International Conference on Systems, Man, and Cybernetics*, pp. 3428-3432, 2007.
 - [72] M. D. McDonnell and D. Abbott, "What Is Stochastic Resonance? Definitions, Misconceptions, Debates, and Its Relevance to Biology," *PLoS Computational Biology* 5, e1000348, 2009.
 - [73] T. Mori and S. Kai, "Noise-induced entrainment and stochastic resonance in human brain waves," *Phy. Rev. Letters* 88, 218101, 2002.
 - [74] P. Hänggi, "Stochastic resonance in biology - How noise can enhance detection of weak signals and help improve biological information processing," *ChemPhysChem* 3, pp. 285-290, 2002.
 - [75] L. Ke, X. Jianping, K. Dongmei, Z. Na, “A Method of Evaluating the Signal to Noise Ratio Based on Duffing Time Series,” *Proc. of the 2009 International Conference on Measuring Technology and Mechatronics Automation*, vol. 1, pp. 399-402, 2009.
 - [76] Y. Hotta, T. Kanki, N. Asakawa, H. Tabata, T. Kawai, "Cooperative Dynamics of an Artificial Stochastic Resonant System," *Appl. Phys. Express* 1, 2008.

- [77] K. Wiesenfeld and F. Jaramillo, "Minireview of stochastic c resonance", *Chaos* 8, pp. 539-548, 1998.
- [78] G. Hiramatsu, Y. Ikeda, S. Imawaki, Y. T. Kitamura, T. Yanagida, S. Kobashi and Y. Hata, "Trans-skull Imaging System by Ultrasonic Array Probe," *Proc. of 2009 IEEE Int. Conf. on Systems, Man and Cybernetics*, pp. 1116-1121, 2009.

Author's Papers Concerning This Dissertation

Chapter 2

1. N. Yagi, Y. Oshiro, O. Ishikawa, K. Oe, and Y. Hata, "Soft Computing Approaches to Identify Cellular Quantity of Artificial Culture Bone," *Proc. of 2010 IEEE World Congress on Computational Intelligence*, pp. 2852-2857, Jul. 2010.
2. N. Yagi, Y. Oshiro, O. Ishikawa and Y. Hata, "Computational Intelligence in Medical Ultrasonic System," *Proc. of Korea Institute of Intelligent Systems Fall Conference 2010*, Vol. 20, No. 2, pp. 9-15, Nov. 2010.
3. N. Yagi, T. Ishikawa, K. Kuramoto, S. Kobashi, and Y. Hata, "Noninvasive Cellular Quantity Measurement in Bone Marrow Stromal Cells/ Beta-tricalcium Phosphate," *Proc. of 35th Annual International Conference of the IEEE Engineering in Medicine and Biology Society*, pp. 2048-2051, Sep. 2013.
4. N. Yagi, T. Ishikawa, K. Kuramoto, S. Kobashi, and Y. Hata, "Ultrasonic Frequency Response Analysis for Quantitative Measurements in Bone Marrow Stromal Cells," *Proc. of 2013 IEEE Int. Conf. on Systems, Man and Cybernetics*, pp. 3420-3424, Oct. 2013.
5. N. Yagi, T. Ishikawa and Y. Hata, "Stem Cell Quantity Determination in Artificial Culture Bone by Ultrasonic Testing," *Journal of The Institute of Electronics, Information and Communication Engineers Information and Systems Society (IEICE)*, Transactions on Fundamentals of Electronics, Vol.E97-A, No.4, Apr. 2014. (in press)

Chapter 3

6. N. Yagi, Y. Oshiro, O. Ishikawa, Y. Hata and N. Shibamura, "Estimation System for Total Hip Arthroplasty by Acoustic Signal," *Proc. of 2011 IEEE Symposium Series on Computational Intelligence Workshop on Robotic Intelligence in Informationally Structured Space*, pp. 32-36, Apr. 2011.
7. N. Yagi, Y. Oshiro, O. Ishikawa, Y. Hata and N. Shibamura, "Fuzzy RASP Determination by 1kHz Ultrasonicprobe for Total Hip Arthroplasty," *Proc. of 2011 IEEE Int. Conf. on Fuzzy Systems*, pp. 1017-1021, Jun. 2011.
8. N. Yagi, Y. Hata and N. Shibamura, "Fuzzy Support System for Total Hip Arthroplasty Stem by Ultrasonic Intraoperative Measurement," *Journal of Hindawi - Advances in Fuzzy Systems*, Vol. 2012, Article ID. 201248, Sep. 2012.

Chapter 4

9. N. Yagi, Y. Oshiro, O. Ishikawa, G. Hiramatsu, Y. Hata, Y. Kitamura, and T. Yanagida, "Data Synthesis for Trans-skull Brain Imaging by 0.5 and 1.0MHz Ultrasonic Array Systems," *Proc. of 2010 IEEE Int. Conf. on Systems, Man and Cybernetics*, pp. 1524-1529, Oct. 2010.
10. N. Yagi, Y. Oshiro, O. Ishikawa, Y. Hata, Y. T. Kitamura and T. Yanagida, "YURAGI: Analysis for Trans-skull Brain Visualizing by Ultrasonic Array Probe," *Proc. of SPIE Defense, Security and Sensing 2011*, pp. 805813-1-9, Apr. 2011.
11. N. Yagi, Y. Oshiro, O. Ishikawa and Y. Hata, "Trans-skull Brain Imaging by Image Registration of 0.5 and 1.0 MHz Waves," *Proc. of 2011 IEEE Int. Conf. on Systems, Man, and Cybernetics*, pp. 706-710, Oct. 2011.

12. Y. Hata, M. Nakamura, N. Yagi and T. Ishikawa, "Trans-skull Ultrasonic Doppler System Aided by Fuzzy Logic," Proc. of SPIE Defense, Security and Sensing 2012, pp. 840118-1-8, Apr. 2012.
13. N. Yagi, Y. Oshiro, T. Ishikawa and Y. Hata, "Ultrasonic Image Synthesis in Fourier Transform," Proc. of 2012 World Automation Congress, 1569535291, Jun. 2012.
14. N. Yagi, Y. Oshiro, T. Ishikawa and Y. Hata, "Human Brain Ultrasound-mediated Diagnosis in Emergency Medicine and Home Health Care," Proc. of the 6th International Conference on Soft Computing and Intelligent Systems and 13th International Symposium on Advanced Intelligent Systems, pp. 1269-1274, Nov. 2012.
15. N. Yagi, Y. Oshiro, T. Ishikawa, and Y. Hata, "YURAGI Synthesis for Ultrasonic Human Brain Imaging," Journal of Advanced Computational Intelligence and Intelligent Informatics, vol. 17, no. 1, pp. 74-82, Dec. 2012.
16. N. Yagi, M. Nakamura, K. Kuramoto, S. Kobashi, and Y. Hata, "Noninvasive Diagnosis of Blood Flow for Transcranial Doppler Ultrasonography," Journal of Intelligent Computing in Medical Sciences and Image Processing, vol. 5, no. 1, pp.67-79, Mar. 2013.
17. N. Yagi, T. Ishikawa, and Y. Hata, "Ultrasonic Image Registration for Multi-frequency Analysis," Journal of Acoustic, vol. 3, no. 3A, pp. 1-8, Sep. 2013.
18. N. Yagi, S. Imawaki, T. Ishikawa, and Y. Hata, "Mobile Health Care Management in Smart Medical System," Proc. of the 14th International Symposium on Advanced Intelligent Systems, F3c-1, Nov. 2013.

International Awards

1. The Best Student Paper Award, World Automation Congress 2012, Jun. 2012
2. Google Anita Borg Memorial Scholarship Asia Scholar's Award, Google, Sep. 2012
3. Best Presentation Award, The 14th International Symposium on Advanced Intelligent Systems, Nov. 2013